NATIONAL TECHNICAL UNIVERCITY OF ATHENS
Faculty of Civil Engineering
Institute of steel structures

Performance assessment of three reinforced concrete buildings and verification of performance based design methodology

MASTER THESIS
MSc in Analysis and Design of Earthquake Resistant Structures

Akrivi S. Chatzidaki

Supervisor: Dimitrios Vamvatsikos

Athens, March 2018

EMK ME 2018/8

Chatzidaki A. (2018).
Performance assessment of three reinforced concrete buildings and verification of performance based design methodology
Master Thesis EMK ME 2018/8
Institute of Steel Structures, National Technical University of Athens, Greece

Contents

NATIONAL TECHNICAL UNIVERSITY OF ATHENS
FACULTY OF CIVIL ENGINEERING
INSTITUTE OF STEEL STRUCTURES

MASTER THESIS
EMK ME 2018/8

Performance assessment of three reinforced concrete buildings

Chatzidaki A. (supervised by Vamvatsikos D.)

Abstract

The performance of a 4-story reinforced concrete moment resisting frame building, a 12-story RC coupled wall building and a 7-story RC shear wall building is evaluated. The moment resisting frame building is designed for USA using three different approaches, namely by using the Yield Point Spectrum as a basis for the design (code compatible design) and two other more advanced methods that rely on the Yield Frequency Spectrum and can account for hazard and uncertainty. These methods offer a direct performance-based seismic design and provide a fast algorithm to achieve compliance of a structure to user-specified performance targets. For the performance assessment of the building two different models are examined: a distributed plasticity model to accurately capture the structural response at low intensity levels and a lumped plasticity model to capture the structural response at high intensity levels. For assessment only the lumped plasticity model is employed, after having been calibrated to match the pre-yield behaviour of the distributed plasticity model. The 12 story coupled wall building and the 7 story shear wall building are designed for Europe using the Yield Point Spectrum and the Yield Frequency spectrum as a basis for the design, respectively. A two dimensional model of each structure is used for the performance assessment, that employs distributed plasticity displacement-based elements.

Non-linear static analyses are performed for the qualitative assessment of all buildings, while nonlinear response history analysis is employed for quantifying the performance. Specifically single and double stripe analyses are employed in tandem with a practical Factored Capacity versus Factored Demand checking format. For verification, the mean annual frequency of exceeding each performance objective of interest is also estimated, based on incremental dynamic analysis results.

Results indicate that the Yield Point Spectrum offers a fair assessment when performance objectives with probability of exceedance 10% in 50 years (code compatible) are examined. The results for performance objectives with different probability of exceedance were not satisfactory. The Yield Frequency Spectra led to a far more accurate design, fulfilling the stated performance objectives. Together with the simple checking format, the two may constitute a viable approach for direct performance based design that can be easily employed in practice.

Acknowledgments

First and foremost, I would like to express my sincere gratitude to my supervisor, Assistant Prof. Dimitrios Vamvatsikos, for the continuous support that he offered, his patience, motivation, enthusiasm and immense knowledge. His office door was always open whenever I ran into a trouble spot or had a question about my research or writing. I could not have imagined having a better supervisor for my thesis.

Besides my supervisor, I would like to thank Dr. Mark Aschheim, Professor at Santa Clara Univercity and Dr. Enrique Hernández-Montes, Professor at the University of Granada, for offering valuable assistance and guidance in topics that fall within their expertise. Their input was crucial for the success of this project.

My sincere thanks also go to Charis Lyritsakis, former student at NTUA, who willingly shared some of results of his own thesis, conducted under the supervision of Prof. Vamvatsikos, with me.

Finally, I must express my very profound gratitude to my parents, Stelios and Voula, and to my sister, Natasha, for providing me with unfailing support and continuous encouragement throughout my years of study and through the process of researching and writing this thesis. Thank you!

1 Introduction

1.1 Overview

Current seismic codes, such as Eurocode 8 (2005) that is used in Europe for the seismic design of structures, follow a force-based design procedure. This means that the lateral forces are calculated according to the elastic demands and a system specific factor (R or q) prescribed by the code is used to account for the inelasticity. These factors usually do not account for the ductility capacity or the overstrength that typically exists in the structures. The code provisions usually intend to achieve life safety performance for ground motions that have a probability of exceedance 10% in 50 years approximately, simply by ensuring that critical member sections have sufficient strength and conform with the detailing requirements provided by the codes. Design codes also incorporate the uncertainties via the use of partial safety factors at the input level of materials and loads instead of the output response, which means that the structural performance under earthquakes may not be the desired one.

The large economic losses in the 1994 Northridge and 1995 Hyogo-Ken Nambu earthquakes highlight the need of performance based seismic design (PBSD). This design approach does not account for the life safety performance level, but multiple performance objectives are incorporated as well. The performance objectives are defined as not exceeding a prescribed structural response level with a mean annual frequency higher than the prescribed one. This design procedure provides a direct way to incorporate uncertainty into a design process that respects user determined limits on drift and system ductility. At its most advanced form, non-exceedance rates of economic losses or casualties are targeted, echoing the definition of decision variables that are embedded in the Cornell – Krawinnkler framework (2000), adopted by the Pacific Earthquake Engineering Research (PEER) Center.

An appropriate method should be established to design a structure to meet the desired performance objectives. Current design procedures solve the inverse problem as seismic loads are applied to the model of the structure and individual member forces and deformations are defined. Then, the minimum required member size is specified. The methodology provided by the code is based on an initial estimation of the fundamental period of the building. The better this estimation is, the less re-design and re-analysis cycles are needed. Priestley (2000) and Aschheim (2002) suggested the use of the yield displacement as the invariant term (displacement based design) as it is a more stable parameter, thus the need of iterations is significantly reduced. Figure 1.1 shows the bilinear fit of the capacity curves obtained for two moment resisting frames (four stories and three bays) that have the same nominal geometry and member depths. The weights of the member cross sections are different for the two frames, so the lateral strength differs. As can easily be noticed, the yield displacements are almost invariant although the strengths and stiffnesses of the two frames differ considerably.

Displacement based seismic design may be employed using the Yield Point Spectrum (YPS) as proposed by Aschheim (2002). The yield point spectra is a visualization of the yield displacements of a system having constant displacement ductility for a range of periods. Using the elastic response spectrum and R-μ-T relationships, such as those discussed by Miranda and Bertero (1994), the strengths corresponding to specific displacement ductilities can be determined. Figure 1.2 shows the ASCE-7 (2010) response spectrum in the YPS format which is used in the design of the four story moment resisting frame building discussed later on (Section 21). Given an initial estimation of the Δ_y of the SDOF system and the ductility limits that correspond to the desired performance objectives, the base shear coefficient at yield C_y can be determined using the YPS. Having established the C_y, member sizes may be determined. If an iteration is needed, a new yield displacement is estimated and the process is repeated.

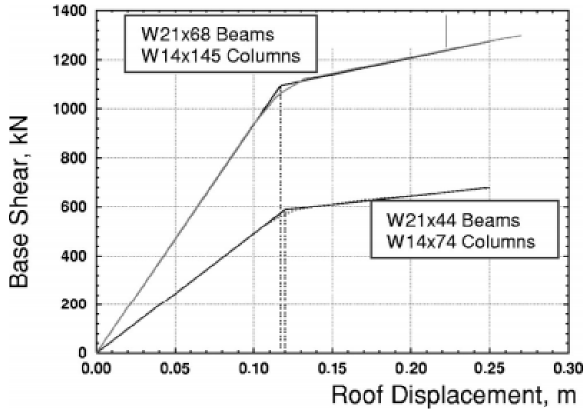

Figure 1.1: Capacity curves determined by nonlinear static (pushover) analysis for two four-story moment-resistant steel frames. The frames have the same nominal section depths but the weights of the sections are changed to change the lateral strength. The yield displacement is almost constant even though the strengths, stiffnesses and periods of vibration of the frames differed substantially, (from Black and Aschheim, 2000).

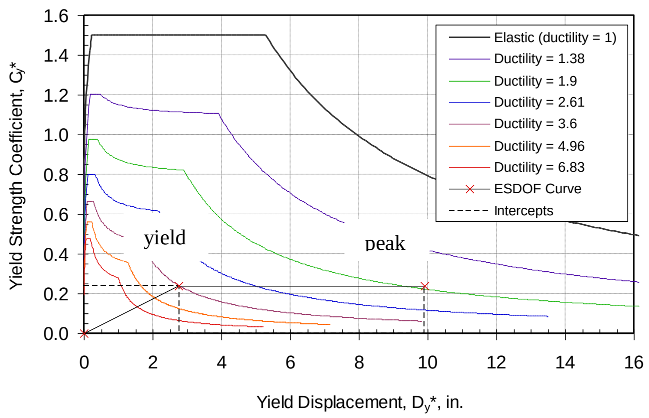

Figure 1.2: Yield point spectra computed for ASCE-7 design spectrum. For a system with yield displacement Δ_y=2.75in and μ=3.6, the corresponding yield strength coefficient is C_y^*=0.24. Given that μ=3 the peak displacement is three times the yield displacement, (from Aschheim et al., forthcoming [7]).

A performance based seismic design methodology that propagates uncertainty at the SDOF level is proposed by Vamvatsikos and Aschheim (2015). The Yield Frequency Spectra (YFS) is a visual representation of a system's performance that links the mean annual frequency (MAF) of exceeding any displacement value with the system yield strength. YFS are plotted for a specified yield displacement, thus the variations in C_y that are shown in the YFS are associated with variation in stiffness and period of vibration. To compute the YFS we need the site hazard and an assumption about the systems behavior (e.g. elastoplastic). Structures can be designed using the YFS but an initial estimation of the δ_y of the SDOF system in necessary. Given the ductility limits that correspond to the desired performance objectives, the base shear coefficient at yield C_y for each PO is determined. The one that demands the higher strength is selected for the design. Figure 1.3 shows an example of the YFS that is used to design the four story moment resisting frame building (Section 3.5).

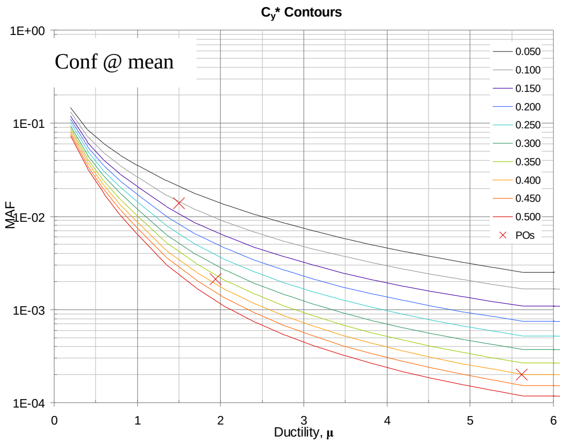

Figure 1.3: Yield frequency spectra contours at C_y = 0.1, … , 0.55 determined for a system with yield displacement equal to Δ_y^*=2.84in. The x symbols represent the performance objectives (μ=1.5, 1.94, 6 at the 50, 10 and 2% in 50 years exceedance rates, respectively). The third objective governs with C_y^*=0.40 (from Aschheim et al., forthcoming [7]).

The structural design that relies on the use of the YPS does not take into account the uncertainty directly but code specific reduction factors are applied in the design. This approach results in a design comparable to the code requirements without explicit consideration of uncertainty. On the contrary, when the YFS is used for the design of the structures, statistical distributions that reflect the dispersion inherent in the values of the estimated parameters are used instead of using point estimates, as in the YPS, hence the uncertainties are incorporated. A desired MAF can be targeted in the design process and the focus is on the MAF of exceeding the parameter value of interest (output), rather than on the MAF of exceeding ground motion intensity (input) as in the YPS. If the YFS is calculated using a linear fit of the hazard curve instead of actual hazard data, some conservatism is introduced, but if the mean hazard information is used then the uncertainties in the hazard are also taken into account.

1.2 Objective

Our aim is to assess the performance of three reinforced concrete buildings: a four story moment resisting frame building, a 12 story coupled wall building and a seven story shear wall building. These structures are designed by Professors Mark Aschheim, Enrique Hernández-Montes and Dimitrios Vamvatsikos using the methodologies mentioned above. The reader who wishes to find more details about the design procedures is encouraged to study Aschheim et al. [7]

The four story reinforced concrete moment resisting frame building is designed using three different approaches. Firstly the YPS is used for the design, which is calculated using the ASCE-7 design spectrum as a basis (design method A). More advanced methods are also employed, which rely on the use of the YFS. In method B the YFS is calculated using the ASCE-7 design spectrum and an estimation of the slope of the hazard curve within the range of interest. Method C also accounts for the epistemic uncertainties in the estimation of the site hazard, thus the YPS is computed using the mean hazard curve at the site of interest.

To assess the performance of the four story moment resisting frame building, two models are prepared: a distributed plasticity model to accurately capture the structural response at low intensity levels and a lumped plasticity model to capture the structural response at high intensity levels. The lumped plasticity model is calibrated so that the pre-yield behaviour better matches the distributed plasticity model.

The coupled wall building is designed for Europe using the Yield Point Spectrum (code-compatible design), (design method A). The shear wall building is designed using the Yield Frequency Spectrum that is calculated using the Eurocode 8 design spectrum and an estimation of the slope of the seismic hazard curve in the range of interest (design method B). Both buildings are modelled using displacement – based fiber elements.

Non-linear static analyses are employed for the qualitative assessment of the buildings. Finally incremental dynamic analyses are performed. The performance of each structure is assessed using the stripe analysis (single and double stripe analysis), simply by checking whether Factored Capacity exceeds Factored Demand. Furthermore, the mean annual frequency of exceeding each performance objective set in the design is estimated, based on the IDA results.

1.3 Chapter layout

In the first chapter the idea of performance based seismic design is introduced along with some current design techniques. Furthermore, the objective of this documentation and the chapter layout are presented.

In the second chapter the methodologies used for the performance assessment of the three structures are presented and briefly discussed.

In the third chapter the design of the reinforced concrete four story moment resisting frame building using the three different methods mentioned above are presented. The non-linear modelling details of the distributed and the lumped plasticity model of the structure are summarized and the results of the calibration procedure are shown. The results of the performance assessment of these design methods are shown.

In the fourth chapter the design of the reinforced concrete 12 story coupled wall building using the YPS (design method A) is summarized. The distributed plasticity model employed for the non-linear analysis of the structure is presented, along with the results of the performance assessment of the building.

In the fifth chapter the design of the 7 story reinforced concrete shear wall building using the YFS (design method B) is presented. The distributed plasticity model used for the non-linear analysis of the building and the results of the performance assessment procedure are shown.

Finally, in the sixth chapter the conclusions that concern the different methodologies used for the design as well as the different methodologies used for the performance assessment of the structures are summarized.

2 Performance assessment

There are many methods to assess the performance of a structure but few of them are in the terms of risk. A definition of performance objective that respects risk should be established. The performance objective is a combination of a threshold or capacity value of response, damage or loss, a maximum allowable mean annual frequency of exceeding this threshold and a desired confidence level (grater or equal to 50%) of meeting this objective, to account for the epistemic uncertainty. The proposed methods for assessing the seismic performance of structures necessitate a compromise between cost and accuracy, with each method offering different balance between these two requirements. Three different methods are used for the performance assessment of the structures named *stripe analysis* (*single* and *double stripe analysis*) and *IDA approach*. These methods are briefly described here. An example of application is also presented for illustrative purposes, which concerns the performance assessment of the four story moment resisting frame building designed using the YPS (design method A).

2.1 IDA approach

The seismic performance of a structure can be evaluated using the incremental dynamic analysis approach (IDA approach), as proposed by Vamvatsikos and Cornell (2002). When performing IDA, the nonlinear model of the structure is subjected to a suit of records, each scaled to several levels of seismic intensity, in order to force the structure all the way from elastic to yielding, then to nonlinear inelastic and finally to global dynamic instability. Analysis results are characterized by two scalars, an Intensity Measure (IM), which represents the scaling factor of the record, and an Engineering Demand Parameter (EDP) which monitors the structural response of the model. Due to considerable record-to-record variability, IDA requires a large enough set of records to cover the full range of responses. For this reason, the 2D models of the structures are here subjected to 44 natural ground motion records (22 seismic events, two components each) obtained from PEER NGA Database (2005). An example of the results of IDA applied for 44 records for the four story moment resisting frame building designed according to the design method A, in terms of the first mode spectral acceleration $S_a(T_1,5\%)$ and maximum interstory drift ratio, θ_{max}, are shown in Figure 2.1 (a) along with their summary 16%, 50% and 84% fractiles (Figure 2.1 (b)).

For each performance objective deformation limit, the IMs that correspond to that limit are calculated through the IDA results. These are assumed to follow the lognormal distribution, with median value m and standard deviation β. The fragility curve for each performance objective is derived. Fragility curves are continuous functions that provide the probability of being in or exceeding predefined POs for specific levels of ground motion intensities. The probability of being in a PO given the IM is calculated using the Equation (2.1), where Φ is the standard normal cumulative distribution function, $\overline{S_a}$ is the median value of the IM at which the building reaches the threshold of the PO and β_{Sa} is the lognormal standard deviation that describes the total variability of the PO. β_{TSa} is calculated according to the Equation (2.2), where β_{Sa} accounts for the aleatory randomness due to natural ground motion variability and β_U can be introduced to account for the epistemic uncertainty owing to modelling assumptions, omissions or errors.

$$P[ds/S_a] = \Phi\left(\frac{lnS_a - ln\overline{S_a}}{\beta_{TS_a}}\right), \quad (2.1)$$

$$\beta_{TS_a} = \sqrt{\beta_{S_a}^2 + \beta_U^2}, \tag{2.2}$$

An example of the computed fragility curve for the PO of maximum interstory drift ratio of 2% of the four story moment resisting frame building designed according to design method A is shown in Figure 2.2. Figure 2.2 (a) shows the $S_a(T_1,5\%)$ values that correspond to the θ_{max}=2% limit. The median value of the lognormal distribution is 0.63g and the standard deviation is equal to 26%. The resulting fragility curve is shown in Figure 2.2 (b).

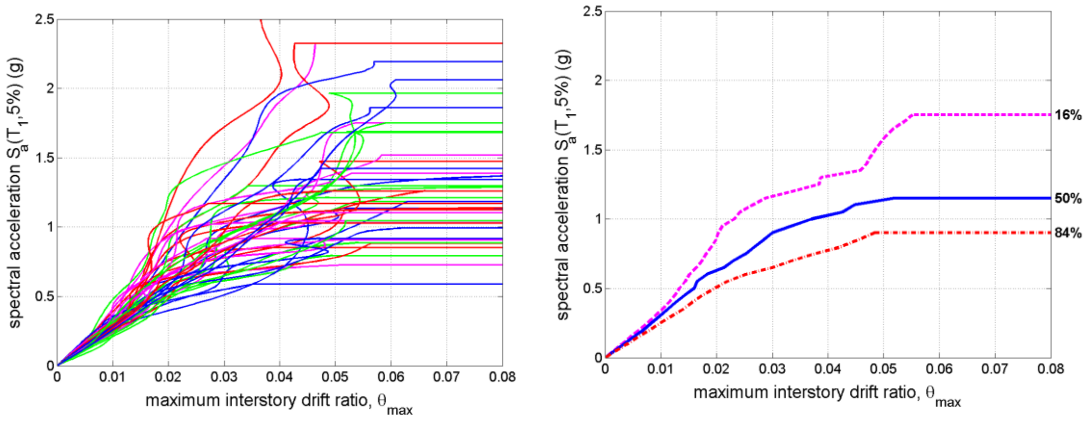

(a) (b)

Figure 2.1: IDA study for 44 records showing a) the 44 individual curves and b) their summary (16, 50 and 84%) fractile curves in terms of Sa(T_1,5%) and maximum interstory drift ratio θ_{max} for the four story moment resisting frame building designed using the YPS.

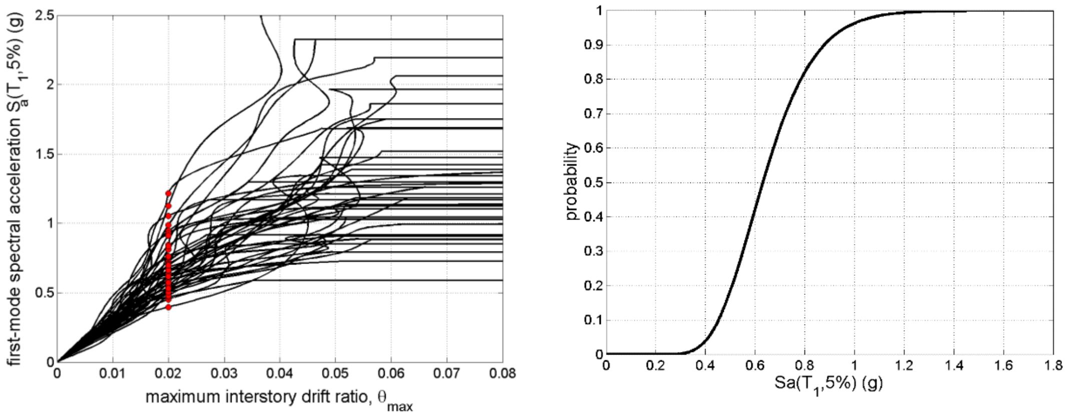

(a) (b)

Figure 2.2: (a) the Sa(T_1,5%) values calculated for the 2% maximum interstory drift ratio limit, θ_{max}, and (b) corresponding fragility curve, derived for the four story moment resisting frame building designed using the YPS.

In order to estimate the mean annual frequency of exceeding each performance objective, two components are needed: (i) the fragility curve and (ii) the seismic hazard curve. The seismic hazard curve for a given site relates the Intensity Measure with its mean annual frequency of exceedance. The seismic hazard curves used for the design (in design method C) and the assessment of the structures is derived for San Jose, California (latitude = 37.33659 and longitude = -121.89056), (established in the 2008 National Seismic Hazard Mapping Project and available at http://geohazards.usgs.gov/hazardtool/ application.php).

In order to offer a fair assessment of the design methodologies that use code design spectrum as a basis (methods A and B), the seismic hazard curve is scaled so as the MAF=0.0021 (10% probability of exceedance in 50 years) matches the spectral acceleration calculated from the design spectrum of the code. An example of a seismic hazard curve is shown in Figure 2.3. This is the scaled curve derived for the four story moment resisting frame building located in San Jose, California.

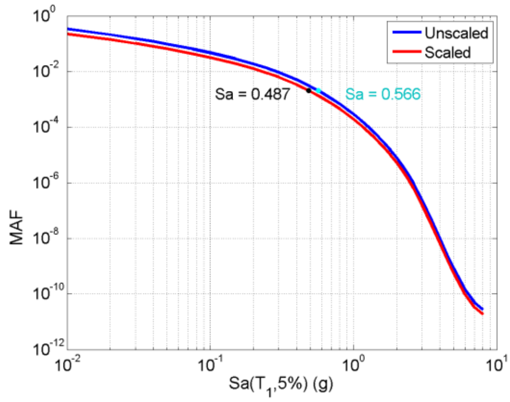

Figure 2.3: Seismic site hazard curve of San Jose site properly scaled to 2% in 50 years for $S_a(T_1)$, used to assess the performance of the four story moment resisting frame building – design method A.

The MAF of exceeding each PO is calculated by integration of the seismic hazard curve over buildings fragility curve, as described by the Equation (2.3):

$$MAF_{LS} = \int_0^{\infty} P(Demand > Capacity|IM) \cdot |d\lambda(IM)|, \tag{2.3}$$

where P (*Demand* > *Capacity* | *IM*) is the probability of demand exceeding capacity given the *IM*, derived by fragility curve, and $|d\lambda(IM)|$ is the slope of the seismic hazard curve. Meeting an objective means that the *x*% percentile estimate (due to epistemic uncertainty) of the mean annual frequency of the demand, *D*, exceeding the capacity *C*, should be lower than λ_{PO}, thus $\lambda_{x\%}(D > C) < \lambda_{PO}$, where *x*% is the desired confidence level at which the PO should be met.

2.2 Stripe analysis

The demand and capacity factored design (DCFD) format developed by Cornell et al. (2002) can be used to check whether a performance objective has been violated, but it cannot provide an estimate of the mean annual frequency of exceeding a given performance objective level. The following inequality is used for safety checking:

$$FC_R \geq FD_{RPo} \cdot \exp(K_x \cdot \beta_{TU}), \tag{2.4}$$

where FC_R is the factored capacity and FD_{RPo} is the factored demand evaluated at the probability P_o associated with the selected performance objective. The subscript *R* is used in order to highlight the fact that only epistemic uncertainties are taken into account. FC_R is estimated as:

$$FC_R = \varphi_R \cdot \mathrm{EDP}_{C,50} \geq \gamma_R \cdot EDP_{50} \cdot \exp(K_x \cdot \beta_{TU}), \tag{2.5}$$

where $EDP_{C,50}$ is the median EDP capacity defining the performance level. EDP_{50} is the median demand evaluated from the non-linear response history analysis (NRHA) of a subset of records scaled at the intensity measure that has probability of exceedance equal to P_o. In the assessment procedure we used 17 records although even less records could have been used. The capacity and demand factors are defined as:

$$\varphi_R = \exp\,[-0.5 \cdot k \cdot \beta_{CR}^2 / b_{EDP}], \tag{2.6}$$

$$\gamma_R = \exp\,[0.5 \cdot k \cdot \beta_{DR}^2 / b_{EDP}], \tag{2.7}$$

where β_{DR} is the demand record to record (aleatory) variability, determined from the results of the NRHAs, and β_{CR} is the aleatory variability in the EDP value of the limit state capacity that can be determined e.g., from experimental tests. We assumed that β_{CR}=0.20. Parameter k is the slope of the hazard curve when plotted in log-log coordinates that can be estimated using the following equation:

$$k = \text{abs}\,[\,(\ln H(S\alpha_1) - \ln H(S\alpha_2)\,) / (\,\ln(S\alpha_1) - \ln(S\alpha_2)\,)\,], \tag{2.8}$$

where $H(\mathrm{Sa_i})$ is the mean annual frequency of exceeding the Sa_i value, calculated according to the hazard curve. The hazard fitting is performed at s_{Po} which is the intensity for which the demand is estimated. The Sa_i values are calculated according to Equation (2.9), where c = 0.0, -1.0, as suggested by Vamvatsikos (2012). The region of the fit is extended further into the lower intensities, since these are the ones that have the higher probabilities of exceedance.

$$S\alpha_i = s_{Po} \cdot \exp\,[\,c_i \cdot (\beta_{CR}^2 + \beta_{DR}^2)^{0.5} / b_{EDP}\,], \tag{2.9}$$

b_{EDP} is equal to 1.0 when single stripe analysis is performed. For double stripe analysis, NRHS is also performed using the selected subset of records (or even fewer records can be used) scaled at an increased intensity measure IM'. The b_{EDP} value is then estimated as the slope of the median demand parameter values calculated through the results of the NRHAs, in a log-log space, thus:

$$b_{EDP} = (\ln(EDP'_{50}) - \ln(EDP_{50})) / \ln(IM' / IM), \tag{2.10}$$

The double stripe analysis, offers improved accuracy compared to the single stripe analysis, as more data are used. Finally, to ensure that FC_R exceeds FD_{RPo} with the designed MAF at confidence level of x, K_x is included in Equation (2.5). This is the standard normal variate corresponding to the desired level x. For example for 90% confidence, K_x=0.0.

2.2.1 Example of application

The safety checks for the maximum interstory drift ratio θ_{max} of the four story moment resisting frame building designed using the YPS (method A) are presented in detail. The results of the incremental dynamic analyses are used as a basis. The results of the 17 ground motion records scaled at the S_a^{design}=0.57g and 1.1S_a^{design}=0.63g level are calculated using IDA results, as we already have them. Alternatively, we could have performed 17 NRHA to compute the desired values. The θ_{max} values calculated for those records are presented in Figure 2.4 (a). The median value of the maximum interstory drift is EDP_{50}=0.0166 and the standard deviation is 28% for the records scaled at the S_a^{design} level. EDP'_{50}=0.0191 calculated according to the results obtained by the records that were scaled at the $1.1S_a^{design}$ level. The slope b_{EDP} is estimated as:

b_{EDP} = - (ln(0.0166)-ln(0.0191))/(ln(1.1)) = 1.47.

The points of the hazard curve needed to estimate the slope k are calculated according to the Equation (2.9) as:

$Sa_1 = 0.57 \cdot \exp[\,0\,] = 0.57$g
$Sa_2 = 0.57 \cdot \exp[\,-1.0 \cdot (0.20^2 + 0.28^2)^{0.5} / 1.47\,] = 0.454$g

and are presented in Figure 2.4 (b). The slope k is 2.63. Comparing the linear fit (blue line) with the hazard curve (red curve), it is obvious that the hazard is overestimated, thus the Sa-based approach results in a conservative evaluation. The Factored Demand and Factored capacity are estimated at the 50% confidence as:

$FD_{RPo} = \theta_{max,50} \exp(0.5 \cdot k \cdot \beta_{\theta max|Sa}^2 / b_{EDP}) = 0.0166 \exp(0.5 \cdot 2.63 \cdot 0.28^2/1.47) = 0.0178$
$FC_R = \theta_{max,C} \exp(-0.5 \cdot k \cdot \beta_{CR}^2 / b_{EDP}) = 0.02 \exp(-0.5 \cdot 2.63 \cdot 0.20^2/1.47) = 0.0193$

hence the result is satisfactory.

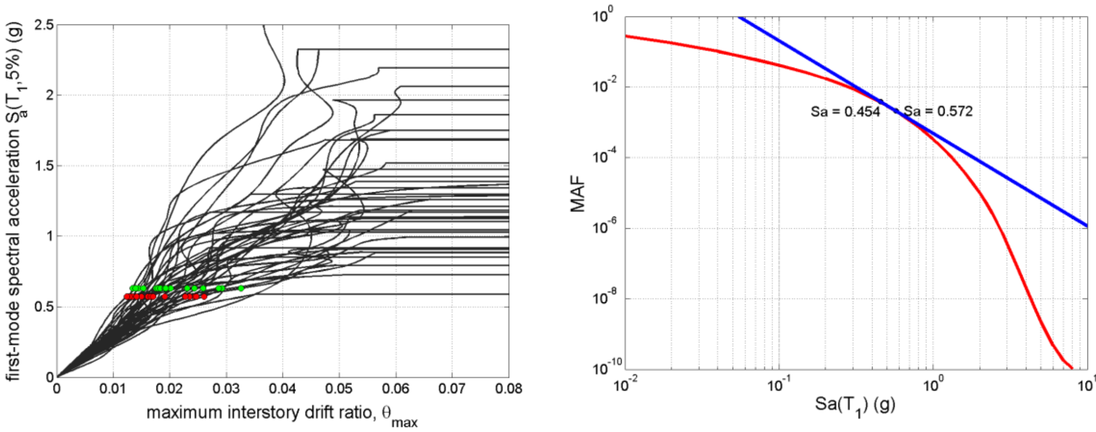

(a) (b)

Figure 2.4: Double stripe analysis method for estimating FD_{RPo} and FC_R for 2% maximum interstory drift ratio: (a) maximum interstory drifts calculated for S_a^{design} (red points) and for $1.1S_a^{design}$ (green points), and (b) the local fit of the seismic hazard curve. This example concerns the four story moment resisting frame building designed using design method A.

3 Four story moment resisting frame

3.1 Building geometry

A four story reinforced concrete moment resisting frame building is examined. The plan of the building has dimensions equal to 120x180ft and is presented in Figure 3.1. The perimeter moment frames resist all the seismic loading, while the inner columns carry only the gravity loads. The height of the first story is 15 feet, while the height of each one of the rest of the stories is 13 feet, resulting in a total height of 54 feet. The frame has four bays, each with 30 feet spans, as presented in Figure 3.1.

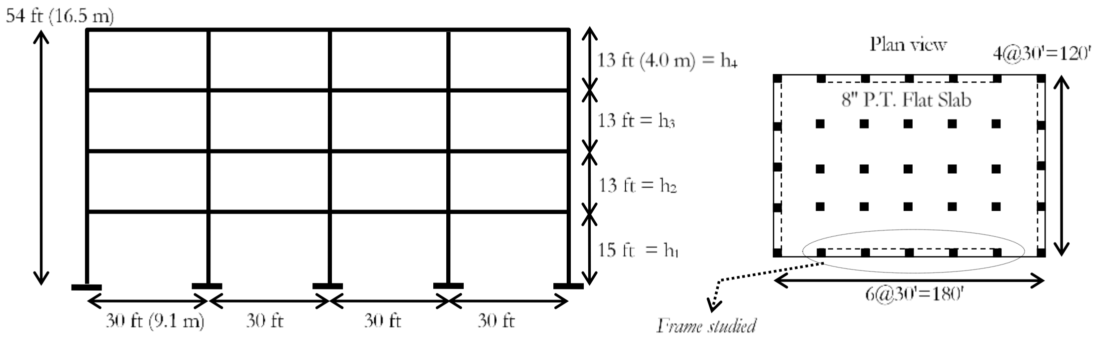

Figure 3.1: Plan and elevation of the four story reinforced concrete perimeter moment resisting frame building.

3.2 Material properties and loading

The moment resisting frames are designed using the nominal material properties. The compressive strength of the concrete is f_c=5ksi and the yield strength of the steel rebars is f_y=60ksi. For the performance assessment, the expected material properties are used, thus f_{ce}= 6.5ksi and f_{ye}= 69ksi and the expected yield strength is ε_{ye}=0.00238. The elastic modulus is estimated as E_c = 57,000(f_{ce})0.5, where f_{ce} and Ec are expressed in psi units.

The dead load is equal to 175psf smeared over the floor plate, while the live load is 50psf per floor plate. The weight of the building is 15120 kips, with half of this (7560 kips) tributary to each frame. During the seismic response, the gravity loads are estimated to be D+0.25L, while only the dead load is assumed to act on the roof.

3.3 Non-linear modelling

The structural model used for the analysis may employ either lumped or distributed plasticity elements. Distributed plasticity elements use fiber sections with each fiber being equivalent to a simple spring that can faithfully represent the uniaxial stress-strain deformation characteristics of steel rebars and concrete fibers, either confined or unconfined. Overall, at the expense of higher computational complexity they allow naturally capturing phenomena such as the cracking of concrete, the spread of plasticity and the axial-moment interaction at the level of the section. At the same time, they typically cannot reproduce well the behavior beyond the maximum strength “capping” point, obviously being unable to capture, e.g., rebar buckling, and cannot directly account for the effect of shear. On the other hand, lumped plasticity phenomenological models only allow a concentrated representation of plasticity at predefined plastic hinge locations. Typically this is a rotational spring with a multi-linear backbone that can capture well enough yielding, capping and the post-capping region but often fails to reproduce the cracking of concrete and the gradual plasticization of sections. Therefore, the transition of the model from its initial uncracked stiffness to the cracked effective stiffness and period often remains an issue that may affect the accuracy of performance assessment. Still, lumped plasticity models are far less complex, numerically more robust and generally better suited to assessing the collapse or near-collapse performance.

In our case, a two dimensional lumped plasticity model of the structure is used. To overcome the initial versus effective stiffness issue, a distributed plasticity model is also created and subjected to static pushover analysis. The elastic stiffness of concentrated plasticity elements is then calibrated (i.e., increased) so that the pre-yield behavior better matches the distributed plasticity model. In both models, a leaning column is added to simulate the effect of the columns that carry the gravity loads. The leaning column is pinned at the foundation and modeled using linear elastic elements having area and moment of inertia that match the corresponding cross sectional properties of one half of the gravity columns of the building, as only one out of two moment-frames is modeled in the direction of interest, due to symmetry.

3.3.1 Distributed plasticity model

To simulate a rigid diaphragm, the frame nodes at any given floor are rigidly connected by stiff truss elements. Still, such a rigid constraint can impose a condition of zero axial strain on the beams, which is not the case for concrete fiber sections where the neutral axis shifts due to inelastic bending. Neglecting this effect can produce fictitious axial compression that will unconservatively increase the moment rotation capacity of the beam plastic hinges due to the moment-axial interaction that fiber sections display. Therefore, according to prof. Zeris (personal communication), one end of each beam element receives a low stiffness axial (i.e., horizontal) spring to connect to the column to avoid generating such compressive forces. The structural model is presented in Figure 3.2 along with some diaphragm modelling details.

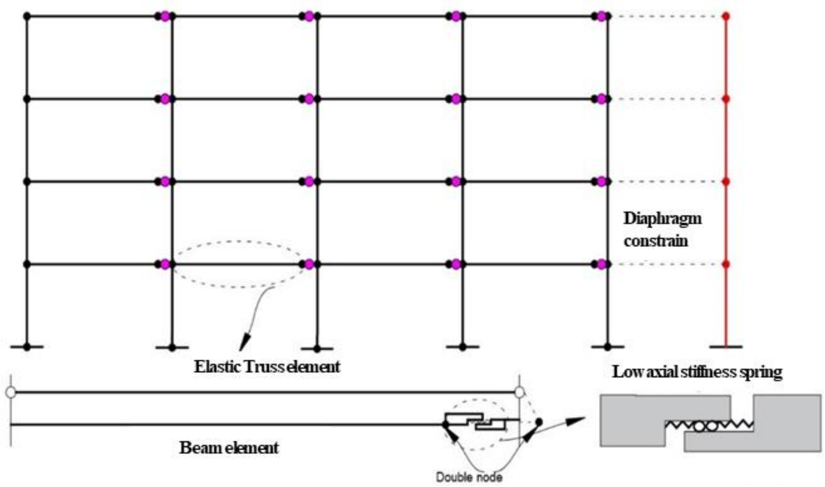

Figure 3.2: Distributed plasticity model of the moment resisting frame showing the beams, the columns (black color) and the leaning column (red color). The diaphragm is modelled using truss elements and low stiffness axial springs (pink color) as professor Zeris suggested (personal communication).

Beams and columns are modelled using force-based distributed plasticity - fiber elements, discretized into longitudinal steel and concrete fibers. A uniaxial nonlinear model, proposed by Kent, Scott and Park and realized in OpenSees [McKenna et al. 2000], is employed for unconfined cover concrete (red color in Figure 3.3), while the confinement related parameters applied in confined core concrete (green color in Figure 3.3) are calculated on the basis of Mander's model [Mander et al. 1988]. Furthermore, steel reinforcing bars (black color in Figure 3.3) are modelled using a bilinear constitutive law accounting for pinching and stiffness degradation. The strength of steel and concrete materials is set at their expected value of f_{ye} =69ksi and f_{ce} =6.5ksi, respectively, rather than at the nominal characteristic strengths. Typical fiber section discretization is shown in Figure 3.3 (a) for beams and (b) for columns.

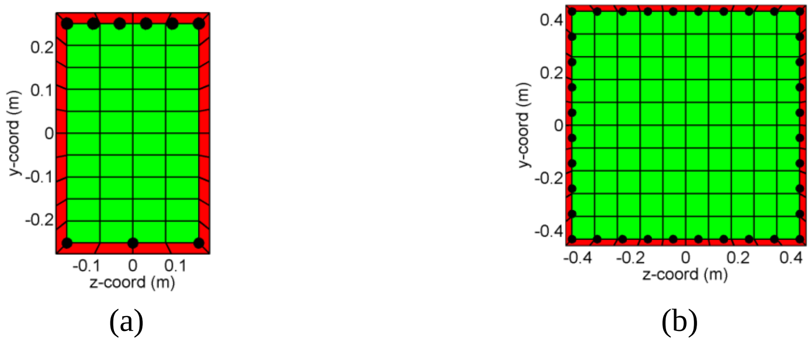

Figure 3.3: Typical section fiber discretization used to model a) a 14x22in beam and b) a 36x36in column, showing the rebars (black), unconfined (red) and confined (green) concrete fibers, (dimensions in m).

3.3.2 Lumped plasticity model

In lumped plasticity models diaphragmatic action can be easily imposed at each floor using rigid kinematic constraints on all nodes, thus enforcing the same lateral displacements. The structural model of the four story moment resisting frame is presented in Figure 3.4, where all nodes in a given floor level are constrained to the leftmost beam-column joint.

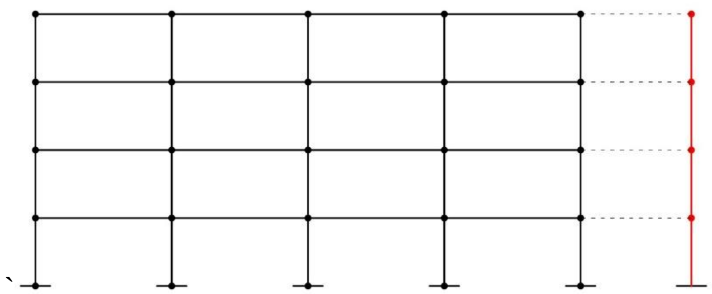

Figure 3.4: Lumped plasticity model of the moment resisting frame showing the beams and columns (black color) and the leaning column (red color). The diaphragmatic action is imposed using rigid kinematic constraints.

In the lumped plasticity approach, beams and columns are modelled using one force based beam-column element per member, having concentrated plastic hinges at the ends. The stiffness properties of the interior elastic part of the member are determined during the calibration procedure of the model. Specifically, an increased moment of inertia is employed for both beams and columns by averaging the initial "uncracked" stiffness and the nominal “cracked” stiffness at yield, as derived from moment-rotation analyses of the fiber sections (rather than prescriptive formulas). For columns with different reinforcement ratio at the two ends, an average value of the moment of inertia of the two end sections is used. This calibration allows for better matching of the period and stiffness between the lumped and distributed plasticity models, helping reconcile their differing predictions at low-to-moderate levels of deformation. Moment-rotation relationships for the plastic hinges are defined based on the generalized backbone curve shown in Figure 3.5 (ASCE SEI-41 (2007)). The plastic hinge behavior can be defined by the five points, named A, B, C, D and E. Details about these points can be found later on.

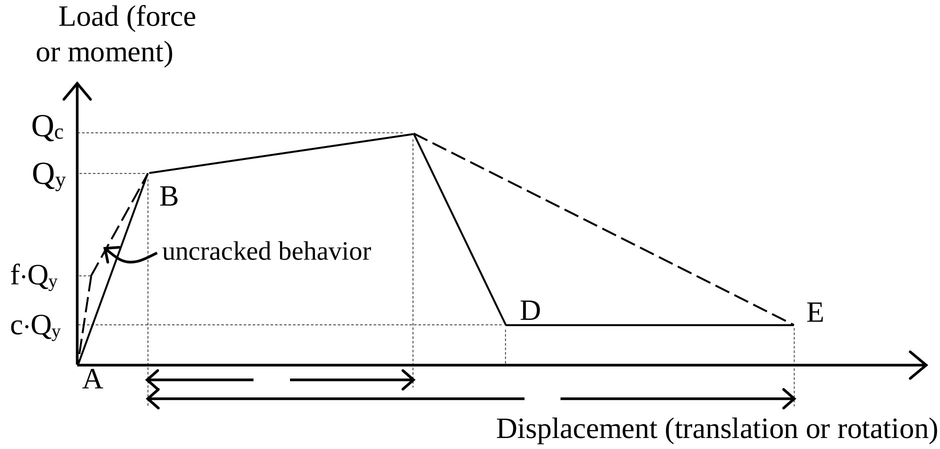

Figure 3.5: Generalized load-displacement (backbone) curve for representing beam and column response (from ASCE SEI-41 (2007)).

Columns

Modelling parameters *a*, *b* and *c* that control capping rotation (point C), ultimate rotation (point E) and residual strength, respectively, are determined according to ASCE SEI-41 (2007). Hardening and capping stiffness are considered to be equal to 0.01 and 0.9 of the initial flexural stiffness, respectively. Yield rotation, θ_y, can be estimated as the product of yield curvature, multiplied by the plastic hinge length which is assumed to be equal to 1.5 times the member depth. The yield curvature is calculated according to Equation 3.1, where $P/A_g f'_c$ is based on the nominal material properties, $\rho_g = A_s/A_g$. A_s is the total area of longitudinal reinforcement and A_g is the gross area of the column section. The yield strain ε_y is given by f'_{ce}/E_s, and d is the depth to the centroid of the extreme layer of the reinforcement.

$$\phi_y = \left(1.8 - 1.3\frac{P}{A_g f'_c} + 9(\rho_g - 0.025)\right)\frac{\varepsilon_y}{d}, \qquad (3.1)$$

The plastic hinge flexural moment at point B is calculated for each section through moment-curvature analysis. Obviously, one may trade simplicity for accuracy by using prescriptive formulas instead. The material properties and section fiber discretization were described earlier in the distributed plasticity approach (Section 3.3.1). The axial loads of the columns used in moment curvature analyses are equal to the ones produced by the gravity loads. In Figure 3.6 the moment-curvature diagram for a first-story external column (above floor section), designed using the Yield Point Spectra (Section 3.4) is presented along with section fiber discretization. M_p is equal to the maximum moment, which is 3281.7 kNm.

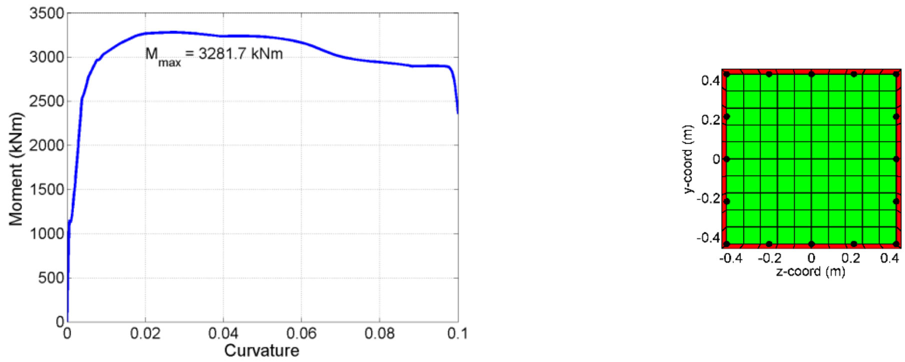

(a) (b)

Figure 3.6: External column of the first story of the moment resisting frame that is designed using method A: a) Moment – curvature diagram and b) section fiber discretization (above cross section).

Table 3.1. Modeling and acceptance criteria for plastic hinges of rectangular cross-section columns, (from ASCE/SEI 41)

Condition			Modeling parameters*			Acceptance Criteria*		
$P/(A_g f_c')$ ‡	$\rho_v = A_v/(b_w s)$	$V/(b_w d f'_c{}^{0.5})$	Plastic rotation angle, radians		Residual strength ratio	Acceptable plastic rotation angle, radians		
						Performance Level		
			a	b	c	IO	LS	CP
Condition i. $V_e/\phi V_n \leq 0.8$ †								
≤ 0.1	≥ 0.006	NA	0.035	0.060	0.2	0.005	0.045	0.060
≥ 0.6	≥ 0.006	NA	0.010	0.010	0.0	0.003	0.009	0.010
≤ 0.1	=0.0036 §	NA	0.030 §	0.044 §	0.2	0.005	0.034	0.044
≥ 0.6	=0.0036 §	NA	0.007 §	0.007 §	0.0	0.002	0.006	0.007
Condition ii. $0.8 \leq V_e/\phi V_n \leq 1.0$ †								
≤ 0.1	≥ 0.006	≤ 3 (0.25)	0.032	0.060	0.2	0.005	0.045	0.060
≤ 0.1	≥ 0.006	≥ 6 (0.50)	0.025	0.060	0.2	0.005	0.045	0.060
≥ 0.6	≥ 0.006	≤ 3 (0.25)	0.010	0.010	0.0	0.003	0.009	0.010
≥ 0.6	≥ 0.006	≥ 6 (0.50)	0.008	0.008	0.0	0.003	0.007	0.008
≤ 0.1	=0.0036 §	≤ 3 (0.25)	0.023 §	0.039 §	0.2	0.005	0.030	0.039
≤ 0.1	=0.0036 §	≥ 6 (0.50)	0.017 §	0.036 §	0.2	0.005	0.028	0.036
≥ 0.6	=0.0036 §	≤ 3 (0.25)	0.007 §	0.007 §	0.0	0.003	0.006	0.007
≥ 0.6	=0.0036 §	≥ 6 (0.50)	0.005 §	0.005 §	0.0	0.002	0.004	0.005

NA = not applicable
f'c in psi (MPa) units
*Values between those listed in the table should be determined by linear interpolation.
†The strength provided by the hoops or spirals (ϕV_s) must be at least three-fourths of the design shear force, V_e
‡Design axial force, *P*, should be based on the maximum expected axial load due to gravity and earthquake loads.
V is the design shear force, V_e, per Section 18.7.6.1.1, ACI 318, unless determined by a nonlinear analysis.
§The transverse reinforcement ratio values in ASCE/SEI 41 were modified per the minimum requirement in ACI 318 and the modeling parameter values were modified by linear interpolation.

Beams

Typically, negative and positive plastic moment strengths differ ($M_p^+ < M_p^-$), thus the plastic hinge moment-curvature relationship used for beams is asymmetrical. Modelling parameters *a*, *b* and *c* that control capping rotation (point C), ultimate rotation (point E) and the residual strength, respectively, are determined according to ASCE SEI 41 (2007), for positive and negative moment separately. Hardening and capping stiffness in both cases are considered to be equal to 0.01 and 0.9 of the initial flexural stiffness, respectively. Yield rotations θ_y^+ and θ_y^- are estimated as the product of yield curvature multiplied by the plastic hinge length (assumed to be equal to twice the member depth). The yield curvature calculated according to Equations 3.2 and 3.3 for positive and negative moment, respectively, where h_b is the overall height of the Tee beam. The effect of reinforcement slip at the anchorage is also taken into account, so the yield rotation is increased by $\theta_{anchslip}$ calculated by Equation 3.4, where d_b is the bar diameter.

$$\phi_y^+ = \frac{1.4\varepsilon_y}{h_b} \text{(flange in compression)}, \tag{3.2}$$

$$\phi_y^- = \frac{1.8\varepsilon_y}{h_b} \text{(flange in tension)}, \tag{3.3}$$

$$\theta_{anchslip} = \begin{cases} \dfrac{\phi_y d_b f_y}{108\sqrt{f_c'}} & \text{psi units} \\ \dfrac{\phi_y d_b f_y}{9\sqrt{f_{ck}}} & \text{MPa units} \end{cases}, \tag{3.4}$$

Moment curvature analysis of beam sections is performed both for positive and for negative moment. The material properties and fiber section discretization used for the analyses were described in the distributed plasticity approach. The axial load imposed in the analyses is equal to zero. In Figures 3.7 (a) and (b) the moment-curvature diagrams for positive and negative moments are shown, along with section fiber discretization, for a first-story beam designed using the Yield Point Spectra (Section 3.4).

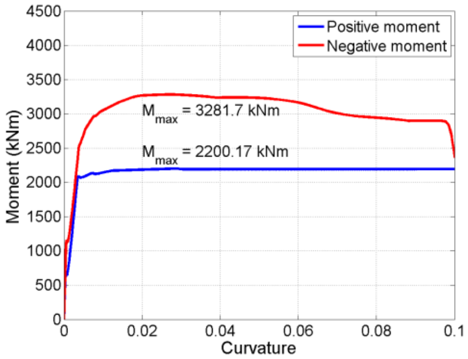

(a)

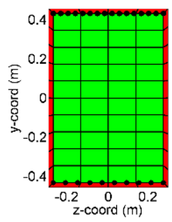

(b)

Figure 3.7: A 24x36in beam at the first story of the four story moment resisting frame designed using the YPS (method A): (a) Moment – curvature diagram and (b) section fiber discretization, dimensions in m.

Table 3.2 Modeling and acceptance criteria for beam plastic hinges (from ASCE/SEI 41 (2007)).

Condition		Modelling parameters*			Acceptance criteria*		
		Plastic rotation angle, radians		Residual strength ratio	Acceptable plastic rotation angle, radians		
					Performance level		
$\frac{\rho - \rho'}{\rho_{bal}}$	$\frac{V}{b_w d \sqrt{f_c'}}$ †‡	a	b	c	IO	LS	CP
≤0.0	≤3 (0.25)	0.025	0.05	0.2	0.010	0.025	0.050
≤0.0	≥6 (0.50)	0.02	0.04	0.2	0.005	0.020	0.040
≥0.5	≤3 (0.25)	0.02	0.03	0.2	0.005	0.020	0.030
≥0.5	≥6 (0.50)	0.015	0.02	0.2	0.005	0.015	0.020

f'_c in psi (MPa) units
*Values between those listed in the table should be determined by linear interpolation.
† The strength provided by the hoops (ϕV_s) must be at least three-fourths of the design shear, V.
‡ V is the design shear unless determined by a nonlinear analysis.

3.4 Four story MRF designed using method A

3.4.1 Initial design

The initial design of the four story moment resisting frame using the Yield Point Spectrum can be found in detail in Aschheim et al. [7] along with an analytical description of this design method. Only some of the key points of the design are listed in this documentation. The design is comparable to that obtained in current codes. The performance objectives that are taken into account are:

- ❖ Ductility limit of 3.6 at the 2% probability of exceedance in 50 years
- ❖ Interstory drift ratio limit of 0.02

The first mode parameters of the four story moment resisting frame are estimated according as Γ_1=1.30 and α_1 =0.88.The yield displacement is estimated as 0.55% of the height of the building, thus Δ_y = 3.56in. Based on the interstory drift ratio limit of 0.02, the peak roof displacement is estimated as $D_{u,drift}$ = 19.1in, so the resulting ductility is μ = 19.1/3.56 = 5.36. The more restrictive ductility limit of 3.6 = min{5.36;3.6} at the 2/50 level is used for the design. The Yield Point Spectrum representation of the 2/50 hazard, that was derived using R-C-T relationships, is presented in Figure 3.8. For a yield displacement of the ESDOF system equal to $\Delta_y^* = \Delta_y/\Gamma_1$ = 2.75 and μ = 3.6, the normalized yield strength coefficient is C_y^* = 0.24, thus $C_y = \alpha_1 \cdot C_y^*$ = 0.211. The design base shear is $V = C_y \cdot W/2$ = 1597kips, and the corresponding period is estimated as 1.08sec, using Equation (3.5).

$$T^* = 2\pi \sqrt{\frac{\Delta_y^*}{C_y^* g}}, \tag{3.5}$$

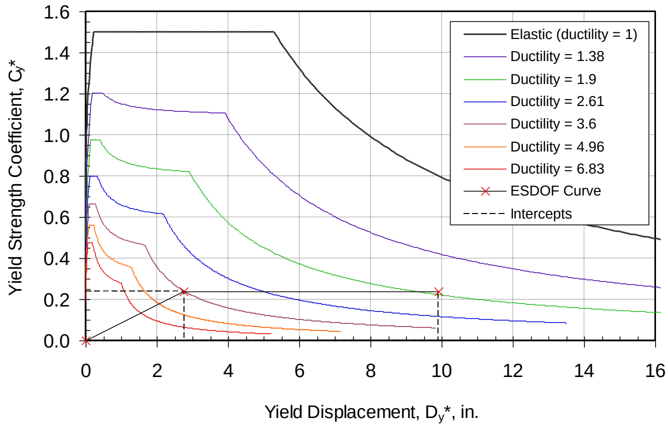

Figure 3.8: Yield point spectra computed for ASCE-7 design spectrum (2%/50). For a system with yield displacement Δ_y^*=2.75in and μ=3.6, the corresponding yield strength coefficient is C_y^*=0.24 – four story moment resisting frame designed using method A (from Aschheim et al., forthcoming [7]).

A first mode proportional lateral force distribution according to ASCE-7 (2005) is used in the design and a weak-beam strong-column mechanism analysis is conducted. Using the Portal Frame Method and assuming that the inflection points for the columns occur at 70% of the height for the first story and at 60% of the height for the others, the moment distribution is calculated for the whole building. The members are designed according to the resulting moment distribution. The expected material properties are used. This quasi static design method does not rely on a non-linear response history analysis to validate performance, just an elastic analysis to validate the estimated parameters of Γ_1, α_1 and T_1. For this reason, beam and column sections are proportioned using the ACI 318 (2008) strength reduction factor, φ. The resulting dimensions and the sizing of the beams and columns are summarized in Tables 3.3, 3.4 and 3.5. The "above floor sections" and "below floor sections" as well as the "external" and "intermmediate" columns of the frame are explained in the Figure 3.9.

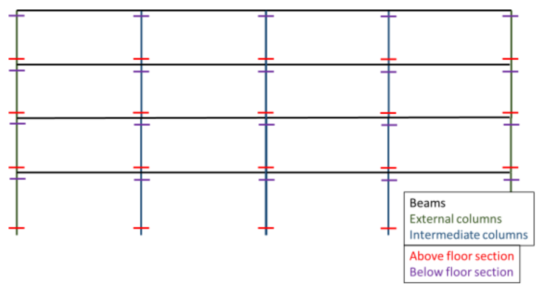

Figure 3.9: Definition of the terms "external" and "intermediate" columns and "above" and "below" floor sections.

Table 3.3: Engineering design for beam sizes and reinforcing – four story moment resisting frame designed using method A (from Aschheim et al., forthcoming [7]).

Story	b_w (in)	h (in)	Top bars	Bottom bars
4	14	22	(6) No 9	(3) No 8
3	18	32	(12) No 9	(7) No 8
2	24	36	(16) No 9	(9) No 8
1	24	36	(16) No 9	(10) No 8

Table 3.4: Design of sections of external and intermediate columns just above floor levels – four story moment resisting frame designed using method A (from Aschheim et al., forthcoming [7]).

Floor level	External columns				Intermediate columns			
	M_c or M_{pc} (k-in)	h (in)	Bars	$A_{s,prov}$ (in^2)	M_c or M_{pc} (k-in)	h (in)	Bars	$A_{s,prov}$ (in^2)
4	NA	NA	NA	NA	NA	NA	NA	NA
3	9602	26	(12) No 10	15.24	15431	26	(20) No 10	25.40
2	15047	30	(16) No 10	20.32	23573	30	(24) No 10	30.48
1	16726	32	(16) No 10	20.32	25089	32	(24) No 10	30.48
footing	23244	36	(16) No 10	20.32	46488	36	(36) No 10	45.72

Table 3.5: Design of sections of external and intermediate columns just below floor levels – four story moment resisting frame designed using method A (from Aschheim et al., forthcoming [7]).

Floor level	External columns				Intermediate columns			
	M_c or M_{pc} (k-in)	h (in)	Bars	$A_{s,prov}$ (in^2)	M_c or M_{pc} (k-in)	h (in)	Bars	$A_{s,prov}$ (in^2)
4	7137	26	(12) No 10	15.24	10705	26	(20) No 10	25.40
3	13260	30	(12) No 10	15.24	18861	30	(20) No 10	25.40
2	18390	32	(16) No 10	20.32	26582	32	(24) No 10	30.48
1	20443	36	(16) No 10	20.32	30665	36	(24) No 10	30.48
footing	NA	NA	NA	NA	NA	NA	NA	NA

The initial design is preliminarily evaluated through an eigenvalue analysis. The modal parameters calculated through SeismoStruct (Seismosoft (2006)) are T_1 = 0.787s, Γ_1 = 1.36 and α_1 = 0.63. A non-linear static analysis using a lateral force vector proportional to the fist mode distribution is carried out using SeismoStruct and the resulting pushover curve is presented in Figure 3.10. The period associated with secant stiffness representative of cracked section behavior is estimated as:

$$T_{\text{eff}} = T_1 \sqrt{\frac{k_{in}}{k_{eff}}} = 1.05\text{sec} \tag{3.6}$$

which compares well to the estimated T* = 1.08sec. The base shear at yield also compares well with the design base shear which equal to 1597kips. The yield displacement of the building is estimated as 4.80in according to Figure 3.10.

Given the reduction in the a_1 and the increase of the yield displacement, a re-design cycle can be obtained using the updated values. The yield displacement of the ESDOF system is $\Delta_y^* = \Delta_y/\Gamma_1$ = 4.8/1.36 = 3.53in. The yield strength coefficient is $C_y=V_y/W$ = 1600/7560=0.211 and $C_y^*=C_y/\alpha_1$=0.336. This point is plotted on the YPS shown in Figure 3.11 and the resulting μ = 2.65, which is lower than the design limit of 3.6. The peak roof displacement is estimated as 4.8·2.65=12.7in. Therefore, the resulting design complies with the performance objectives that were taken into account.

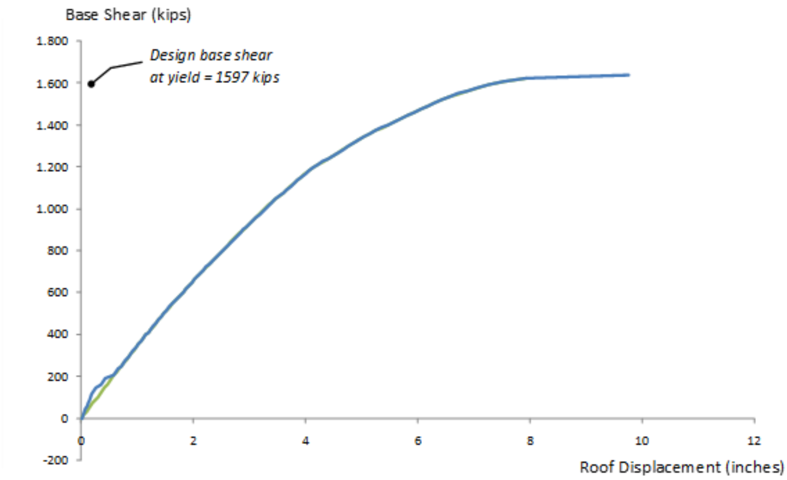

Figure 3.10: Capacity curve observed in a first-mode pushover analysis for the four story moment resisting frame designed using method A (from Aschheim et al., forthcoming [7]).

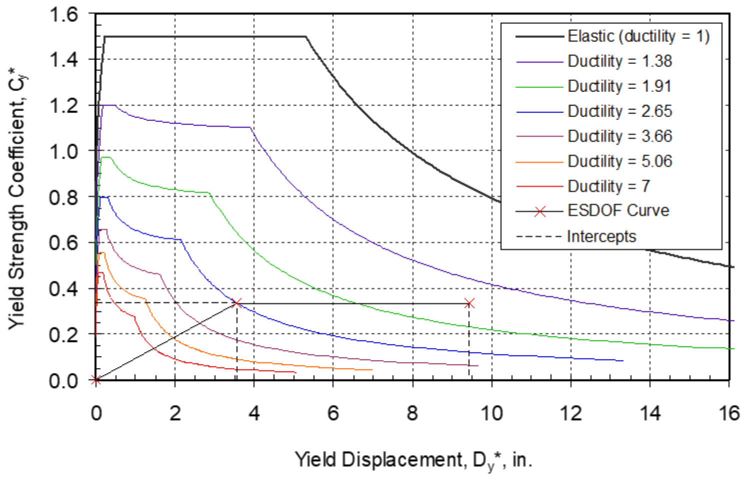

Figure 3.11: Yield point spectra used for evaluation of the first design realization of the four story moment resisting frame building designed using method A. For a system with yield displacement Δ_y^*=3.53in and μ=2.65, the corresponding yield strength coefficient is C_y^*=0.336 (from Aschheim et al., forthcoming [7]).

3.4.2 Non-linear modeling and acceptance criteria

Although it is not explicitly required by the methodological layout of the quasi-static approach used in the design of the moment frame, we shall nevertheless perform nonlinear response history analysis to evaluate the performance of the moment-frame and provide a basis for comparison with the other two approaches to follow. In Tables 3.6 and 3.28 the modelling parameters for columns and beams, respectively, are summarized. In Tables 3.27 and 3.28 the acceptance criteria for columns and beams are also presented.

Table 3.6: Plastic hinge modelling parameters for columns – four story moment resisting frame designed using method A.

Story	External columns				Internal columns			
	M_p (kNm)	a	b	c	M_p (kNm)	a	b	c
4	1562.7	0.030	0.044	0.20	2377.9	0.030	0.044	0.20
3	1955.4 (top) 2433.0 (bot)				2916.8 (top) 3415.5 (bot)			
2	2731.8				3785.3			
1	3281.7				4468.6			

Table 3.7: Plastic hinge modelling parameters for beams – four story moment resisting frame designed using method A.

Story	Negative moment				Positive moment			
	M_y^- (kNm)	a	b	c	M_y^+ (kNm)	a	b	c
4	959.2	0.0210	0.0338	0.20	390.5	0.025	0.050	0.20
3	2836.8	0.0211	0.0346		1359.1			
2	4337.7	0.0215	0.0359		1981.4			
1	4364.7	0.0218	0.0371		2200.2			

Table 3.8: Maximum column plastic rotation for all stories, for IO, LS and CP – four story moment resisting frame designed using method A.

Story	Positive rotation (rad)		
	IO	LS	CP
$\theta_{p,max}$ (rad)	0.005	0.034	0.044

Table 3.9: Maximum beam plastic rotation for IO, LS and CP – four story moment resisting frame designed using method A.

Story	Positive rotation (rad)			Negative rotation (rad)		
	IO	LS	CP	IO	LS	CP
4	0.010	0.025	0.050	0.0060	0.0210	0.0338
3				0.0061	0.0211	0.0346
2				0.0065	0.0215	0.0359
1				0.0068	0.0218	0.0371

Going back to the discussion of Section 3.3, we have two models to contend with, the distributed plasticity model and the lumped plasticity model. The fundamental period of the latter, after the calibration step of Section 3.3.2 is T_1=1.04sec. Note that this is obviously larger than the initial period of the distributed plasticity model of T_1 = 0.98sec. Our aim is not to perfectly capture this, as it only persists for minor deformations, but instead to be able to capture the effective stiffness (and secant period) that characterizes the majority of the pre-yield segment. The static pushover capacity curve resulting from a first-mode-proportional lateral load pattern is presented in Figure 3.12 for both lumped and distributed plasticity models. The effect of the calibration of member elastic stiffness is obvious in the matching of the pre-yield segments of the two curves. The yield displacement is calculated according to Figure 3.13. Assuming a bilinear approximation of the capacity curve having the same effective stiffness as the lumped plasticity model yields Δ_y = 4.05in. The computed parameters of C_y, Δ_y and T_1 compare well to the estimated ones.

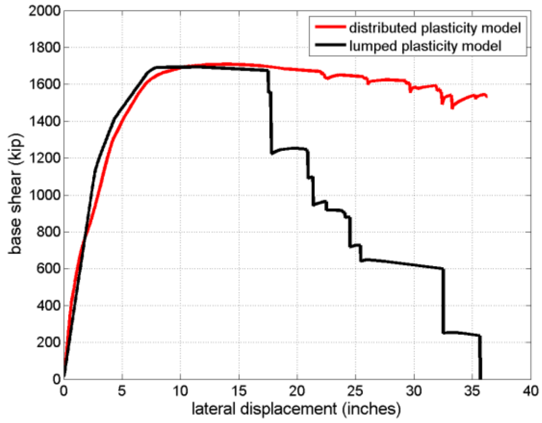

Figure 3.12: Static pushover curves of the distributed (black color) and the lumped plasticity (red color) model for the four story moment resisting frame designed using method A. The effect of the calibration is obvious in the matching pre-yielding segment of the two models.

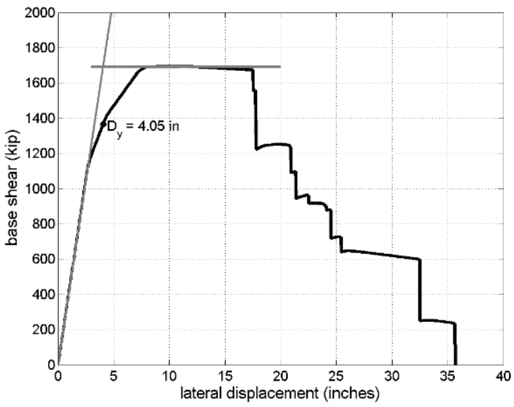

Computed performance:

W = 7560 kips

V_{max} = 1693 kips

$C_y = V_{max}/W = 1693/7560 = 0.224$

Δ_y = 4.05in

T_1 = 1.04sec

Figure 3.13: Calculation of the yield displacement Δ_y of the four story moment resisting frame designed using method A.

3.4.3 Performance evaluation of the initial design by nonlinear dynamic analysis

The acceptability of peak dynamic interstory drifts, plastic hinge rotations and ductility limit of 3.6 is assessed using the three different methods introduced in Section 2: (i) by convolving the seismic hazard curve with the fragility curve (IDA), and by (ii) single and (iii) double stripe analysis (at 2/50 level for the ductility limit and at 10/50 level for the others). For each performance objective, the results are summarized in Tables 3.10 and 3.11. For IDA, the first two values of each PO correspond to the estimated and allowable MAF, and for the stripe analysis they correspond to factored demand and factored capacity, respectively.

Table 3.10: Verification of the maximum interstory drift and beam plastic rotations for the four story moment resisting frame designed using method A.

	IDR			beam plastic rotation		
	IDA	Single	Double	IDA	Single	Double
	(yrs^{-1})	–	–	(yrs^{-1})	(rad)	(rad)
Demand	0.0019	0.0182	0.0178	0.0020	0.9630	0.9413
Capacity	0.0021	0.0190	0.0193	0.0021	0.9530	0.9632
Check	✓	✓	✓	✓	✗	✓
Confidence	50 %			60 %		

Table3.11: Verification of column plastic rotations and global ductility for the four story moment resisting frame designed using method A.

	column plastic rotation			global ductility		
	IDA	Single	Double	IDA	Single	Double
	(yrs^{-1})	(rad)	(rad)	(yrs^{-1})	–	–
Demand	0.0005	0.2548	0.2405	0.0009	0.0236	0.0228
Capacity	0.0021	0.9515	0.9885	0.0004	0.0210	0.0216
Check	✓	✓	✓	✗	✗	✗
Confidence	60 %			50 %		

IDA is first employed to estimate the MAF of exceeding the maximum interstory drift ratio limit of θ_{max} = 2%. The fragility curve is calculated based on the $S_a(T_1$,5%) values that correspond to the 2% drift limit (Figure 3.15). The median value of the lognormal distribution is equal to 0.63g and the standard deviation is 26%. The hazard curve is presented in Figure 3.14, having been scaled to the design spectrum to offer a fair assessment of quasi static approach used in the design. The estimated mean annual frequency of exceeding the maximum interstory drift limit of 2%, at 50% confidence, equals 0.00190, which is lower than the corresponding code value of 0.0021 (10% probability of exceeding PO in 50 years). This means that the performance objective is met.

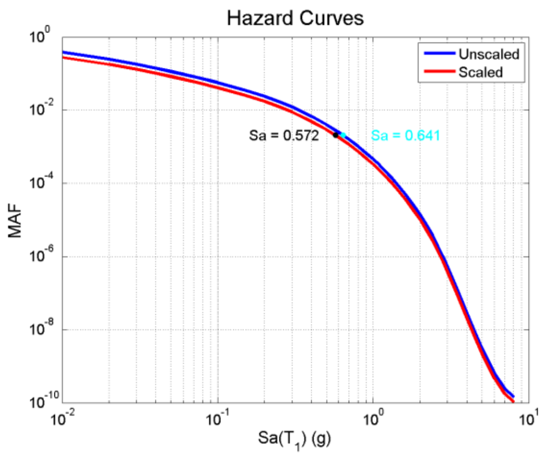

Figure 3.14: Seismic site hazard curve scaled to match the 10% in 50 years value of $S_a(T_1)$ as provided by the design spectrum – four story moment resisting frame designed using method A.

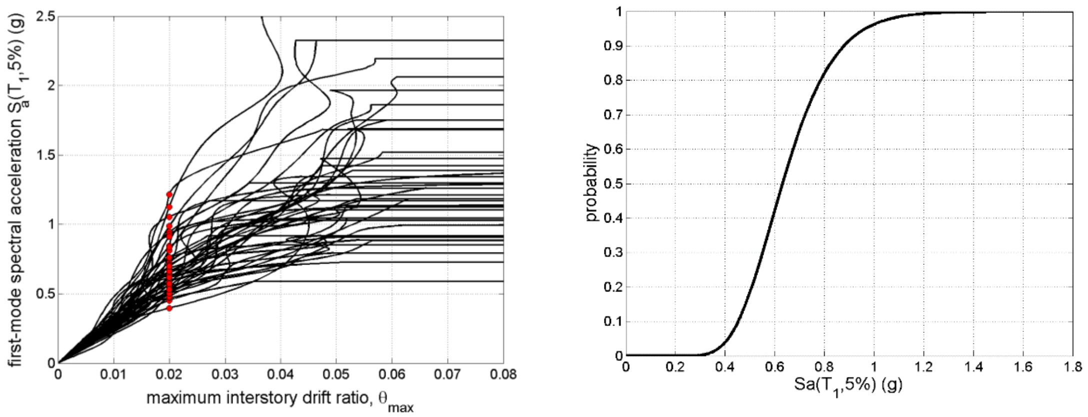

(a) (b)

Figure 3.15: IDA approach for estimating the mean annual frequency of exceeding 2% maximum interstory drift ratio: (a) the $S_a(T_1,5\%)$ values calculated for 2% maximum interstory drift ratio limit, θ_{max}, and (b) corresponding fragility curve (four story moment resisting frame designed using method A).

For the stripe analysis, factored demand (FD) is calculated and compared to factored capacity (FC). The interstory drift ratio values are calculated for 17 records for S_a^{design}=0.57g, as shown in Figure 3.16 (a). The points of the hazard curve needed to estimate the slope k are presented in Figure 3.16 (b). FD and FC at 50% confidence are estimated as:

$FD_{RPo}=\theta_{max,50}\ \exp(0.5\cdot k\cdot \beta_{\theta max|Sa}{}^2/b) = 0.0166\ \exp(0.5\cdot 2.43\cdot 0.28^2/1) = 0.0182$
$FC_R=\theta_{max,C}\ \exp(-0.5\cdot k\cdot \beta_{CR}{}^2/b) = 0.02\ \exp(-0.5\cdot 2.43\cdot 0.20^2/1) = 0.0190$

Since the factored capacity of 0.0190 is greater than the factored demand of 0.0182 the result is satisfactory at the 50% confidence level.

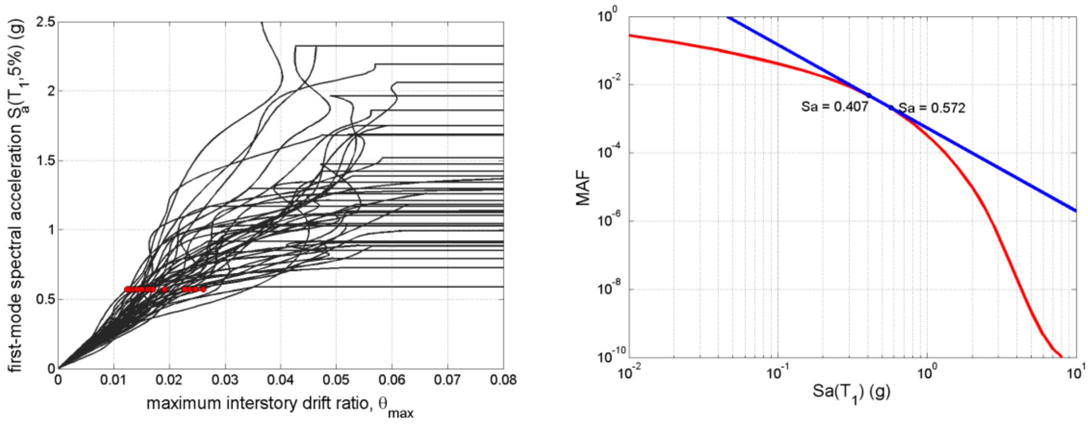

(a) (b)

Figure 3.16: Single stripe analysis method for estimating FD_{RPo} and FC_R for 2% maximum interstory drift ratio: (a) maximum interstory drifts calculated for S_a^{design}, and (b) the local fit of the seismic hazard curve – four story moment resisting frame designed using method A.

For the double stripe analysis, the interstory drift values are calculated for 17 records at S_a^{design}=0.57g (red points) and at $1.1S_a^{design}$=0.63g (green points), as shown in Figure 3.17

(a). The points of the hazard curve needed to estimate the slope k are presented in Figure 3.17 (b). FD and FC at 50% confidence are estimated as:

$$FD_{RPo}=\theta_{max,50}\ \exp(0.5\cdot k\cdot \beta_{\theta max|Sa}{}^{2}/b) = 0.0166\ \exp(0.5\cdot 2.63\cdot 0.28^{2}/1.47) = 0.0178$$
$$FC_{R}=\theta_{max,\mathrm{C}}\ \exp(-0.5\cdot k\cdot \beta_{CR}{}^{2}/b) = 0.02\ \exp(-0.5\cdot 2.63\cdot 0.20^{2}/1.47) = 0.0193$$

Since the factored capacity of 0.0193 is greater than the factored demand of 0.0178 the result is satisfactory at the 50% confidence level.

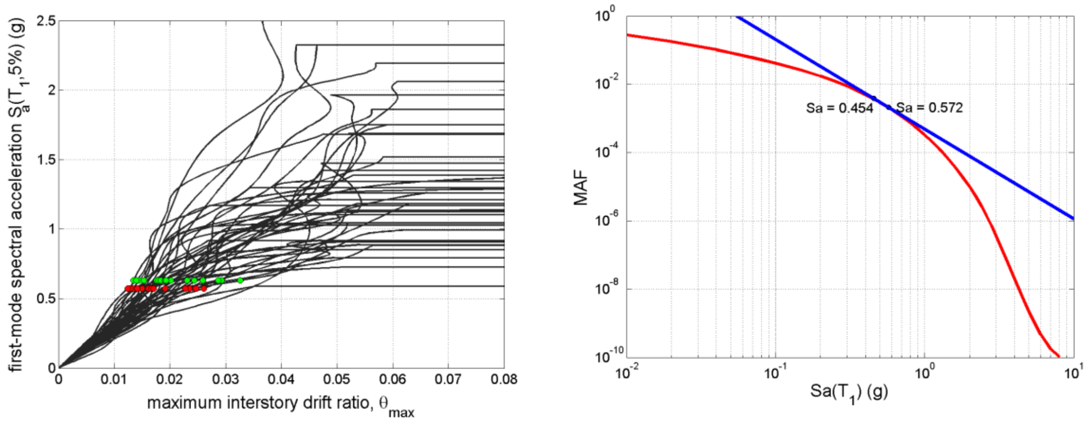

(a) (b)

Figure 3.17: Double stripe analysis method for estimating FD_{RPo} and FC_{R} for 2% maximum interstory drift ratio: (a) maximum interstory drifts calculated for S_a^{design} (red points) and for $1.1Sa^{design}$ (green points), and (b) the local fit of the seismic hazard curve – four story moment resisting frame designed using method A.

Due to having different beam plastic rotation capacities, the maximum demand capacity ratio, DCR=$(\theta_{demand}{}^{pl}/\ \theta_{capacity}{}^{pl})_{\max}$ is employed to facilitate calculation, where $\theta_{capacity}{}^{pl}$ is presented in Table 3.9. The MAF of exceeding DCR=1.0 is estimated using the fragility curve that is calculated based on $S_a(T_1,5\%)$ values that correspond to the DCR limit, according to the IDA results (Figure 3.36 (a)). The median value of the lognormal distribution equals to 0.65g and the standard deviation to 26%. The estimated mean annual frequency of exceeding DCR=1.0 at 60% confidence equals 0.0020, which is lower than the corresponding code value of 0.0021 (10% probability of exceeding PO in 50 years), thus the performance objective is met.

For the single stripe analysis, factored demand (FD) is calculated and compared to the factored capacity (FC). Maximum demand capacity ratio for beams is calculated for 17 records at S_a^{design}=0.57g, as shown in Figure 3.19 (a). Note therein that interpolating the IDA curves for near-zero or zero values of the plastic rotation causes a minor overshoot and the appearance of seemingly negative rotations, without any consequence for the much higher demands that we are interested in. The points of the hazard curve that define the slope k are presented in Figure 3.19 (b). FD and FC are estimated as:

$$FD_{RPo}=DCR_{max,50}\ \exp(0.5\cdot k\cdot \beta_{\theta max|Sa}{}^{2}/b) = 0.82\ \exp(0.5\cdot 2.41\cdot 0.29^{2}/1.0) = 0.9154$$
$$FC_{R}=DCR_{max,\mathrm{C}}\ \exp(-0.5\cdot k\cdot \beta_{CR}{}^{2}/b) = 1.0\ \exp(-0.5\cdot 2.41\cdot 0.20^{2}/1.0) = 0.9530$$

For a confidence level of 60%, the lognormal standard variate is K_x=0.253 and the evaluation inequality becomes:

$FC_R > FD_{RPo} \exp(K_x \cdot \beta_{TU}) = 0.9154 \exp(0.253 \cdot 0.20) = 0.9630$

Since the factored capacity of 0.9530 is lower than the factored demand of 0.9630 the result is marginally unsatisfactory at the 60% confidence level. This is in general the price we pay for using a simpler (and generally more conservative) approach than the full IDA. Seeing that the difference between factored demand and factored capacity is small, one may opt to further test it by employing a second stripe (or IDA), or accept the result and seek a redesign.

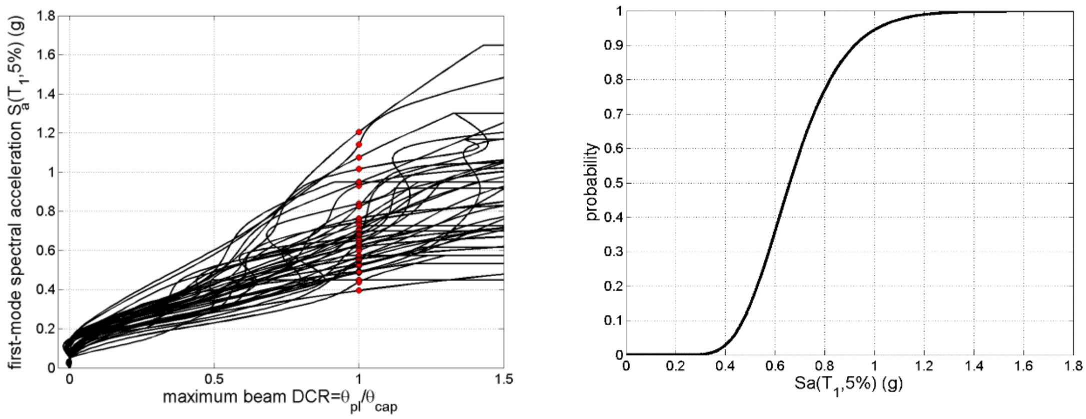

(a) (b)

Figure 3.18: Analytical approach for estimating mean annual frequency of exceeding demand capacity ratio limit of 1.0 for beams: (a) the $S_a(T_1,5\%)$ values calculated for DCR=1, and (b) corresponding fragility curve – four story moment resisting frame designed using method A.

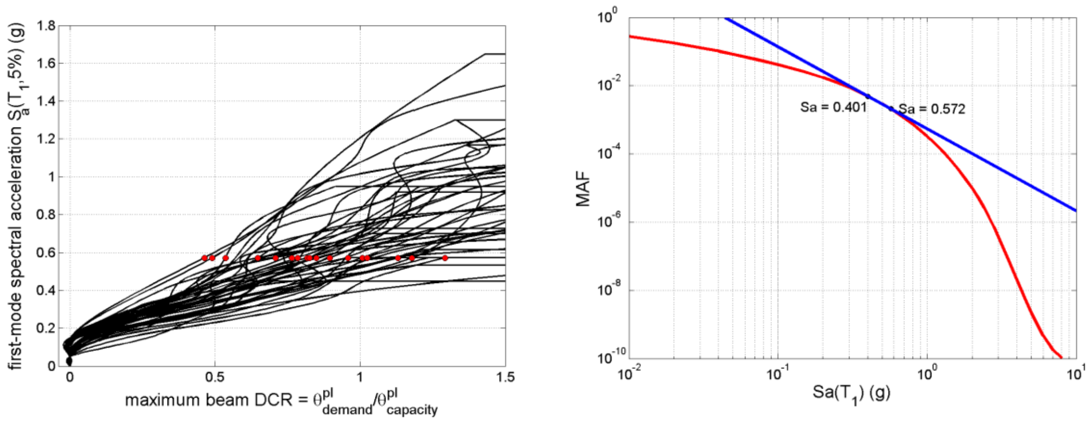

(a) (b)

Figure 3.19: Single stripe analysis method for estimating FD_{RPo} and FC_R for DCR=1 of beams: (a) maximum beam DCR calculated for S_a^{design}, and (b) the local fit of the seismic hazard curve – four story moment resisting frame designed using method A.

For the double stripe analysis, the DCR values are calculated for 17 records for S_a^{design}=0.57g (red points) and for $1.1S_a^{design}$=0.63g (green points). The points of the hazard curve that define the slope k are presented in Figures 3.20 (a) and (b), respectively. FD and FC are estimated as:

$FD_{RPo}=DCR_{max,50} \exp(0.5 \cdot k \cdot \beta_{\theta max|Sa}{}^2/b) = 0.82 \exp(0.5 \cdot 2.59 \cdot 0.29^2/1.38) = 0.8948$
$FC_R=DCR_{max,\mathrm{C}} \exp(-0.5 \cdot k \cdot \beta_{CR}{}^2/b) = 1.0 \exp(-0.5 \cdot 2.59 \cdot 0.20^2/1.38) = 0.9632$

For a confidence level of 60%, the lognormal standard variate is K_x=0.253 and the evaluation inequality becomes:

$FC_R > FD_{RPo}\ \exp(K_x \cdot \beta_{TU}) = 0.8948\ \exp(0.253 \cdot 0.20) = 0.9413$

Since the factored capacity of 0.9632 is greater than the factored demand of 0.9413 the result is now satisfactory at 60% confidence level. The improved accuracy offered by the double stripe has allowed us to avoid the need for a redesign in this case. An IDA would be even more accurate, although this does not necessarily mean that it would necessarily increase the margin between demand and capacity, as Table 3.10 attests.

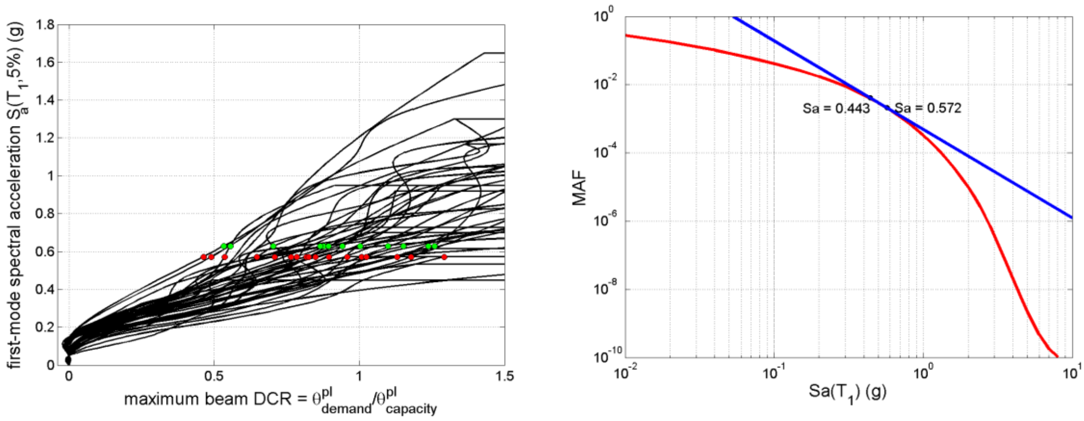

(a) (b)

Figure 3.20: Double stripe analysis method for estimating FD_{RPo} and FC_R for DCR=1 of beams: (a) maximum beam DCR calculated for S_a^{design} (red points) and for $1.1S_a^{design}$ (green points), and (b) the local fit of the seismic hazard curve – four story moment resisting frame designed using method A.

IDA curves in terms of the first mode spectral acceleration $S_a(T_1,5\%)$ and maximum demand capacity ratio, DCR=$(\theta_{demand}^{pl}/\ \theta_{capacity}^{pl})_{\max}$ for columns are presented in Figure 3.21 (a). The median value of the fragility curve equals to 1.02g and the standard deviation to 26%. The estimated mean annual frequency of exceeding DCR=1.0 at 60% confidence equals to 0.00053, which is lower than the corresponding code value of 0.0021 (10% probability of exceeding PO in 50 years). This means that the performance objective is met.

For the single stripe analysis, the maximum demand capacity ratio for columns is calculated for 17 records for S_a^{design}=0.57g, as shown in Figure 3.22 (a). The points of the hazard curve that define the slope k are presented in Figures 3.22 (b). FD and FC are estimated as:

$FD_{RPo}=DCR_{max,50}\ \exp(0.5 \cdot k \cdot \beta_{\theta max|Sa}^2/b) = 0.22\ \exp(0.5 \cdot 2.48 \cdot 0.25^2/1.0) = 0.2422$
$FC_R=DCR_{max,C}\ \exp(-0.5 \cdot k \cdot \beta_{CR}^2/b) = 1.0\ \exp(-0.5 \cdot 2.48 \cdot 0.20^2/1.0) = 0.9515$

For a confidence level of 60%, the lognormal standard variate is K_x=0.253 and the evaluation inequality becomes:

$FC_R > FD_{RPo}\ \exp(K_x \cdot \beta_{TU}) = 0.2422\ \exp(0.253 \cdot 0.20) = 0.2548$

Since the factored capacity of 0.9515 is greater than the factored demand of 0.2548 the result is satisfactory at 60% confidence level.

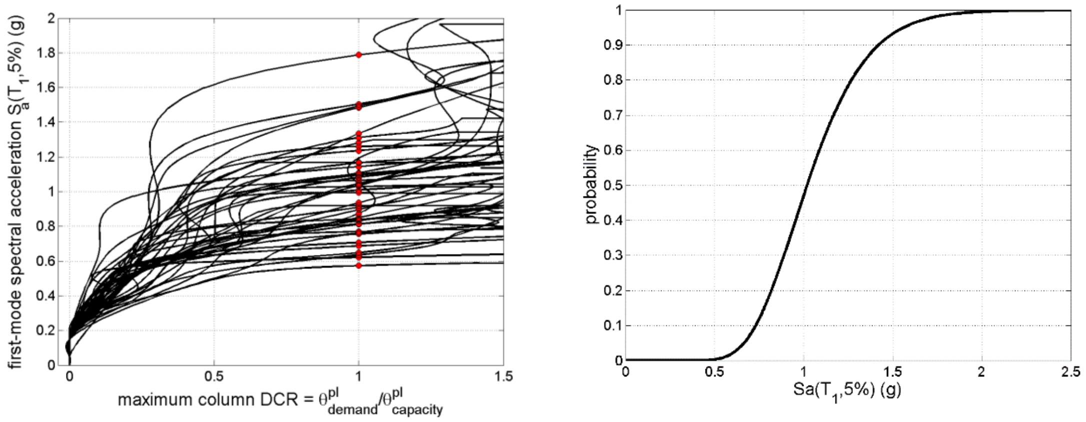

(a) (b)

Figure 3.21: Analytical approach for estimating mean annual frequency of exceeding demand capacity ratio limit of 1.0 for columns: (a) the $S_a(T_1,5\%)$ values calculated for DCR=1, and (b) corresponding fragility curve – four story moment resisting frame designed using method A.

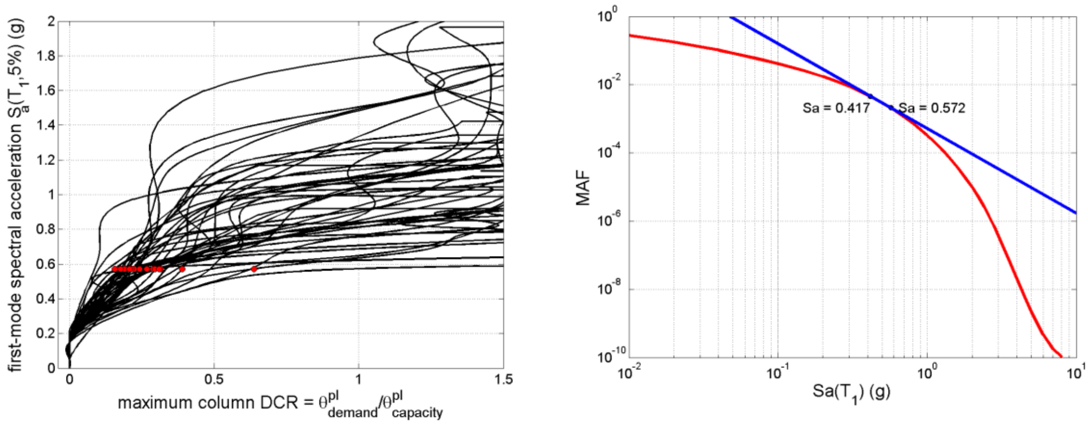

(a) (b)

Figure 3.22: Single stripe analysis method for estimating FD_{RPo} and FC_R for DCR=1 of columns: (a) maximum column DCR calculated for S_a^{design}, and (b) the local fit of the seismic hazard curve – four story moment resisting frame designed using method A.

For the double stripe analysis, the DCR values are calculated for 17 records for S_a^{design}=0.57g (red points) and for $1.1S_a^{design}$=0.63g (green points) (Figure 3.23 (a)). The points of the hazard curve needed to estimate the slope k are presented in Figure 3.23 (b). FD and FC are estimated as:

$FD_{RPo}=DCR_{max,50}\ \exp(0.5\cdot k\cdot \beta_{\theta max|Sa}{}^2/b) = 0.225\ \exp(0.5\cdot 2.71\cdot 0.25^2/4.7) = 0.2286$
$FC_R=DCR_{max,C}\ \exp(-0.5\cdot k\cdot \beta_{CR}{}^2/b) = 1.0\ \exp(-0.5\cdot 2.71\cdot 0.20^2/4.7) = 0.9885$

Note the rather large value of b = 4.7 estimated from the two stripes and employed above. This is in general an indication that this verification is performed relatively close to the onset of global collapse, as also observed by the proximity of the second stripe to the flatlines in Figure 3.23 (a). In such cases, some care should be exercised to make sure that no more than 16% of the runs are non-convergent (i.e., indicative of global collapse in a good model), otherwise the approximation underlying the Factored Demand and Factored Capacity approach will fail. In such cases IDA is the recommended approach.

For a confidence level of 60%, the lognormal standard variate is K_x=0.253 and the evaluation inequality becomes:

$FC_R > FD_{RPo} \exp(K_x \cdot \beta_{TU}) = 0.2286 \exp(0.253 \cdot 0.20) = 0.2405$

Since the factored capacity of 0.9885 is greater than the factored demand of 0.2405 the result is satisfactory at 60% confidence level.

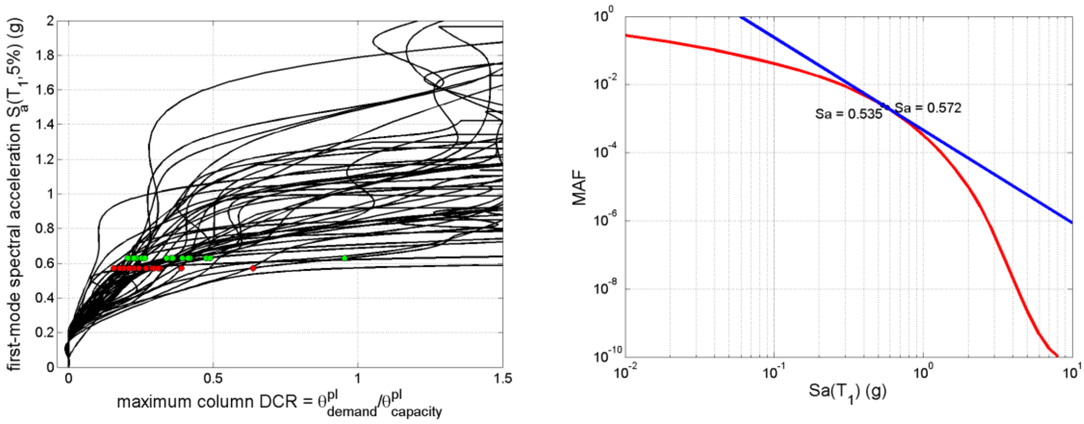

(a) (b)

Figure 3.23: Double stripe analysis method for estimating FD_{RPo} and FC_R for DCR=1 of columns: (a) maximum column DCR calculated for S_a^{design} (red points) and for $1.1S_a^{design}$ (green points), and (b) the local fit of the seismic hazard curve – four story moment resisting frame designed using method A.

The acceptability of the ductility limit of 3.6 is assessed at the 2/50 level. This ductility limit is equivalent to a roof drift ratio capacity of $\theta_{roof} = 3.6\ \Delta_y/H_{tot} = 3.6 \cdot 4.05\text{in} / 648\text{in} = 0.0225$. IDA curves in terms of the first mode spectral acceleration $S_a(T_1,5\%)$ and roof drift ratio, θ_{roof} are presented in Figure 3.24 (a). The MAF of exceeding $\theta_{roof} = 0.0225$ is estimated using the fragility curve calculated based on the $S_a(T_1,5\%)$ values that correspond to the roof drift limit (red points in Figure 3.24 (a)), and is presented in Figure 3.24 (b). The median value of the lognormal distribution equals 0.84g and the standard deviation is 27%. The estimated mean annual frequency of exceeding θ_{roof} =0.0225 at 50% confidence equals 0.00087, which is higher than the corresponding value of 0.000404 (2% in 50 years). This means that the performance objective is not met. Note, though that the difference in MAF terms may seem large but it translates to a much smaller difference in terms of $Sa(T_1)$ due to their exponential relationship.

For the single stripe analysis, the maximum roof drift ratio is calculated for 17 records at acceleration $S_a^{2\%/50}$=0.95g, as shown in Figure 3.25 (a). This is the acceleration value that corresponds to MAF=0.000404 and is calculated via the hazard curve. The points of the hazard curve defining the slope k are presented in Figure 3.25 (b). FD and FC are estimated as:

$FD_{RPo}=\theta_{roof,50} \exp(0.5 \cdot k \cdot \beta_{\theta max|Sa}{}^2/b) = 0.0216 \exp(0.5 \cdot 3.35 \cdot 0.23^2/1.0) = 0.02364$
$FC_R=\theta_{roof,C} \exp(-0.5 \cdot k \cdot \beta_{CR}{}^2/b) = 0.0225 \exp(-0.5 \cdot 3.35 \cdot 0.20^2/1.0) = 0.02104$

Since the factored capacity of 0.02104 is lower than the factored demand of 0.02364 the result is not satisfactory at the 50% confidence level.

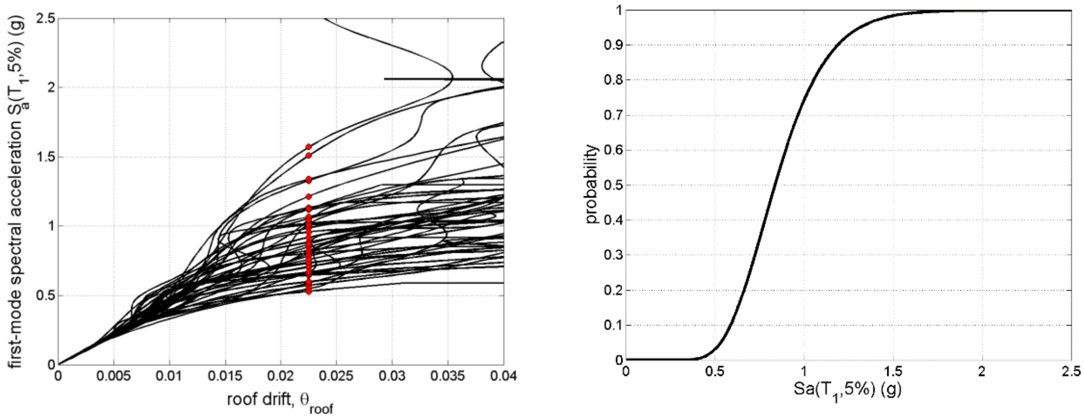

(a) (b)

Figure 3.24: IDA approach for estimating mean annual frequency of exceeding ductility limit of 3.6: (a) the $S_a(T_1,5\%)$ values calculated for $\theta_{roof}=0.0226$, and (b) corresponding fragility curve – four story moment resisting frame designed using method A.

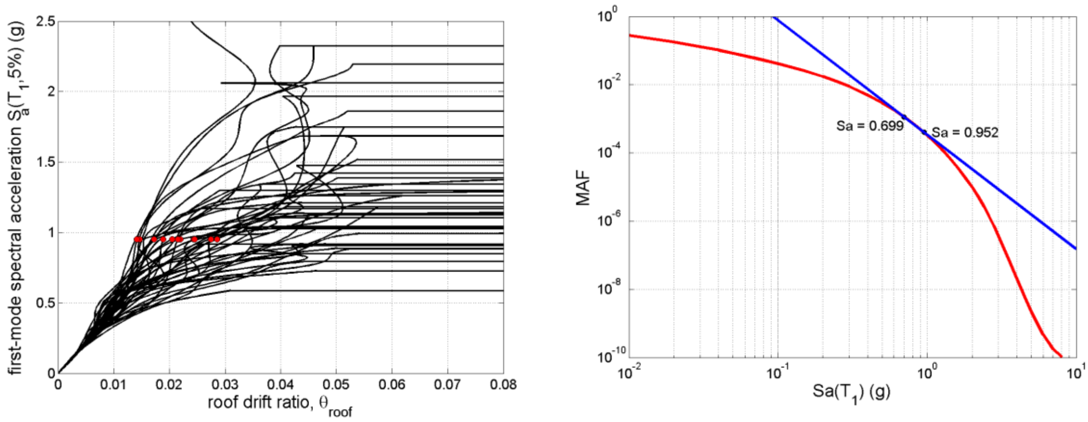

(a) (b)

Figure 3.25: Single stripe analysis method for estimating FD_{RPo} and FC_R for ductility limit of 3.6: (a) roof drift ratio calculated for $S_a^{2\%/50}$, and (b) the local fit of the seismic hazard curve – four story moment resisting frame designed using method A.

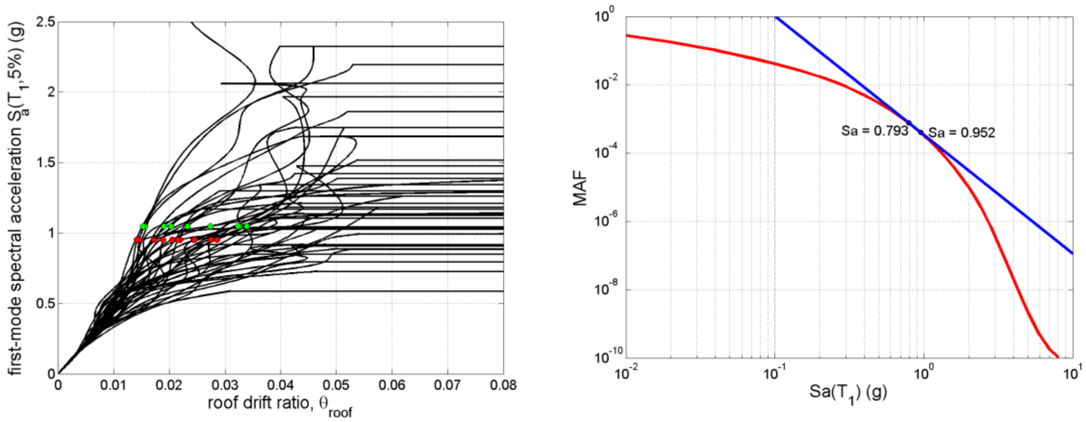

(a) (b)

Figure 3.26: Double stripe analysis method for estimating FD_{RPo} and FC_R for ductility limit of 3.6: (a) roof drift ratio calculated for $S_a^{2\%/50}$ (red points) and for $1.1S_a^{2\%/50}$ (green points), and (b) the local fit of the seismic hazard curve – four story moment resisting frame designed using method A.

For the double stripe analysis, the θ_{roof} values are calculated for 17 records for $S_a^{2\%/50}$=0.95g (red points) and for $1.1S_a^{2\%/50}$=1.05g (green points) (Figure 3.26 (a)). The points of the hazard curve that define the slope k are presented in Figure 3.26 (b). FD and FC at 50% confidence (K_x=0) are estimated as:

$FD_{RPo}=\theta_{roof,50}\ \exp(0.5\cdot k\cdot\beta_{\theta max|Sa}{}^2/b) = 0.0216\ \exp(0.5\cdot 3.48\cdot 0.23^2/1.68) = 0.0228$
$FC_R=\theta_{roof,C}\ \exp(-0.5\cdot k\cdot\beta_{CR}{}^2/b) = 0.0225\ \exp(-0.5\cdot 3.48\cdot 0.20^2/1.68) = 0.0216$

Since the factored capacity of 0.0216 is lower than the factored demand of 0.0228 the result is not satisfactory at 50% confidence level.

3.5 Four story MRF designed using method B

3.5.1 Initial design

The design method of the four story moment resisting frame using the YFS and an estimation of the slope of the hazard curve within the range of interest (design method B) can be found in detail in Aschheim et al. [7] along with an analytical description of this design method. Only some of the key points of the design are listed in this documentation. The design aims to limit the mean annual frequency of exceeding interstory drift ratio of 2% to $2.11\cdot 10^{-3}$ (10% probability of exceedance in 50years). A first mode nonlinear static pushover analysis is used to evaluate the initial design and a single stipe analysis should be used to evaluate the acceptability of all performance objectives. Nevertheless, the results of all the three methods for the performance assessment of a structure that are presented in Section 2 are shown below.

As mentioned in the introduction, the first mode parameters of the building as well as the yield displacement must be estimated. As starting parameters for this design approach the ones calculated through the eigenvalue and the pushover analyses of the previous example are used, thus Δ_y =4.8in, Γ_1 =1.36 and α_1=0.63. The yield displacement of the ESDOF system is $\Delta_y^*=\Delta_y/\Gamma_1$=4.8/1.36=3.53in. The roof displacement is estimated as D_u =8.94 in, so the resulting ductility is μ=8.94/4.8=1.86. The mean annual frequency of exceeding this ductility limit should be lower than the $2.11\cdot 10^{-3}$. Using the Yield Frequency Spectra at 50% confidence which is calculated using an estimation of the slope of the seismic hazard curve (and can be found in detail in Aschheim et al., [7]) shown in Figure 3.27, the required normalized yield strength coefficient is estimated as C_y^*=0.463. This means that $C_y=C_y^*\cdot\alpha_1$=0.463·0.63=0.275 and the design base shear at yield is $V=C_y\cdot W/2$=2079kips. The corresponding period is calculated using the Equation 3.5 as T^* = 0.91sec.

The Equivalent Lateral Force Method of ASCE-7 is used in the design, thus the lateral forces are associated with a base shear at yield equal to 1941kips. Using the Portal Frame Method and assuming that the inflection points for the columns occur at 60% of the height for the first story and at 50% of the height for the others, the moment distribution is calculated for the whole building. A weak-beam strong-column mechanism is used in the design. A non-linear response history analysis will be used to assess the initial design, thus the strength reduction factors are set equal to 1.0. More details about the design procedure can be found in Aschheim et al., [7].

The resulting dimensions and the sizing of the beams and columns is summarized in Tables 3.3, 3.4 and 3.5. The “above floor sections” and “below floor sections” as well as the “external” and “intermmediate” columns of the frame are explained in Figure 3.9.

The initial design is preliminarily evaluated through an eigenvalue analysis. The modal parameters calculated through SeismoStruct are T_1 = 0.73s, Γ_1 = 1.35 and α_1 = 0.63. A nonlinear static analysis using a lateral force vector proportional to the fist mode distribution is carried out using SeismoStruct and the resulting pushover curve is presented in Figure 3.10. The base shear at yield is 1870kips which is lower than the design base shear of 2079kips. This difference appears because of the approximate formula of the ASCE-7 that is used to calculate the design base shear using the resultant of the force distribution. The period associated with secant stiffness representative of cracked section behavior is estimated as 1.01sec which is a little higher than the estimated $T^* = 0.91$sec.

Table 3.12: Engineering design for beam sizes and reinforcing – four story moment resisting frame designed using method B (from Aschheim et al., forthcoming [7]).

Story	b_w (in)	h (in)	Top bars	Bottom bars
4	14	24	(7) No 9	(3) No 9
3	20	32	(14) No 9	(6) No 9
2	22	36	(18) No 9	(8) No 9
1	22	38	(18) No 9	(9) No 9

Table 3.13: Design of sections of external and intermediate columns just above floor levels – four story moment resisting frame designed using method B (from Aschheim et al., forthcoming [7]).

Floor level	External columns				Intermediate columns			
	M_c or M_{pc} (k-in)	h (in)	Bars	$A_{s,prov}$ (in^2)	M_c or M_{pc} (k-in)	h (in)	Bars	$A_{s,prov}$ (in^2)
4	NA	NA	NA	NA	NA	NA	NA	NA
3	12672	28	(12) No 10	15.24	19008	28	(20) No 10	25.40
2	21792	32	(20) No 10	25.40	32688	32	(28) No 10	35.56
1	27571	36	(20) No 10	25.40	41357	36	(32) No 10	40.64
footing	34944	36	(24) No 10	30.48	52416	36	(40) No 10	50.80

Table 3.14: Design of sections of external and intermediate columns just below floor levels – four story moment resisting frame designed using method B (from Aschheim et al., forthcoming [7]).

Floor level	External columns				Intermediate columns			
	M_c or M_{pc} (k-in)	h (in)	Bars	$A_{s,prov}$ (in^2)	M_c or M_{pc} (k-in)	h (in)	Bars	$A_{s,prov}$ (in^2)
4	12672	28	(12) No 10	15.24	19008	28	(20) No 10	25.40
3	21792	32	(20) No 10	25.40	32688	32	(28) No 10	35.56
2	27571	36	(20) No 10	25.40	41357	36	(32) No 10	40.64
1	34944	36	(24) No 10	30.48	41933	36	(32) No 10	40.64
footing	NA	NA	NA	NA	NA	NA	NA	NA

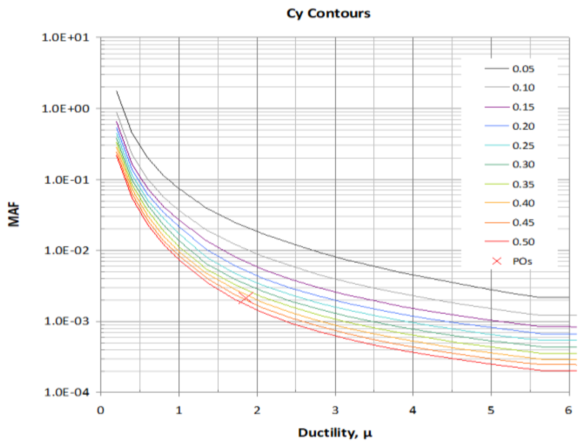

Figure 3.27: Yield Frequency Spectra contours at C_y = 0.05, …, 0.50 determined for a system with Δ_y^*=3.53in at the 50% confidence level. The x symbol represent the performance objective (μ=1.86 and 10% probability of exceedance in 50 years), thus C_y^*=0.463, (four story moment resisting frame building designed using method B) (from Aschheim et al., forthcoming [7]).

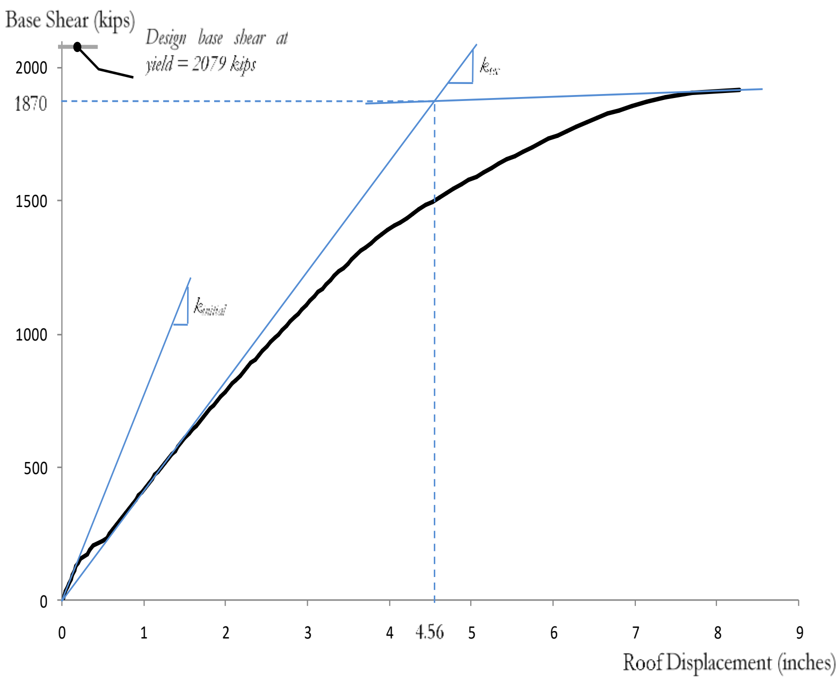

Figure 3.28: Capacity curve observed in a first-mode pushover analysis – four story moment resisting frame designed using method B (from Aschheim et al., forthcoming [7]).

Given the differences in the a_1 and the design base shear, the yield displacement of the ESDOF system is $\Delta_y^* = \Delta_y/\Gamma_1 = 4.56/1.35 = 3.38$in. The yield strength coefficient is $C_y = V_y/W$ = 1870/7560=0.247 and $C_y^* = C_y/\alpha_1$=0.393. The YFS for this yield displacement is shown in Figure 3.11. For a peak roof displacement equal to 8.94in, the resulting ductility limit is μ = 8.94/4.56=1.96, thus the required normalized base shear coefficient at yield is C_y^*=0.419. This value is greater than the estimated one, so either a re-design cycle could be obtained or a stipe analysis could be established to validate the initial design.

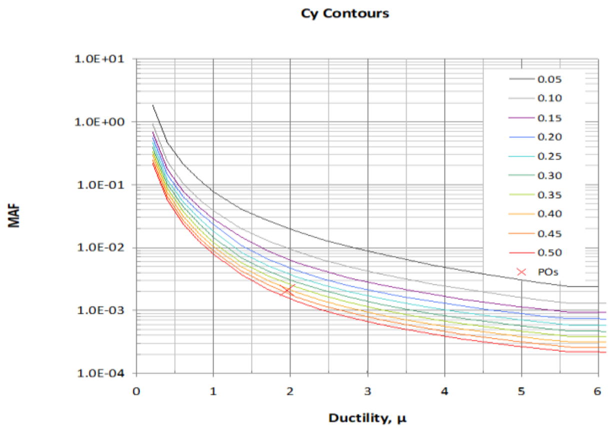

Figure 3.29: Yield frequency spectra contours at C_y = 0.05, …, 0.50 determined for a system with Δ_y^*=3.38in at the 50% confidence level that is used for the evaluation of the first design realization (four story moment resisting frame building designed using method B), (from Aschheim et al., forthcoming [7]).

3.5.2 Non-linear modeling and acceptance criteria

In Table 3.15 and Table 3.16 the modelling parameters for columns and beams, respectively, are summarized. In Tables 3.17 and 3.18 the acceptance criteria for beams and columns are presented.

The static pushover capacity curve resulting from a first-mode-proportional lateral load pattern is presented in Figure 3.30, both for the distributed and for the lumped plasticity model. The fundamental period of the lumped plasticity model is T_1=0.97sec. Note that this is obviously larger than the initial (uncracked) period of the fiber model of T_1 = 0.79. As discussed in Section 3.4.2 matching the initial stiffness is not our target; matching the effective one is. Yield displacement is calculated according to Figure 3.31. Assuming a bilinear approximation of the capacity curve having the same effective stiffness as the lumped plasticity model yields Δ_y=4.10in.

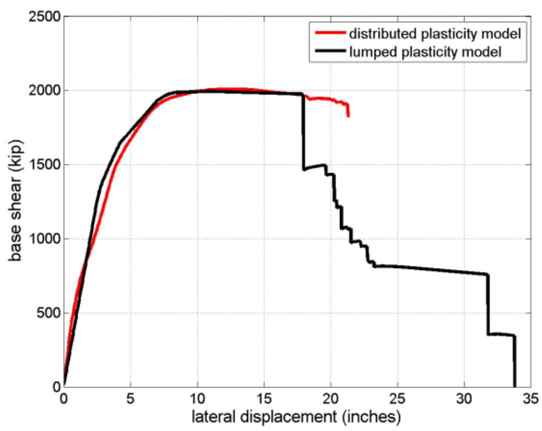

Figure 3.30: Static pushover curves of the distributed (black color) and the lumped plasticity (red color) model for the four story moment resisting frame designed using method B. The effect of the calibration is obvious in the matching pre-yielding segment of the two models.

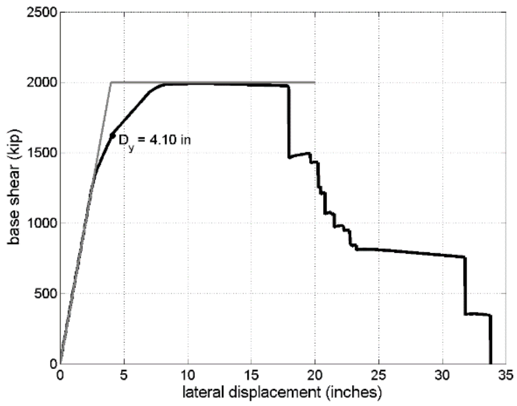

Computed performance:

W = 7560 kips

V_{max} = 1999.5 kips

C_y = Vmax/W = 1999.5/7560 = 0.264

Δ_y = 4.10 inches

T_1 = 0.97 sec

Figure 3.31: Calculation of the yield displacement Δ_y of the four story moment resisting frame designed using method B.

Table 3.15: Plastic hinge modelling parameters for columns – four story moment resisting frame designed using method B.

Story	External columns				Internal columns			
	M_y (kNm)	a	b	c	M_y (kNm)	a	b	c
4	1703.1	0.030	0.044	0.20	2602.1	0.030	0.044	0.20
3	3154.3				4210.6			
2	3753.3				5553.8			
1	3860.9 (top) 468.6 (bot)				5657.6 (top) 6847.4 (bot)			

Table 3.16: Plastic hinge modelling parameters for beams – four story moment resisting frame designed using method B.

Story	Positive moment				Negative moment			
	M_y^+ (kNm)	a	b	c	M_y^- (kNm)	a	b	c
4	524.3	0.025	0.050	0.20	1227.9	0.021	0.033	0.20
3	1474.8	0.025	0.049		3318.8	0.020	0.032	
2	2226.1	0.024	0.048		4827.3	0.020	0.031	
1	2650.3	0.024	0.047		5159.1	0.020	0.032	

Table 3.17: Maximum beam plastic rotation for IO, LS and CP – four story moment resisting frame designed using method B.

Story	Positive rotation (rad)			Negative rotation (rad)		
	IO	LS	CP	IO	LS	CP
4	0.0100	0.0250	0.050	0.0062	0.0210	0.0385
3			0.049	0.0067	0.0209	0.0495
2	0.0090	0.0240	0.048	0.0075	0.0210	0.0632
1			0.047	0.0092	0.0224	0.0825

Table 3.18: Maximum column plastic rotation for all stories, for IO, LS and CP – four story moment resisting frame designed using method B.

Story	Positive rotation (rad)		
	IO	LS	CP
$\theta_{p,max}$ (rad)	0.005	0.034	0.044

3.5.3 Performance evaluation of the initial design by nonlinear dynamic analysis

The acceptability of peak dynamic interstory drift and plastic hinge rotations is assessed at the 10/50 level by using the three methods introduced in Section 2, i.e., IDA, single and double stripe analysis. For each performance objective, the results are summarized in

Table 3.19 and Table 3.20. For IDA, the first two values of each PO correspond to estimated and allowable MAF, and for the stripe analysis they correspond to factored demand and factored capacity, respectively.

Table 3.19: Verification of the maximum interstory drift and beam plastic rotations for the four story moment resisting frame building designed using method B.

	IDR			beam plastic rotation		
	IDA	Single	Double	IDA	Single	Double
	(yrs^{-1})	–	–	(yrs^{-1})	(rad)	(rad)
Demand	0.0012	0.0167	0.0171	0.0012	0.8274	0.9013
Capacity	0.0021	0.0190	0.0187	0.0021	0.9511	0.9245
Check	✓	✓	✓	✓	✓	✓
Confidence	50 %			60%		

Table 3.20: Verification of column plastic rotations and global ductility for the four story moment resisting frame building designed using method B.

	column plastic rotation		
	IDA	Single	Double
	(yrs^{-1})	(rad)	(rad)
Demand	0.0006	0.2594	0.2209
Capacity	0.0021	0.9531	0.9721
Check	✓	✓	✓
Confidence	60 %		

IDA is first employed to estimate the MAF of exceeding the maximum interstory drift ratio limit of θ_{max} = 2%. The median value of the fragility curve is equal to 0.82g and the standard deviation is 29%. The hazard curve is presented in Figure 3.32. Note that despite the simplification of the seismic hazard curve adopted for design, assessment will progress by using the actual hazard data, scaled to match the 10/50 $S_a(T_1)$ value of the design spectrum to ensure a fair comparison of the different methodologies. The estimated mean annual frequency of exceeding maximum interstory drift limit of 2%, at 50% confidence, equals

0.00121, which is lower than the corresponding code value of 0.0021 (10% probability of exceeding PO in 50 years). This means that the performance objective is met.

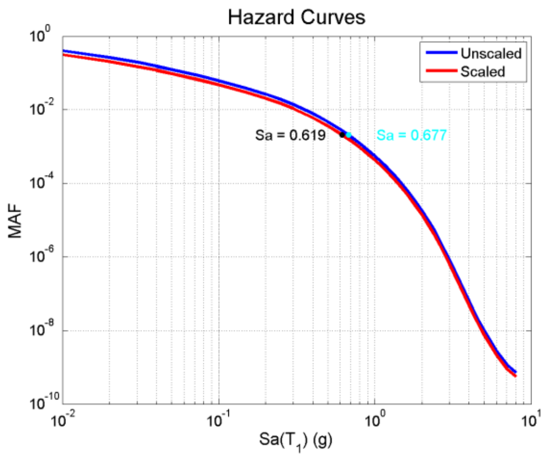

Figure 3.32: Seismic site hazard curve properly scaled to 10% in 50 years for $S_a(T_1)$ for the four story moment resisting frame building designed using method B.

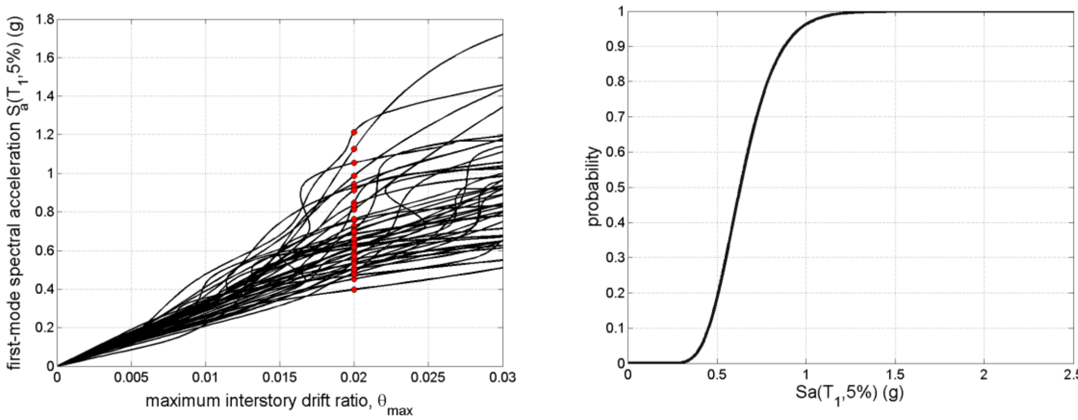

(a) (b)

Figure 3.33: IDA approach for estimating the mean annual frequency of exceeding 2% maximum interstory drift ratio: (a) the $Sa(T_1,5\%)$ values calculated for 2% maximum interstory drift ratio limit, θ_{max}, and (b) corresponding fragility curve – four story moment resisting frame designed using method B.

The maximum interstory drift ratio demand as calculated for 17 records for S_a^{design}=0.62g, appears in Figure 3.34 (a) and the corresponding hazard fit to define the slope k is presented in Figure 3.34 (b). FD and FC at 50% confidence are estimated as:

$$FD_{RPo}=\theta_{max,50}\ \exp(0.5\cdot k\cdot\beta_{\theta max|Sa}{}^2/b) = 0.015\ \exp(0.5\cdot 2.59\cdot 0.29^2/1) = 0.0167$$
$$FC_R=\theta_{max,C}\ \exp(-0.5\cdot k\cdot\beta_{CR}{}^2/b) = 0.02\ \exp(-0.5\cdot 2.59\cdot 0.20^2/1) = 0.0190$$

Since the factored capacity of 0.0190 is greater than the factored demand of 0.0167 the result is satisfactory at 50% confidence level.

For the double stripe analysis, the interstory drift values are calculated for 17 records at S_a^{design}=0.62g (red points) and at $1.1S_a^{design}$=0.68g (green points), as shown in Figure 3.35 (a) and the corresponding hazard fit to define the slope k is presented in Figure 3.35 (b). FD and FC at 50% confidence are estimated as:

$FD_{RPo}=\theta_{max,50}\ \exp(0.5\cdot k\cdot \beta_{\theta max|Sa}{}^{2}/b) = 0.015\ \exp(0.5\cdot 2.47\cdot 0.29^{2}/0.76) = 0.0171$
$FC_{R}=\theta_{max,C}\ \exp(-0.5\cdot k\cdot \beta_{CR}{}^{2}/b) = 0.02\ \exp(-0.5\cdot 2.47\cdot 0.20^{2}/0.76) = 0.0187$

Since the factored capacity of 0.0187 is greater than the factored demand of 0.0171 the result is satisfactory at 50% confidence level.

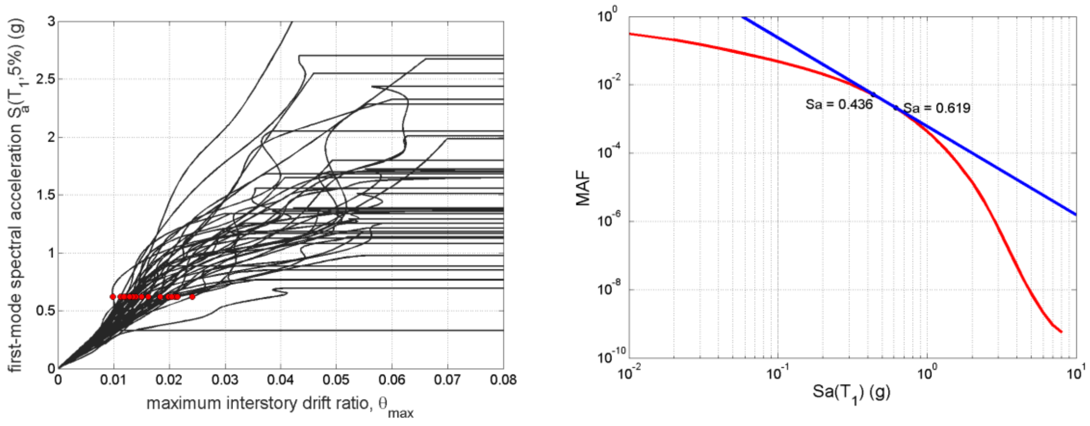

(a) (b)

Figure 3.34: Single stripe analysis method for estimating FD_{RPo} and FC_R for 2% maximum interstory drift ratio: (a) maximum interstory drifts calculated for S_a^{design}, and (b) the local fit of the seismic hazard curve – four story moment resisting frame designed using method B.

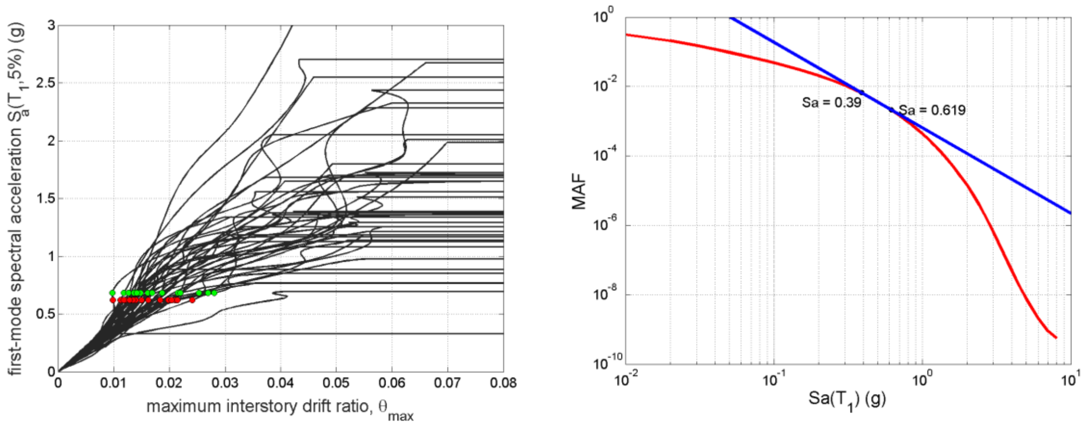

(a) (b)

Figure 3.35: Double stripe analysis method for estimating FD_{RPo} and FC_R for 2% maximum interstory drift ratio: (a) maximum interstory drifts calculated for S_a^{design} (red points) and for $1.1Sa^{design}$ (green points), and (b) the local fit of the seismic hazard curve – four story moment resisting frame designed using method B.

The MAF of exceeding DCR=1.0 for beams is estimated using the fragility curve that is calculated based on the $S_a(T_1,5\%)$ values that correspond to the DCR limit. The median value of the fragility curve (Figure 3.36 (b)) equals to 0.87g and the standard deviation is equal to 30%. The hazard curve used to estimate MAF is presented in Figure 3.32. The estimated mean annual frequency of exceeding DCR=1.0, at 60% confidence, equals to 0.0012, which is lower than the corresponding code value of 0.0021 (10% probability of exceeding PO in 50 years). This means that the performance objective is met.

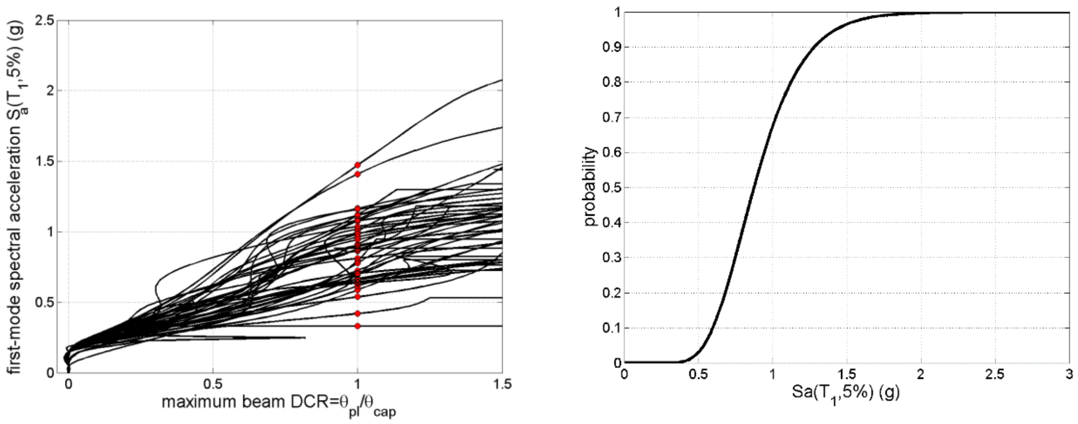

(a) (b)

Figure 3.36: IDA approach for estimating mean annual frequency of exceeding demand capacity ratio limit of 1.0 for beams: (a) the $S_a(T_1,5\%)$ values calculated for DCR=1, and (b) corresponding fragility curve – four story moment resisting frame designed using method B.

The maximum demand capacity ratio demand for beams as calculated for 17 records for S_a^{design}=0.62g, appears in Figure 3.36 (a) and the corresponding hazard fit to define the slope k is presented in Figure 3.36 (b). FD and FC are estimated as:

$FD_{RPo}=DCR_{max,50}$ $\exp(0.5\cdot k\cdot \beta_{\theta max|Sa}{}^2/b) = 0.676 \exp(0.5\cdot 2.50\cdot 0.35^2/1.0) = 0.7865$
$FC_R=DCR_{max,C}$ $\exp(-0.5\cdot k\cdot \beta_{CR}{}^2/b) = 1.0 \exp(-0.5\cdot 2.50\cdot 0.20^2/1.0) = 0.9511$

For a confidence level of 60%, the lognormal standard variate is K_x=0.253 and the evaluation inequality becomes:

$FC_R > FD_{RPo} \exp(K_x\cdot \beta_{TU}) = 0.7865 \exp(0.253\cdot 0.20) = 0.8274$

Since the factored capacity of 0.9511 is greater than the factored demand of 0.8274 the result is satisfactory at the 60% confidence level.

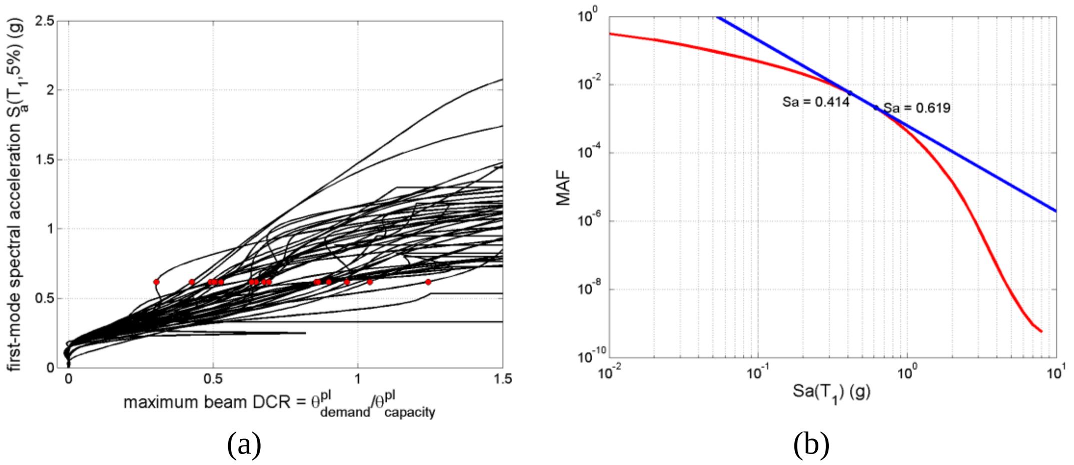

(a) (b)

Figure 3.37: Single stripe analysis method for estimating FD_{RPo} and FC_R for DCR=1 of beams: (a) maximum beam DCR calculated for S_a^{design}, and (b) the local fit of the seismic hazard curve – four story moment resisting frame designed using method B.

The DCR values are calculated for 17 records for S_a^{design}=0.62g (red points) and for 1.1S_a^{design}=0.68g (green points) are shown in Figure 3.38 (a) and the corresponding hazard fit to define the slope k is presented in Figure 3.38 (b). FD and FC are estimated as:

$FD_{RPo}=DCR_{max,50}\ \exp(0.5\cdot k\cdot \beta_{\theta max|Sa}{}^2/b) = 0.676\ \exp(0.5\cdot 2.31\cdot 0.35^2/0.68) = 0.8568$
$FC_R=DCR_{max,C}\ \exp(-0.5\cdot k\cdot \beta_{CR}{}^2/b) = 1.0\ \exp(-0.5\cdot 2.31\cdot 0.20^2/0.68) = 0.9245$

For a confidence level of 60%, the lognormal standard variate is K_x=0.253 and the evaluation inequality becomes:

$FC_R > FD_{RPo}\ \exp(K_x\cdot \beta_{TU}) = 0.8568\ \exp(0.253\cdot 0.20) = 0.9013$

Since the factored capacity of 0.9245 is greater than the factored demand of 0.9013 the result is satisfactory at 60% confidence level.

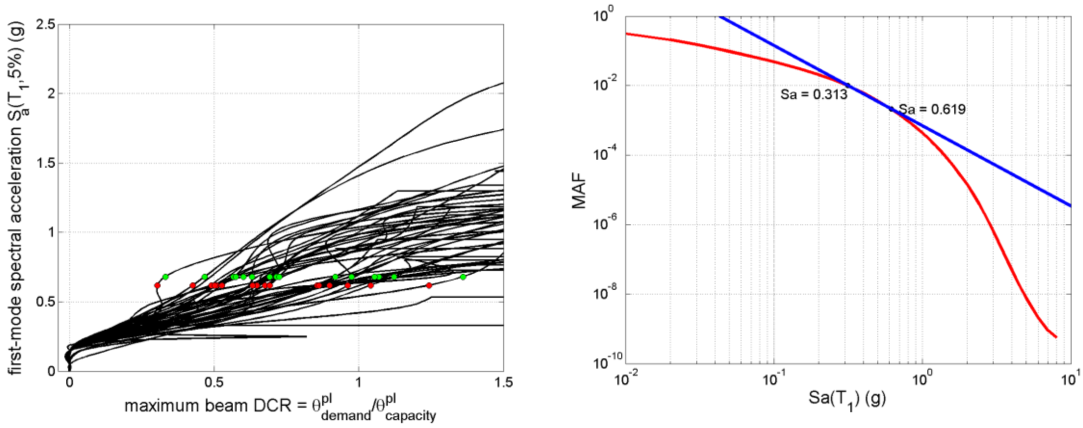

(a) (b)

Figure 3.38: Double stripe analysis method for estimating FD_{RPo} and FC_R for DCR=1 of beams: (a) maximum beam DCR calculated for S_a^{design} (red points) and for $1.1S_a^{design}$ (green points), and (b) the local fit of the seismic hazard curve – four story moment resisting frame designed using method B.

IDA curves in terms of the first mode spectral acceleration $S_a(T_1,5\%)$ and maximum demand capacity ratio, DCR=$(\theta_{demand}{}^{pl}/\ \theta_{capacity}{}^{pl})_{\max}$ for columns are presented in Figure 3.39 (a). The median value of the fragility curve (Figure 3.39 (b)) equals to 1.14g and the standard deviation is equal to 34%. The hazard curve is presented in Figure 3.32. The estimated mean annual frequency of exceeding DCR=1.0, at 60% confidence, equals to 0.00057, which is lower than the corresponding code value of 0.0021 (10% probability of exceeding PO in 50 years). This means that the performance objective is met.

The maximum demand capacity ratio demand for columns is calculated for 17 records for S_a^{design}=0.62g, as shown in Figure 3.40 (a) and the corresponding hazard fit to define the slope k is presented in Figure 3.40 (b). FD and FC are estimated as:

$FD_{RPo}=DCR_{max,50}\ \exp(0.5\cdot k\cdot \beta_{\theta max|Sa}{}^2/b) = 0.167\ \exp(0.5\cdot 2.40\cdot 0.57^2/1.0) = 0.2466$
$FC_R=DCR_{max,C}\ \exp(-0.5\cdot k\cdot \beta_{CR}{}^2/b) = 1.0\ \exp(-0.5\cdot 2.40\cdot 0.20^2/1.0) = 0.9531$

For a confidence level of 60%, the lognormal standard variate is K_x=0.253 and the evaluation inequality becomes:

$FC_R > FD_{RPo}\ \exp(K_x\cdot \beta_{TU}) = 0.2466\ \exp(0.253\cdot 0.20) = 0.2594$

Since the factored capacity of 0.9531 is greater than the factored demand of 0.2594 the result is satisfactory at 60% confidence level.

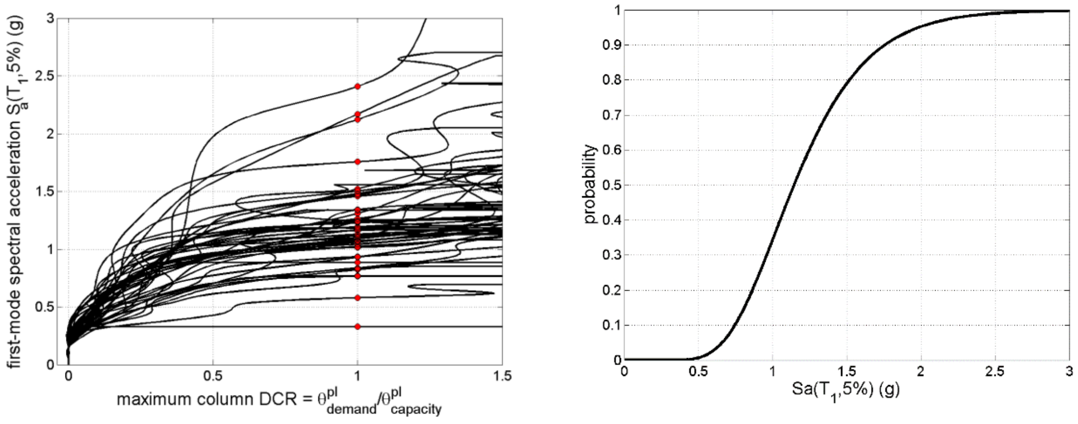

(a) (b)

Figure 3.39: IDA approach for estimating mean annual frequency of exceeding demand capacity ratio limit of 1.0 for columns: (a) the $S_a(T_1,5\%)$ values calculated for DCR=1, and (b) corresponding fragility curve – four story moment resisting frame designed using method B.

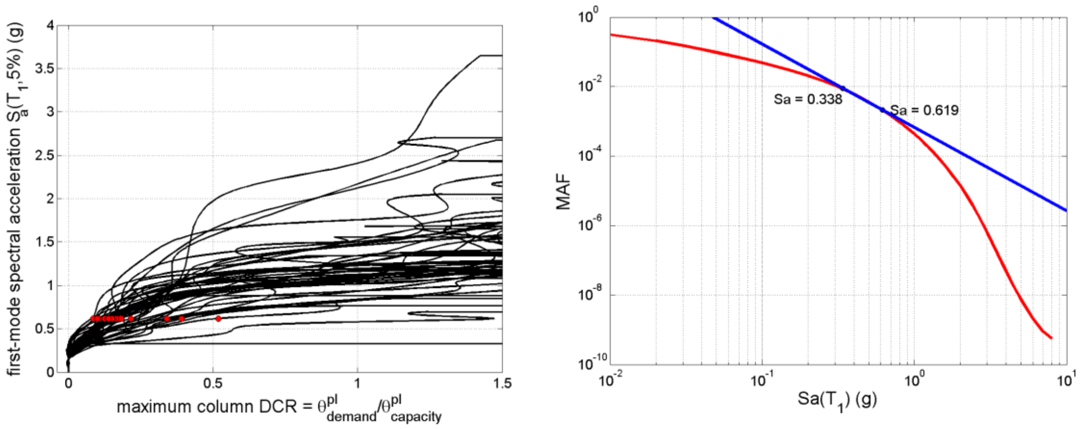

(a) (b)

Figure 3.40: Single stripe analysis method for estimating FD_{RPo} and FC_R for DCR=1 of columns: (a) maximum column DCR calculated for S_a^{design}, and (b) the local fit of the seismic hazard curve – four story moment resisting frame designed using method B

For the double stripe analysis, the DCR values is calculated for 17 records for S_a^{design}=0.62g (red points) and for $1.1S_a^{design}$=0.68g (green points), as shown in Figure 3.41 (a). The slope k is presented in Figure 3.41 (b). FD and FC are estimated as:

$$FD_{RPo}=DCR_{max,50}\ \exp(0.5\cdot k\cdot \beta_{\theta max|Sa}{}^2/b) = 0.167\ \exp(0.5\cdot 2.63\cdot 0.57^2/1.86) = 0.2100$$
$$FC_R=DCR_{max,C}\ \exp(-0.5\cdot k\cdot \beta_{CR}{}^2/b) = 1.0\ \exp(-0.5\cdot 2.63\cdot 0.20^2/1.86) = 0.9721$$

For a confidence level of 60%, the lognormal standard variate is K_x=0.253 and the evaluation inequality becomes:

$$FC_R > FD_{RPo}\ \exp(K_x\cdot \beta_{TU}) = 0.2100\ \exp(0.253\cdot 0.20) = 0.2209$$

Since the factored capacity of 0.9721 is greater than the factored demand of 0.2209 the result is satisfactory at 60% confidence level.

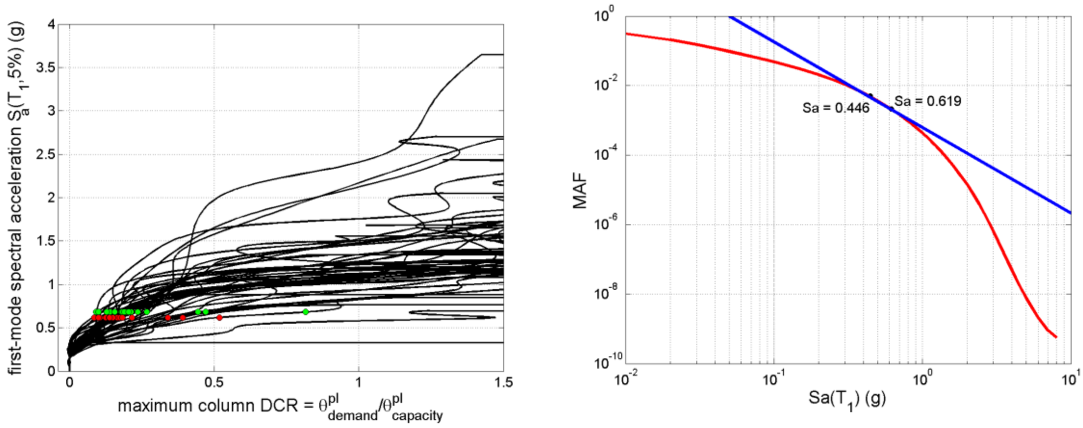

(a) (b)

Figure 3.41: Double stripe analysis method for estimating FD_{RPo} and FC_R for DCR=1 of columns: (a) maximum column DCR calculated for S_a^{design} (red points) and for $1.1S_a^{design}$ (green points), and (b) the local fit of the seismic hazard curve – four story moment resisting frame designed using method B.

3.6 Four story MRF designed using method C

3.6.1 Initial design

The initial design of the four story moment resisting frame using the Yield Frequency Spectra derived using actual hazard data (design method C) can be found in detail in Aschheim et al., [7] along with an analytical description of this design method. Only some of the key points of the design are listed in this documentation. The design of the building aims to limit the mean annual frequency of exceeding the following performance objectives:

❖ Limit the MAF of exceeding ductility limit of 1.5 to $1.39\cdot10^{-2}$ (50% probability of exceedance in 50 years) at the 50% confidence
❖ Limit the MAF of exceeding interstory drift ratio of 2% to $2.11\cdot10^{-3}$ (10% probability of exceedance in 50 years) at the 50% confidence
❖ Limit the MAF of collapse of the ESDOF system to $2.01\cdot10^{-4}$ (1% probability of exceedance in 50 years) at the 90% confidence (we seek high confidence that this PO is achieved)

As mentioned in the previous examples, the first mode parameters of the building as well as the yield displacement are firstly estimated. As starting parameters for this design approach the ones calculated through the eigenvalue and the pushover analyses of the previous example are used, thus Δ_y =4.6in, Γ_1 =1.35 and α_1=0.63. The yield displacement of the ESDOF system is $\Delta_y^*=\Delta_y/\Gamma_1$=4.6/1.35=3.41in. The roof displacement is estimated as D_u =8.94 in, so the resulting ductility is μ=8.94/4.6=1.94. The mean annual frequency of exceeding this ductility limit should be lower than the $2.11\cdot10^{-3}$ (second PO). For the third PO the ductility limit is determined at the point where the constant flatline of the YFS appears.

The Yield Frequency Spectra at the 50% confidence is shown in Figure 3.42, computed using actual hazard data. Each PO is plotted the YFS considering its desired MAF. Because we wish to avoid collapse, the 90% confidence level is chosen for the third PO, so the YFS at the 90% confidence level that is presented in Figure 3.43, is also used. The resulting values of the C_y^* are summarized in Table 3.21. The greatest value of C_y^* is used for the design, thus $C_y^*=\max\{0.108;0.377;0.577\}=0.577$. The design base shear coefficient at yield is $C_y=C_y^*\cdot\alpha_1=0.577\cdot0.63=0.364$, thus $V_y=C_y\cdot W/2=2752$kips. The period associated with C_y^* and Δ_y^* is 0.79sec.

The beta distribution of lateral forces is used in the design, thus design base shear at yield is modified to 2502kips. Using the Portal Frame Method and assuming that the inflection points for the columns occur at 60% of the height for the first story and at 50% of the height for the others, the moment distribution is calculated for the whole building. A weak-beam strong-column mechanism is used in the design. More details about the design procedure can be found in Aschheim et al., [7].

The resulting dimensions and the sizing of the beams and columns is summarized in Tables 3.3, 3.4 and 3.5. The "above floor sections" and "below floor sections" as well as the "external" and "intermmediate" columns of the frame are explained in Figure 3.9.

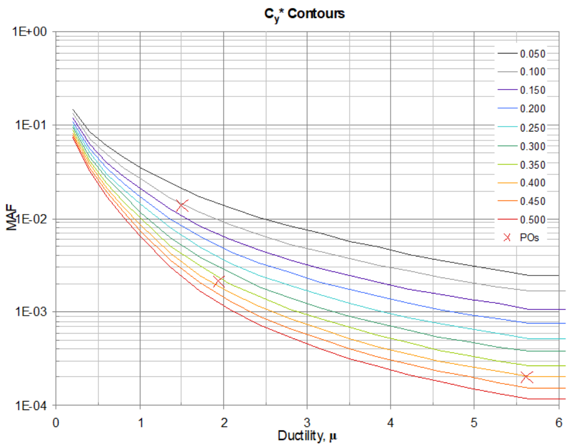

Figure 3.42: Yield Frequency Spectra contours at C_y = 0.15, …, 0.60 for Δ_y^*=3.41in at the 50% confidence level. The x symbol represent the performance objectives, (four story moment resisting frame building designed using method C), (from Aschheim et al., forthcoming [7]).

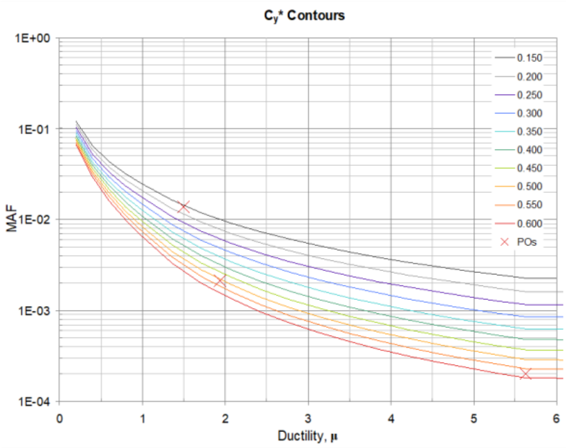

Figure 3.43: Yield Frequency Spectra contours at C_y = 0.15, …, 0.60 for Δ_y^*=3.41in at the 90% confidence level. The x symbol represent the performance objectives, (four story moment resisting frame building designed using method C), (from Aschheim et al., forthcoming [7]).

The initial design is preliminarily evaluated through an eigenvalue analysis. The modal parameters calculated through SeismoStruct are T_1 = 0.60s, Γ_1 = 1.35 and α_1 = 0.65. A nonlinear static analysis using a lateral force vector proportional to the fist mode distribution is carried out using SeismoStruct and the resulting pushover curve is presented in Figure 3.44. The base shear at yield is 2250kips which is lower than the design base shear of 2752kips. This difference appears because of the use of the formula of the ASCE-7 to calculate the design base shear, which takes into account the resultant of the lateral force distribution, which was at first estimated approximately. If the results of the eigenvalue analysis were considered, the design base shear would have increased from 2550kips to approximately 2720kips. The period associated with secant stiffness representative of cracked section behavior is estimated as 0.79sec which matches the estimated period of the ESDOF, $T^* = 0.79$sec. The roof displacement at yield is 3.84in.

Table 3.21: Normalized base shear coefficient at yield calculated for each PO at 50% and 90% confidence level – four story moment resisting frame building designed using method C (from Aschheim et al., forthcoming [7]).

Probability of exceeding in 50 years	MAF of exceedance	Mean return period (yrs)	Ductility μ	C_y^* Confidence 50%	C_y^* Confidence 90%
50%	$1.39\cdot10^{-2}$	72	1.50	0.108	0.159
10%	$2.11\cdot10^{-3}$	475	1.94	0.377	0.513
1%	$2.01\cdot10^{-4}$	4975	6.0*	0.402	0.577

* flatline in YFS

Table 3.22: Engineering design for beam sizes and reinforcing – four story moment resisting frame building designed using method C (from Aschheim et al., forthcoming [7]).

Story	b_w (in)	h (in)	Top bars	Bottom bars
4	16	28	(10) No 9	(5) No 9
3	22	36	(16) No 9	(8) No 9
2	26	42	(20) No 9	(10) No 9
1	26	42	(22) No 9	(10) No 9

Table 3.23: Design of sections of external and intermediate columns just above floor levels – four story moment resisting frame building designed using method C (from Aschheim et al., forthcoming [7])

Floor level	External columns				Intermediate columns			
	M_c or M_{pc} (k-in)	h (in)	Bars	$A_{s,prov}$ (in^2)	M_c or M_{pc} (k-in)	h (in)	Bars	$A_{s,prov}$ (in^2)
4	NA	NA	NA	NA	NA	NA	NA	NA
3	18624	30	(20) No 10	25.40	27936	30	(28) No 10	35.56
2	29088	34	(24) No 10	30.48	43632	34	(36) No 10	45.72
1	35654	38	(24) No 10	30.48	53482	38	(36) No 10	45.72
footing	33780	38	(20) No 10	25.40	67560	38	(48) No 10	60.96

Table 3.24: Design of sections of external and intermediate columns just below floor levels – four story moment resisting frame building designed using method C (from Aschheim et al., forthcoming [7]).

Floor level	External columns				Intermediate columns			
	M_c or M_{pc} (k-in)	h (in)	Bars	$A_{s,prov}$ (in^2)	M_c or M_{pc} (k-in)	h (in)	Bars	$A_{s,prov}$ (in^2)
4	18624	30	(20) No 10	25.40	27936	30	(28) No 10	35.56
3	29088	34	(24) No 10	30.48	43632	34	(36) No 10	45.72
2	35654	38	(24) No 10	30.48	53482	38	(36) No 10	45.72
1	36038	38	(24) No 10	30.48	54058	38	(36) No 10	45.72
footing	NA	NA	NA	NA	NA	NA	NA	NA

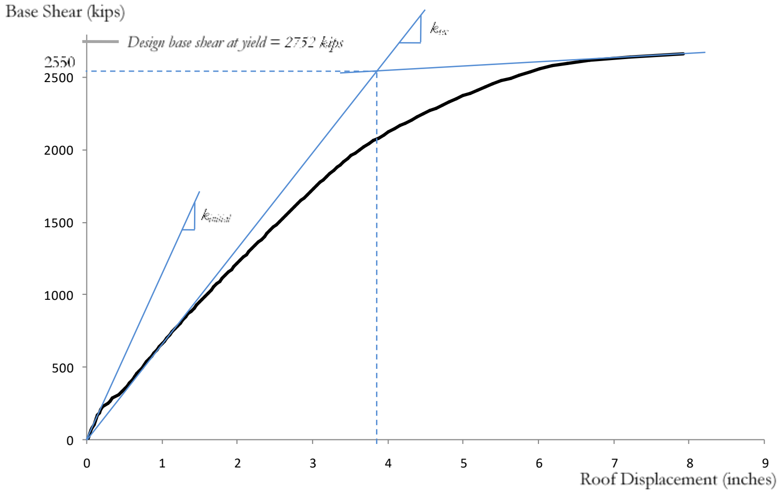

Figure 3.44: Capacity curve observed in a first-mode pushover analysis for the four story moment resisting frame building designed using method C (from Aschheim et al., forthcoming [7]).

Given the results of the eigenvalue analysis, the performance of the initial design can be evaluated. The yield displacement of the ESDOF system is $\Delta_y^* = \Delta_y/\Gamma_1 = 3.84/1.35 = 2.48$in. The yield strength coefficient is $C_y=V_y/W$ = 2550/7560=0.337 and $C_y^*=C_y/\alpha_1$=0.518. The YFSs for this yield displacement are shown in Figures 3.45 and 3.46 at the 50% and 90% confidence levels, respectively. For a peak roof displacement equal to 8.94in, the resulting ductility limit is μ = 8.94/3.84=2.33. The required normalized base shear coefficient at yield is C_y^*=0.626. This value is greater than the estimated one, so either a re-design cycle could be obtained or a multiple stripe analysis could be established to determine a better estimate of the MAF of collapse of the MDOF system.

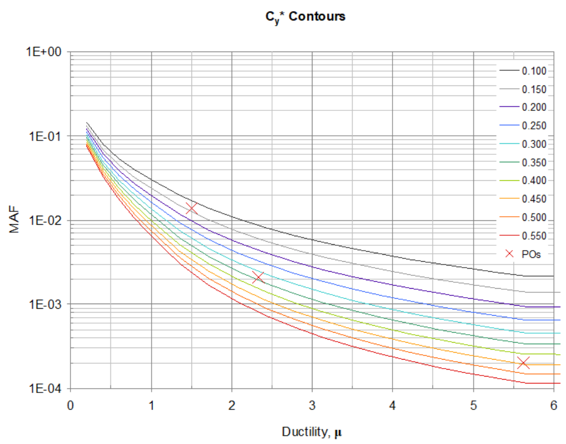

Figure 3.45: Yield Frequency Spectra contours at C_y = 0.10, …, 0.550 for Δ_y^*=2.48in at the 50% confidence level for evaluation of the first design realization – four story moment resisting frame building designed using method C (from Aschheim et al., forthcoming [7]).

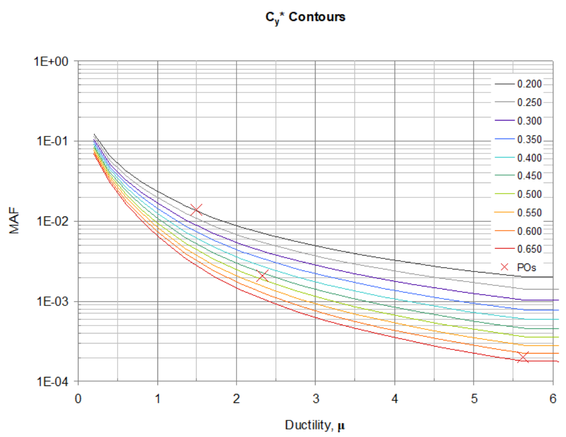

Figure 3.46: Yield Frequency Spectra contours at C_y = 0.10, …, 0.550 for Δ_y^*=2.48in at the 90% confidence level for evaluation of the first design realization – four story moment resisting frame building designed using method C (from Aschheim et al., forthcoming [7]).

3.6.2 Non-linear modeling and acceptance criteria

In Tables 3.25 and 3.26 the modelling parameters for columns and beams, respectively, are summarized. In Tables 3.27 and 3.28 the acceptance criteria for columns and beams are presented.

The static pushover capacity curve resulting from a first-mode-proportional lateral load pattern is presented in Figure 3.47, both for lumped and for the distributed plasticity model. The fundamental period of the lumped plasticity model is T_1=0.79sec. Note that this is obviously larger than the initial period of the fiber model of T_1 = 0.65, as explained in Section 19.6.7. The same comments apply here as well. Yield displacement is calculated according to Figure 3.48, assuming a bilinear approximation of the capacity curve having the same effective stiffness as the lumped plasticity model, resulting to Δ_y=3.7in.

Table 3.25: Plastic hinge modelling parameters for columns – four story moment resisting frame building designed using method C.

Story	External columns				Internal columns			
	M_p (kNm)	a	b	c	M_p (kNm)	a	b	c
4	2828.7	0.030	0.044	0.200	3838.5	0.030	0.044	0.200
3	3967.9				5655.3			
2	4654.5				6565.9			
1	4770.5 (top) 4128.3 (bot)				6677.9 (top) 3838.5 (bot)			

Table 3.26: Plastic hinge modelling parameters for beam – four story moment resisting frame building designed using method C.

Story	Positive moment				Negative moment			
	M_p^+ (kNm)	a	b	c	M_p^- (kNm)	a	b	c
4	1065.0	0.025	0.050	0.20	2076.7	0.021	0.035	0.20
3	2226.4	0.024	0.049		4348.1	0.020	0.031	
2	3274.0	0.025	0.049		6412.1	0.021	0.034	
1	3273.7	0.024	0.048		6979.0	0.020	0.033	

Table 3.27: Maximum column plastic rotation for all stories, for IO, LS and CP – four story moment resisting frame building designed using method C.

Story	Positive rotation		
	IO	LS	CP
$\theta_{p,max}$ (rad)	0.005	0.034	0.044

Table 3.28: Maximum beam plastic rotation for IO, LS and CP – four story moment resisting frame building designed using method C.

Story	Positive rotation (rad)			Negative rotation (rad)		
	IO	LS	CP	IO	LS	CP
4	0.0088	0.0238	0.0477	0.0062	0.0212	0.0347
3	0.0096	0.0246	0.0492	0.0056	0.0199	0.0311
2	0.0092	0.0242	0.0485	0.0061	0.0208	0.0341
1	0.0100	0.0250	0.0500	0.0059	0.0201	0.0326

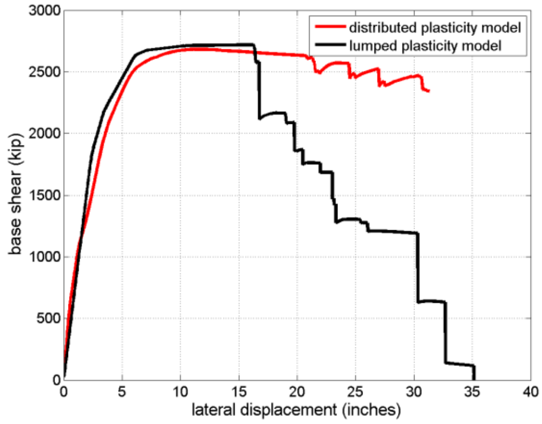

Figure 3.47: Static pushover curves of the distributed (black color) and the lumped plasticity (red color) model for the four story moment resisting frame designed using method C. The effect of the calibration is obvious in the matching pre-yielding segment of the two models.

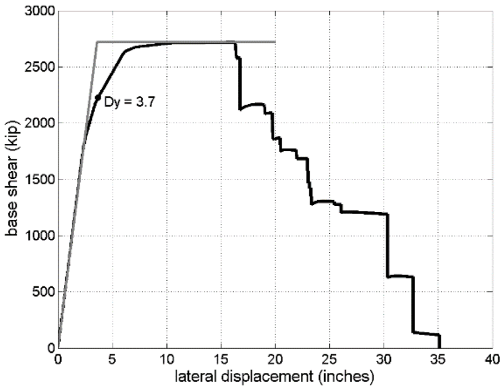

<u>Computed performance:</u>

W = 7560 kips

V_{max} = 2720 kips

$C_y = V_{max}/W$ = 2720/7560 = 0.360

Δ_y = 3.7 inches

T_1 = 0.79sec

Figure 3.48: Calculation of the yield displacement Δ_y of the four story moment resisting frame designed using method C.

3.6.3 Performance evaluation of the initial design by nonlinear dynamic analysis

Four different types of performance criteria are checked: (i) peak dynamic interstory drifts at a MAF of 10/50 with confidence of 50%, (ii) plastic hinge rotations of beams and columns at 10/50, 60% confidence, (iii) the global ductility limit of 1.5 at 50/50, 50% confidence, and (iv) the global collapse limit-state versus 1/50 at 90% confidence. All three methods introduced in Section 2 are employed, i.e., IDA, single and double stripe analysis. For each performance objective, the results are summarized in Table 3.29 and 3.30. For IDA, the first two values of each PO correspond to estimated and allowable MAF, and for the stripe analysis they correspond to factored demand and factored capacity, respectively.

Table 3.29: Verification of the maximum interstory drift and beam plastic rotations for the four story moment resisting frame building designed using method C.

	IDR			beam plastic rotation		
	IDA	Single	Double	IDA	Single	Double
	(yrs^{-1})	–	–	(yrs^{-1})	(rad)	(rad)
Demand	0.0005	0.0108	0.0011	0.0005	0.4288	0.4202
Capacity	0.0021	0.0189	0.0190	0.0021	0.9463	0.9681
Check	✓	✓	✓	✓	✓	✓
Confidence		50 %			60%	

Table 3.30: Verification of column plastic rotations, global ductility and global collapse for the four story moment resisting frame building designed using method C.

	column plastic rotation			global ductility			collapse
	IDA	Single	Double	IDA	Single	Double	IDA
	(yrs^{-1})	(rad)	(rad)	(yrs^{-1})	–	–	(yrs^{-1})
Demand	0.0003	0.2075	0.1998	0.0028	0.0046	0.0046	0.000457
Capacity	0.0021	0.9481	0.9629	0.0139	0.0083	0.0083	0.000201
Check	✓	✓	✓	✓	✓	✓	✗ *
Confidence		60 %			50 %		90%

* Initial estimate. Refer to later discussion on improvements at the end of the Section

IDA is first employed to estimate the MAF of exceeding the maximum interstory drift ratio limit of θ_{max} = 2%. The median value of the fragility curve (Figure 3.15 (b)) is equal to 1.70g and the standard deviation is 34%. In this case, since we directly use the site-specific hazard data in the YFS design, the assessment will be fair by default, without requiring any scaling of the hazard curve. Thus, the latter can be employed directly as estimated from USGS (see Figure 3.49). The estimated mean annual frequency of exceeding maximum interstory drift limit of 2%, at 50% confidence, equals 0.00048, which is lower than the corresponding code value of 0.0021 (10% probability of exceeding PO in 50 years). This means that the performance objective is met.

The maximum interstory drift ratio demand as calculated for 17 records for S_a^{design}=0.76g, appears in Figure 3.51 (a) and the corresponding hazard fit to define the slope k is presented in Figure 3.51 (b). FD and FC at 50% confidence are estimated as:

$$FD_{RPo}=\theta_{max,50}\exp(0.5\cdot k\cdot \beta_{\theta max|Sa}{}^2/b) = 0.0104\exp(0.5\cdot 2.74\cdot 0.15^2/1) = 0.0108$$
$$FC_R=\theta_{max,C}\exp(-0.5\cdot k\cdot \beta_{CR}{}^2/b) = 0.02\exp(-0.5\cdot 2.74\cdot 0.20^2/1) = 0.0189$$

Since the factored capacity of 0.0189 is greater than the factored demand of 0.0108 the result is satisfactory at 50% confidence level.

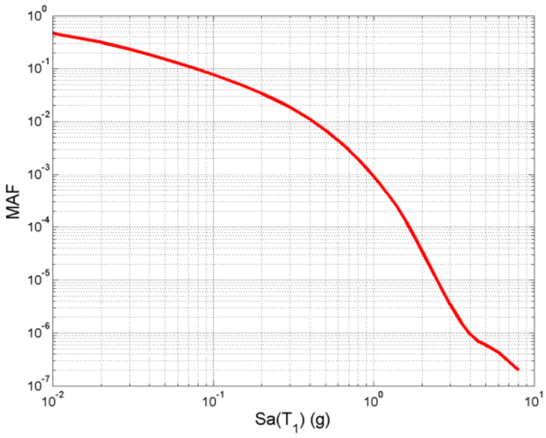

Figure 3.49: Seismic site hazard curve as determined from USGS data used in the performance assessment of the four story moment resisting frame building designed using method C.

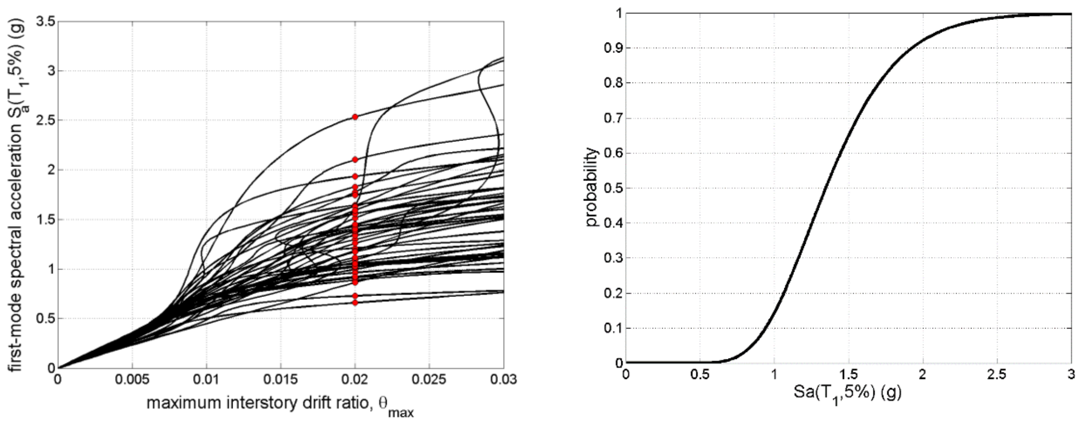

(a) (b)

Figure 3.50: IDA approach for estimating the mean annual frequency of exceeding 2% maximum interstory drift ratio: a) the $S_a(T_1,5\%)$ values calculated for 2% maximum interstory drift ratio limit, θ_{max}, and (b) corresponding fragility curve – four story moment resisting frame building designed using method C.

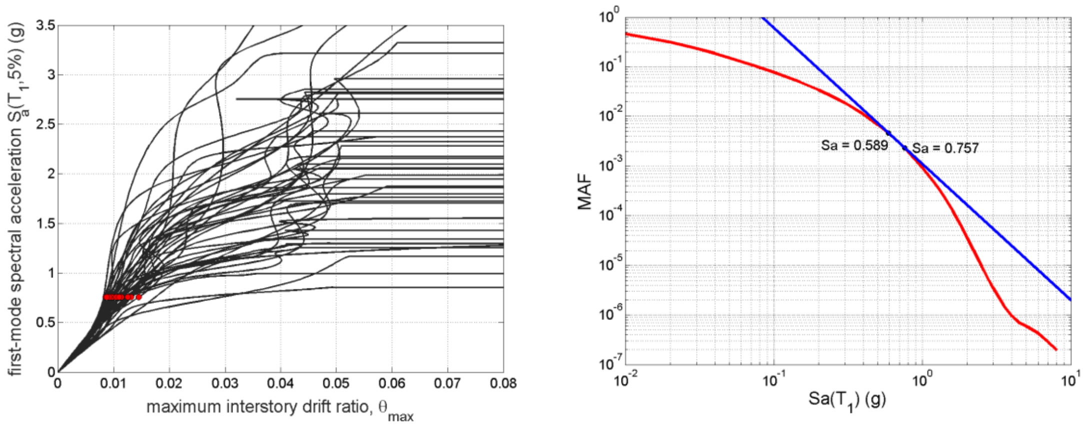

(a) (b)

Figure 3.51: Single stripe analysis method for estimating FD_{RPo} and FC_R for 2% maximum interstory drift ratio: (a) maximum interstory drifts calculated for S_a^{design}, and (b) the local fit of the seismic hazard curve – four story moment resisting frame building designed using method C.

For the double stripe analysis, the interstory drift values are calculated for 17 records for S_a^{design}=0.76g (red points) and for 1.1S_a^{design}=0.83g (green points) (Figure 3.52 (a)) and the corresponding hazard fit to define the slope k is presented in Figure 3.52 (b). FD and FC at 50% confidence are estimated as:

$FD_{RPo}=\theta_{max,50}\ \exp(0.5\cdot k\cdot \beta_{\theta max|Sa}{}^2/b) = 0.0104\ \exp(0.5\cdot 2.71\cdot 0.15^2/1.06) = 0.0107$
$FC_R=\theta_{max,C}\ \exp(-0.5\cdot k\cdot \beta_{CR}{}^2/b) = 0.02\ \exp(-0.5\cdot 2.71\cdot 0.20^2/1.06) = 0.0190$

Since the factored capacity of 0.0190 is greater than the factored demand of 0.0107 the result is satisfactory at the 50% confidence level.

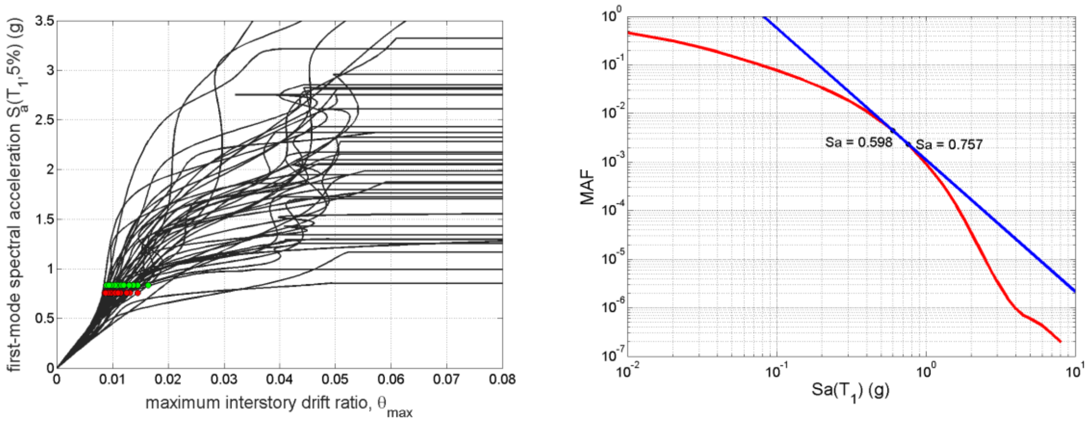

(a) (b)

Figure 3.52: Double stripe analysis method for estimating FD_{RPo} and FC_R for 2% maximum interstory drift ratio: (a) maximum interstory drifts calculated for S_a^{design} (red points) and for 1.1S_a^{design} (green points), and (b) local fit of the seismic hazard curve – four story moment resisting frame building designed using method C.

The MAF of exceeding DCR=1.0 for beams is also estimated using the fragility curve that is calculated based on the $S_a(T_1,5\%)$ values that correspond to the DCR limit, according to IDA results and is shown in Figure 3.53 (b). The median value of the lognormal distribution equals to 1.42g and the standard deviation is equal to 30%. The hazard curve used to estimate MAF is presented in Figure 3.49. The estimated mean annual frequency of exceeding DCR=1.0, at 60% confidence, equals to 0.00049, which is lower than the corresponding code value of 0.0021 (10% probability of exceeding PO in 50 years). This means that the performance objective is met.

The maximum demand capacity ratio demand for beams as calculated for 17 records for S_a^{design}=0.76g, appears in Figure 3.54 (a) and the corresponding hazard fit to define the slope k is presented in Figure 3.54 (b). FD and FC are estimated as:

$FD_{RPo}=DCR_{max,50}\ \exp(0.5\cdot k\cdot \beta_{\theta max|Sa}{}^2/b) = 0.388\ \exp(0.5\cdot 2.76\cdot 0.19^2/1.0) = 0.4076$
$FC_R=DCR_{max,C}\ \exp(-0.5\cdot k\cdot \beta_{CR}{}^2/b) = 1.0\ \exp(-0.5\cdot 2.76\cdot 0.20^2/1.0) = 0.9463$

For a confidence level of 60%, the lognormal standard variate is K_x=0.253 and the evaluation inequality becomes:

$FC_R > FD_{RPo}\ \exp(K_x\cdot \beta_{TU}) = 0.4076\ \exp(0.253\cdot 0.20) = 0.4288$

Since the factored capacity of 0.9463 is greater than the factored demand of 0.4288 the result is satisfactory at the 60% confidence level.

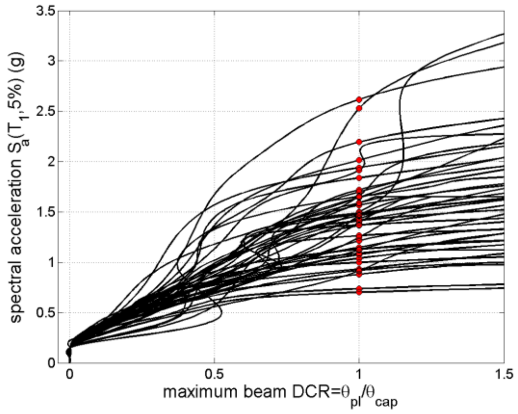

(a)

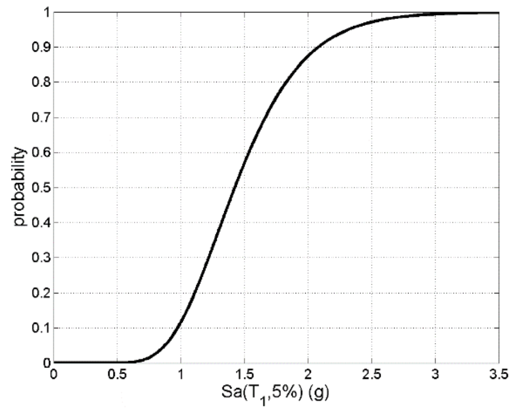

(b)

Figure 3.53: IDA approach for estimating mean annual frequency of exceeding demand capacity ratio limit of 1.0 for beams: (a) the $S_a(T_1,5\%)$ values calculated for DCR=1, and (b) corresponding fragility curve – four story moment resisting frame building designed using method C.

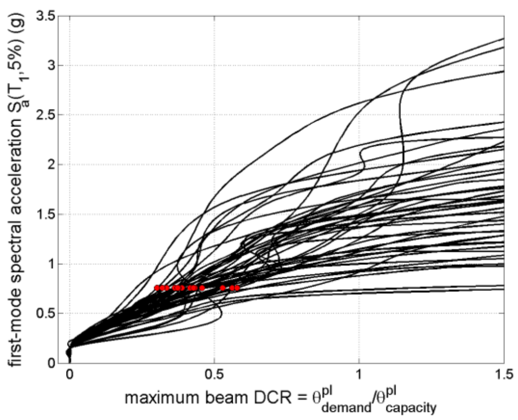

(a)

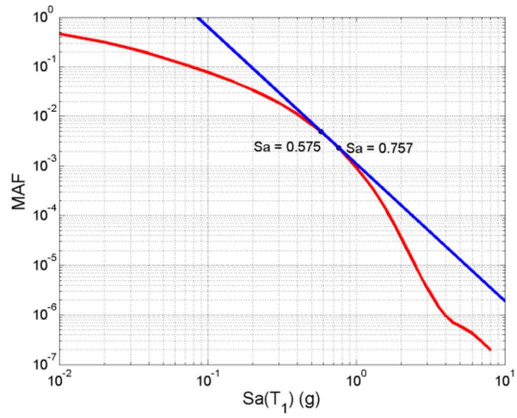

(b)

Figure 3.54: Single stripe analysis method for estimating FD_{RPo} and FC_R for DCR=1 of beams: (a) maximum beam DCR calculated for S_a^{design}, and (b) the local fit of the seismic hazard curve – four story moment resisting frame building designed using method C.

DCR values for the plastic rotation of beams are also calculated for 17 records for S_a^{design}=0.76g (red points) and for $1.1S_a^{design}$=0.83g (green points) (Figure 3.55 (a)) and the corresponding hazard fit to define the slope k is presented in Figure 3.55 (b). FD and FC are estimated as:

$FD_{RPo}=DCR_{max,50}\ \exp(0.5\cdot k\cdot \beta_{\theta max|Sa}{}^2/b) = 0.388\ \exp(0.5\cdot 2.88\cdot 0.19^2/1.78) = 0.3995$
$FC_R=DCR_{max,C}\ \exp(-0.5\cdot k\cdot \beta_{CR}{}^2/b) = 1.0\ \exp(-0.5\cdot 2.88\cdot 0.20^2/1.78) = 0.9681$

For a confidence level of 60%, the lognormal standard variate is K_x=0.253 and the evaluation inequality becomes:

$FC_R > FD_{RPo}\ \exp(K_x\cdot \beta_{TU}) = 0.3995\ \exp(0.253\cdot 0.20) = 0.4202$

As the factored capacity of 0.9681 is greater than the factored demand of 0.4202 the result is satisfactory at the 60% confidence level.

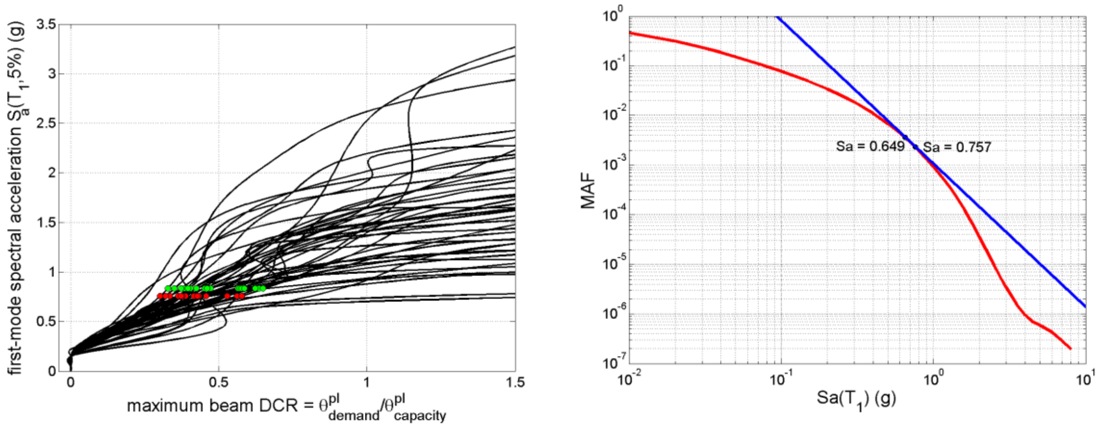

(a) (b)

Figure 3.55: Double stripe analysis method for estimating FD_{RPo} and FC_R for DCR=1 of beams: (a) maximum beam DCR calculated for S_a^{design} (red points) and for $1.1S_a^{design}$ (green points), and (b) local fit of the seismic hazard curve – four story moment resisting frame building designed using method C.

IDA curves in terms of the first mode spectral acceleration $S_a(T_1,5\%)$ and maximum demand capacity ratio, DCR=$(\theta_{demand}{}^{pl}/\ \theta_{capacity}{}^{pl})_{\max}$ for columns are presented in Figure 3.56 (a). Similarly, the MAF of exceeding DCR=1.0 is estimated using the fragility curve with median value of equal to 1.70g and standard deviation to 34%. The estimated mean annual frequency of exceeding *DCR*=1.0 at 60% confidence equals to 0.00030, which is lower than the corresponding code value of 0.0021 (10% probability of exceeding PO in 50 years). This means that the performance objective is met.

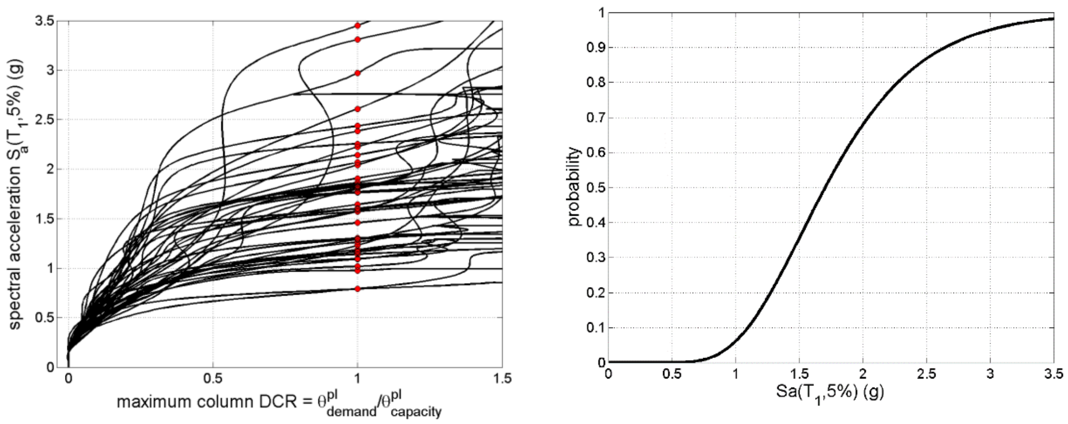

(a) (b)

Figure 3.56: IDA approach for estimating mean annual frequency of exceeding demand capacity ratio limit of 1.0 for columns: (a) the $S_a(T_1,5\%)$ values calculated for DCR=1, and (b) corresponding fragility curve– four story moment resisting frame building designed using method C.

The maximum demand capacity ratio demand for columns as calculated for 17 records for S_a^{design}=0.76g, appears in Figure 3.57 (a) and the corresponding hazard fit to define the slope *k* is presented in Figure 3.57 (b). FD and FC are estimated as:

FD_{RPo}=$DCR_{max,50}$ exp(0.5·k·$\beta_{\theta max|Sa}{}^2$/$b$) = 0.173 exp(0.5·2.68·0.31^2/1.0) = 0.1973
FC_R=$DCR_{max,C}$ exp(-0.5·k·$\beta_{CR}{}^2$/b) = 1.0 exp(-0.5·2.68·0.20^2/1.0) = 0.9481

For a confidence level of 60%, the lognormal standard variate is K_x=0.253 and the evaluation inequality becomes:

FC_R > FD_{RPo} exp(K_x·β_{TU}) = 0.1973 exp(0.253·0.20) = 0.2075

Since the factored capacity of 0.9481 is greater than the factored demand of 0.2075 the result is satisfactory at 60% confidence level.

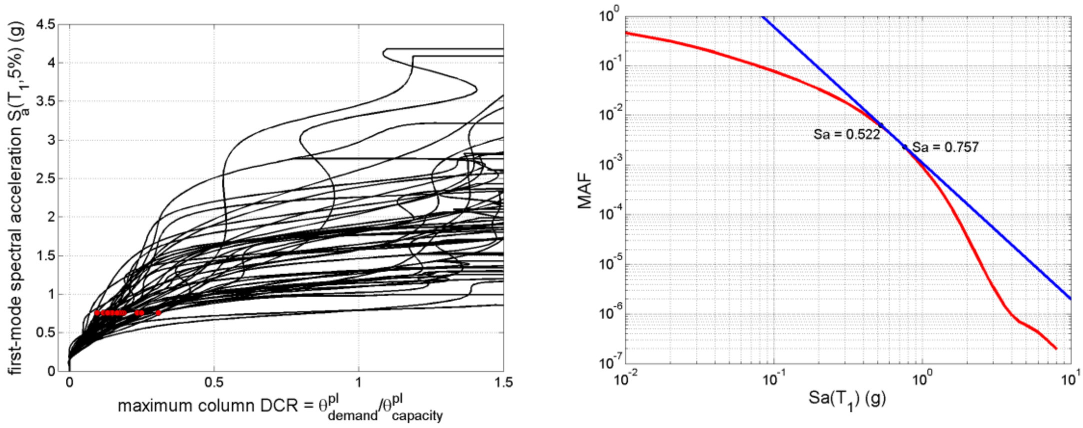

(a) (b)

Figure 3.57: Single stripe analysis method for estimating FD_{RPo} and FC_R for DCR=1 of columns: (a) maximum column DCR calculated for $S_a{}^{design}$, and (b) the local fit of the seismic hazard curve – four story moment resisting frame building designed using method C.

Similarly, the DCR values for the plastic rotation of columns are also calculated at $S_a{}^{design}$=0.76g (red points) and at 1.1$S_a{}^{design}$=0.83g (green points) (Figure 3.58 (a)). The points of the hazard curve that define the slope k are presented in Figure 3.58 (b). FD and FC are estimated as:

FD_{RPo}=$DCR_{max,50}$ exp(0.5·k·$\beta_{\theta max|Sa}{}^2$/$b$) = 0.173 exp(0.5·2.75·0.31^2/1.45) = 0.1899
FC_R=$DCR_{max,C}$ exp(-0.5·k·$\beta_{CR}{}^2$/b) = 1.0 exp(-0.5·2.75·0.20^2/1.45) = 0.9629

For a confidence level of 60%, the lognormal standard variate is K_x=0.253 and the evaluation inequality becomes:

FC_R > FD_{RPo} exp(K_x·β_{TU}) = 0.1899 exp(0.253·0.20) = 0.1998

Since the factored capacity of 0.9629 is greater than the factored demand of 0.1998 the result is satisfactory at the 60% confidence level.

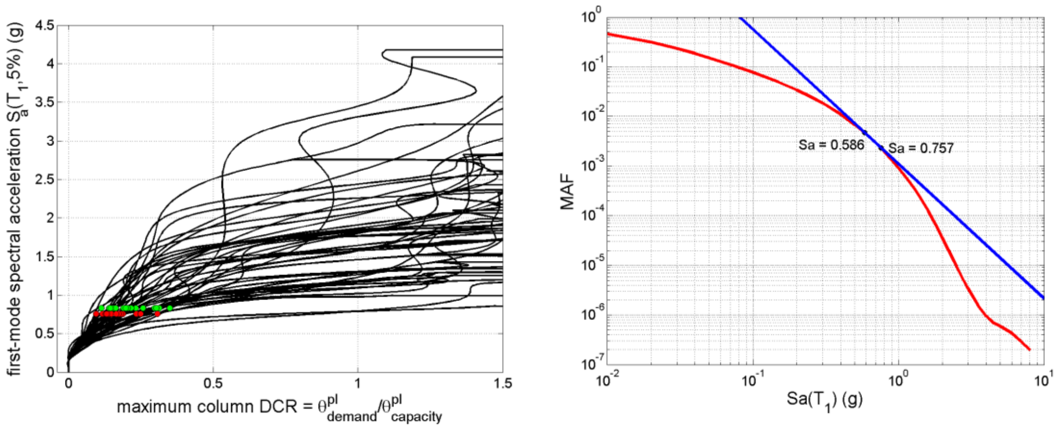

(a) (b)

Figure 3.58: Double stripe analysis method for estimating FD_{RPo} and FC_R for DCR=1 of columns: (a) maximum column DCR calculated for S_a^{design} (red points) and for $1.1S_a^{design}$ (green points), and (b) local fit of the seismic hazard curve – four story moment resisting frame building designed using method C.

The acceptability of ductility limit of 1.5 is assessed at the 50/50 level. This ductility limit is equivalent to a roof drift ratio capacity of $\theta_{roof} = 3.6\ \Delta_y/H_{tot} = 3.6 \cdot 3.7 / 648 = 0.0086$. IDA curves in terms of the first mode spectral acceleration $S_a(T_1,5\%)$ and roof drift ratio, θ_{roof} are presented in Figure 3.59 (a). The MAF of exceeding $\theta_{roof} = 0.0086$ is estimated using the fragility curve with median value equal to 0.74g and standard deviation to 21%. The estimated mean annual frequency of exceeding θ_{roof} =0.0086 at 50% confidence equals 0.0028, which is higher than the corresponding value of 0.0139 (50% in 50 years).

The θ_{roof} demand as calculated for 17 records for S_a^{design}=0.76g, appears in Figure 3.60 (a) and the corresponding hazard fit to define the slope k is presented in Figure 3.60 (b). FD and FC at 50% confidence are estimated as:

$FD_{RPo}=\theta_{max,50}\ \exp(0.5\cdot k\cdot \beta_{\theta max|Sa}{}^2/b) = 0.0046\ \exp(0.5\cdot 1.59\cdot 0.06^2/1) = 0.0046$
$FC_R=\theta_{max,C}\ \exp(-0.5\cdot k\cdot \beta_{CR}{}^2/b) = 0.02\ \exp(-0.5\cdot 1.59\cdot 0.20^2/1) = 0.0083$

Since the factored capacity of 0.0083 is greater than the factored demand of 0.0046 the result is satisfactory at 50% confidence level.

θ_{roof} demand values are calculated for 17 records for $S_a^{50\%/50}$=0.36g (red points) and for $1.1S_a^{50\%/50}$=0.40g (green points) (Figure 3.61 (a)). The points of the hazard curve needed to estimate the slope k are presented in Figure 3.61 (b). FD and FC at 50% confidence (K_x=0) are estimated as:

$FD_{RPo}=\theta_{roof,50}\ \exp(0.5\cdot k\cdot \beta_{\theta max|Sa}{}^2/b) = 0.0046\ \exp(0.5\cdot 1.59\cdot 0.056^2/0.97) = 0.0046$
$FC_R=\theta_{roof,C}\ \exp(-0.5\cdot k\cdot \beta_{CR}{}^2/b) = 0.0086\ \exp(-0.5\cdot 1.59\cdot 0.20^2/0.97) = 0.0083$

Since the factored capacity of 0.0083 is greater than the factored demand of 0.0046 the result is satisfactory at the 50% confidence level.

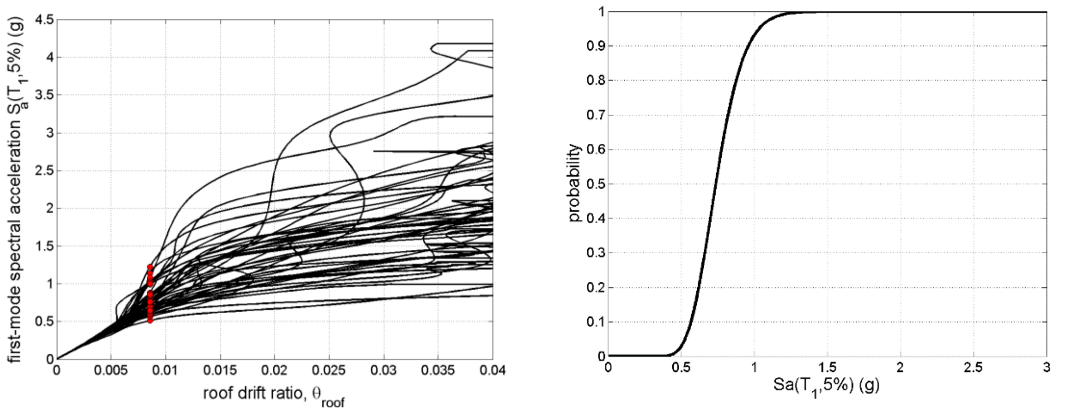

(a) (b)

Figure 3.59: IDA approach for estimating mean annual frequency of exceeding ductility limit of 1.5: (a) the $S_a(T_1,5\%)$ values calculated for $\theta_{roof} = 0.0086$, and (b) corresponding fragility curve – four story moment resisting frame building designed using method C.

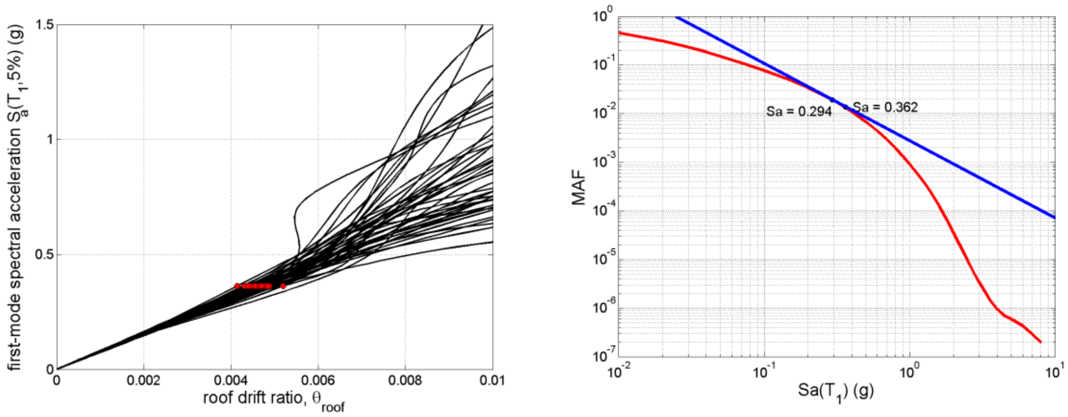

(a) (b)

Figure 3.60: Single stripe analysis method for estimating FD_{RPo} and FC_R for ductility limit of 1.5: (a) roof drift ratio values calculated for $S_a^{50\%/50}$ (red points), and (b) local fit of the seismic hazard curve – four story moment resisting frame building designed using method C.

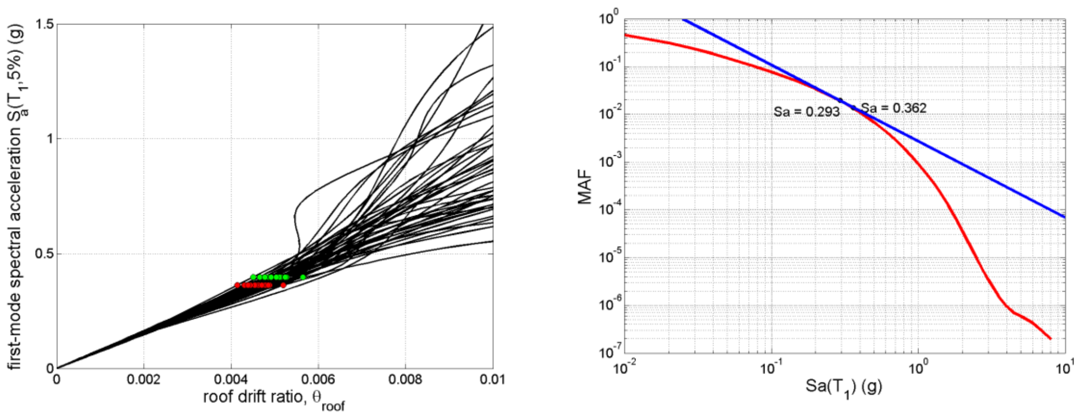

(a) (b)

Figure 3.61: Double stripe analysis method for estimating FD_{RPo} and FC_R for ductility limit of 3.6: (a) θ_{roof} calculated for $S_a^{50\%/50}$ (red points) and for $1.1S_a^{50\%/50}$ (green points), and (b) local fit of the seismic hazard curve – four story moment resisting frame building designed using method C.

Global collapse is deemed to occur when numerical non-convergence appears or a large maximum interstory drift of 8% is exceeded, whichever occurs first. In this case, the first criterion governed, and the corresponding values of $S_a(T_1,5\%)$ at the onset of collapse are employed to define the fragility curve (Figure 3.62). The median value of the lognormal distribution equals 2.08g and the standard deviation is 38%. By convolving with the hazard curve of Figure 3.49, the estimated MAF at 90% confidence, equals 0.000456, which is about 2.5 times the required target of 1% in 50yrs, or 0.000201, while only slightly greater than 2% in 50yrs value of 0.000404. Note that there is an exponential relationship between the C_y and the MAF, therefore such large differences in MAF actually translate to much smaller difference in design strength. Obviously, the performance objective is not met. Here, the analyst has two choices, namely redesign or attempt an even more accurate (and elaborate) assessment. The reason for the latter is that IDA can be conservative close to global collapse (Luco and Bazzurro, 2007), as the simple amplitude scaling that it employs may not allow for capturing the appropriate spectral shape of high intensity ground motions (Baker and Cornell 2006). Specifically, FEMA P-695 (FEMA 2009) recommends employing a spectral shape factor (SSF), which by the way has been determined specifically for the employed suite of 44 ground motions, to adjust *upwards* the collapse capacity. Although this remains a crude approximation and better methods do exist for achieving unbiased assessment of global collapse (e.g., see Lin et al. 2013, Kohrangi et al. 2017), it can help us achieve our goal. For the case at hand, for a global ductility of 6, period $T_1 \approx 0.8$s and assuming Seismic Design Category D_{max}, Table 7-1b of FEMA P695 suggests SSF = 1.35. Now, the adjusted global collapse fragility has a median value of 1.35·2.08g = 2.81g with the same standard deviation of 38%. This results to an improved MAF estimate of 0.000148 that meets the performance objective of 0.000201. It is noted that no such easy shortcut exists in current literature for limit-states other than global collapse; therefore, if higher accuracy is sought, the aforementioned advanced methods involving record selection would need to be considered.

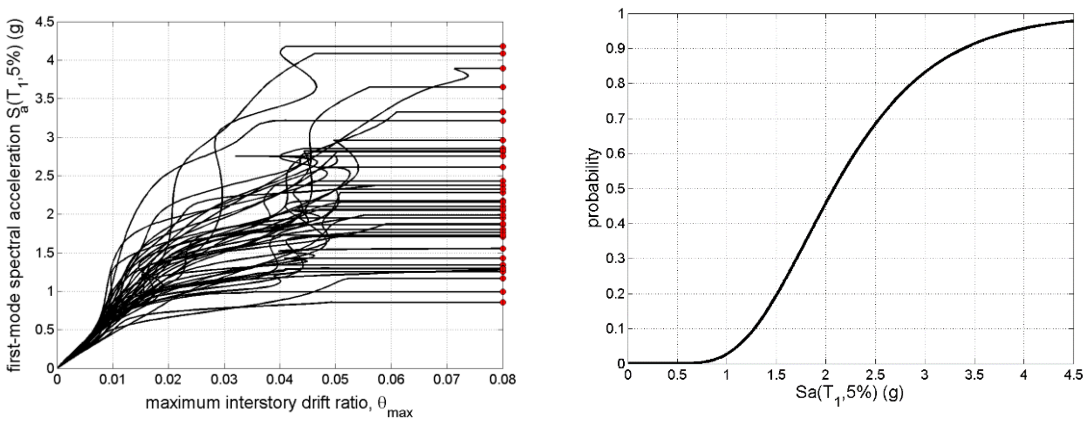

(a) (b)

Figure 3.62: IDA approach for estimating mean annual frequency of collapse: (a) the $S_a(T_1,5\%)$ values calculated for 8% maximum interstory drift ratio limit, θ_{max}, and (b) corresponding fragility curve – four story moment resisting frame building designed using method C.

4 Coupled wall

4.1 Building geometry

A 12-story reinforced concrete frame structure is examined. The plan of the building is shown in Figure 3.1 (b), having dimensions equal to 30x20 m. The perimeter coupled walls resist all the seismic loading in the y direction, while the inner columns carry only the gravity loads. The coupled wall consists of two rectangular cross section walls having plan length of 4.5m and thickness of 0.4m. The coupling beams that connect the two walls have 1m length, 0.7m height and 0.4m width. The height of the first story is 4.5m while the rest of the stories are 3.5m height, resulting in a total height of 41.9m. The coupled wall is presented in Figure 4.1 (a).

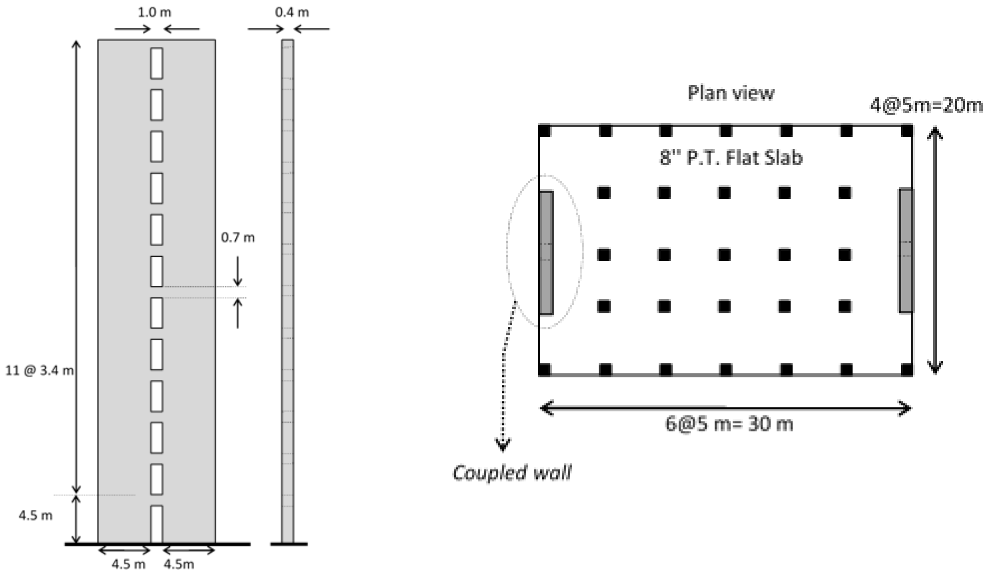

(a) (b)

Figure 4.1: Coupled wall building: (a) coupled wall consisting of two rectangular cross section walls and coupling beams, and (b) typical plan of the building.

4.2 Material properties

C30 concrete and B500 steel reinforcement is used. The coupled wall is designed using nominal material properties, thus the compressive strength of the concrete is f_{ck} = 30MPa and the yield strength of the steel rebars is f_{yk} = 500MPa. The material safety factors used in the design are γ_s = 1.0 and γ_c = 1.0. For the performance assessment, the expected material properties are used, thus f_{ce}= 38MPa, f_{ye}= 575MPa and f_{ye}= 680MPa. The elastic modulus is estimated as $E_c = 4700(f_{ce})^{0.5}$, where f_{ce} and Ec are expressed in MPa units.

4.3 Initial design

The initial design of the coupled wall using the YPS (design method A) can be found in detail in Aschheim et al., [7] along with an analytical description of this design method. Only some of the key points of the design are listed in this documentation. The design is comparable to that obtained in current codes. The performance objectives that are taken into account are:

❖ Ductility limit of 3.3 at the 10% probability of exceedance in 50 years

❖ Interstory drift ratio limit of 0.02

The first mode parameters of the coupled wall are estimated as α_1 =0.79 and Γ_1=1.45.The yield displacement is estimated as Δ_y = 0.102m. Based on the interstory drift ratio limit of 0.02, the peak roof displacement is $D_{u,drift}$ = 0.71m, so the resulting ductility is μ = 0.70/0.102 = 6.96. The more restrictive ductility limit of 3.3 = min{6.96;3.3} at the 10/50 level is used for the design. The Yield Point Spectrum representation, that is generated using the elastic response spectrum reduced by the behavior factor q representing different ductilities, is presented in Figure 4.2. For a yield displacement of the ESDOF system equal to $\Delta_y^* = \Delta_y/\Gamma_1$ = 0.07m and μ = 3.3, the required design spectra acceleration is S_d =1.17g, thus $C_y^* = S_d/g$ = 0.12. The base shear coefficient at yield is thus $C_y = \alpha_1 \cdot C_y^*$ = 0.095 and the design base shear is $V = C_y \cdot W$ = 2615kN. The associated period of vibration is estimated as 1.54sec, using Equation (3.5).

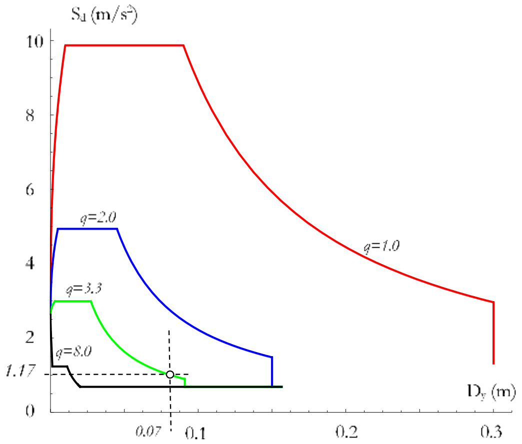

Figure 4.2: Yield Point Spectrum (YPS) representation of EC-8 Design Spectra for initial proportioning of the coupled wall. For a system with yield displacement Δ_y^*=0.07m and μ=3.3 the required design spectra acceleration is S_d =1.17m/s2, thus C_y^* = 0.12 (twelve story coupled wall building designed using method A), (from Aschheim et al., forthcoming [7]).

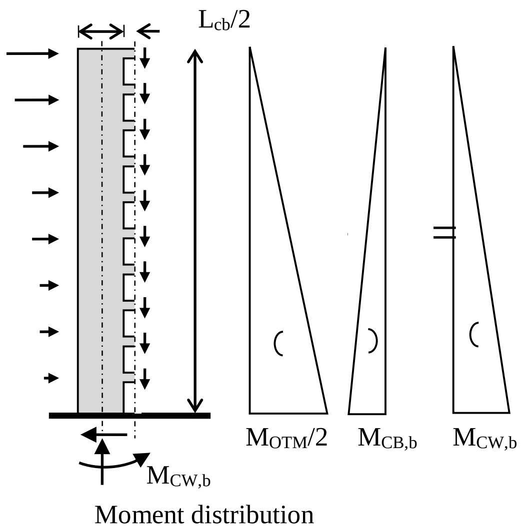

Figure 4.3: Coupled wall mechanism analysis – twelve story coupled wall building designed using method A (from Aschheim et al., forthcoming [7]).

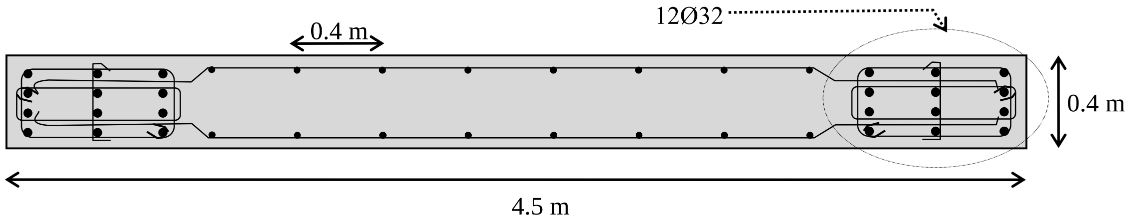

Figure 4.4: Longitudinal reinforcement of the wall – twelve story coupled wall building designed using method A (from Aschheim et al., forthcoming [7]).

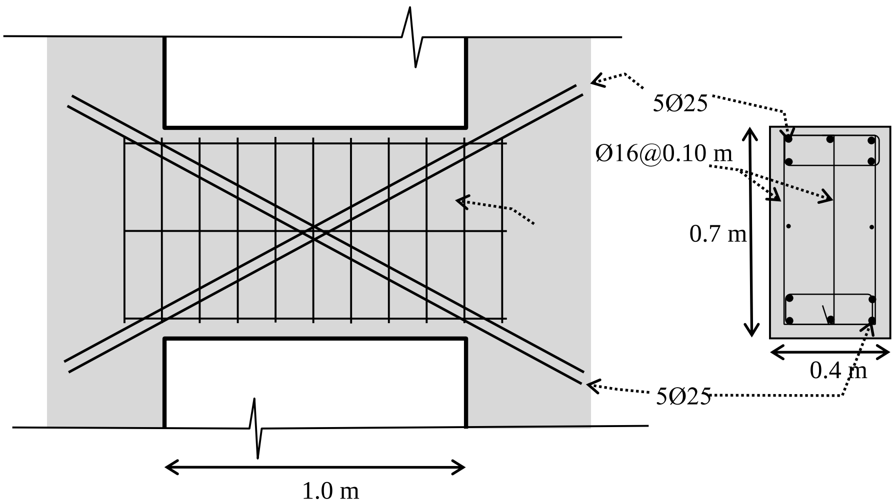

Figure 4.5: Reinforcement of the coupling beams – twelve story coupled wall building designed using method A (from Aschheim et al., forthcoming [7]).

A first mode proportional lateral force distribution according to EC-8 is used in the design. The desired mechanism of failure is the one presented in Figure 4.3, where M_{OTM} is the overturning moment at the base of the wall due to the horizontal seismic forces and $M_{CB,h}$ is the total moment of the coupling beams at the base. The members are designed according to the resulting moment distribution. The cross section of the wall is designed to satisfy the EC-2 detailing requirements and is shown in Figure 4.4. The reinforcement of the coupling beams is shown in Figure 4.5.

Although it is not explicitly required by the design method, the initial design is assessed using IDA and single and double stripe analysis.

4.4 Non-linear modeling and acceptance criteria

A two dimensional model of the structure is shown in Figure 4.6. Only one out of the two coupled walls is modeled in the direction of interest. A leaning column is added to simulate the effect of the columns that carry the gravity loads. The leaning column is pinned at the foundation and modeled using linear elastic elements having area and moment of inertia that match the corresponding cross sectional properties of one half of the gravity columns of the building. A beam-column element is placed at the centerline of each of the two coupled walls (blue color) and it is connected at the level of each floor to the coupling beams (green color) by using rigid links (black color) with a length equal to one half of the wall length. The diaphragm constraint is imposed using the same technique is in the distributed plasticity model of the four story moment resisting frame (Section 3.3.1), in order to avoid generating of fictitious axial forces on the beam. The leaning column (red color) is constrained to the leftmost nodes of the coupled wall at each floor.

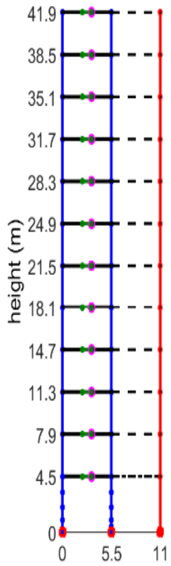

Figure 4.6: Two dimensional structural model used for the analysis showing the walls (blue color), beams (green color), rigid links (black color), the leaning column (red color) and the rotational spring (pink color) used with the truss elements to model the diaphragm, (dimensions in m) for the 12 story coupled wall building.

Each of the two coupled walls is modelled by using a single displacement-based distributed plasticity element per each story, with fiber section representation monitored at five integration points along the member's length. Force-based elements are usually preferable due to their improved capability at capturing plastic hinges along their length, yet at the same time they complicate the response history analysis and introduce many convergence issues. Displacement based elements offer easier convergence, at the cost of requiring improved element discretization where inelasticity will appear. Since all plastic rotations are expected to appear at the base, the first-story walls are discretized into five displacement based elements per member having progressively diminishing length with the height from the ground, as shown in Figure 4.6. A comparison of the model to its force-based analogue showed excellent agreement at all levels of inelasticity.

The wall section is discretized into longitudinal steel and concrete fibers (Figure 4.7), the latter having different confinement factors for the cover, the well-confined core at the edges (green) and the semi-confined core of the web (red). The effect of confinement is calculated on the basis of the Mander et al. (1988) model with a resulting confinement ratio of 1.4 for the edge core concrete (green) at the base of the wall, assuming a 10mm diameter for the transverse reinforcement, placed as indicated in Figure 4.4 every 10cm along the height in the region of the expected plastic hinge. The confinement ratio of the web core concrete (red) is estimated at 1.1. Furthermore, steel reinforcing bars (black color in Figure 4.7) are modelled using a bilinear constitutive law accounting for pinching and stiffness degradation. Each beam is modelled using six displacement based elements, with similarly modelled behavior of steel and cover/confined concrete as applied in the wall section. As mentioned earlier, the expected material properties are used for the analysis, i.e., f_{ce} = 39MPa and f_{ye} = 575MPa.

A number of different assumptions were made for the post-capping behavior of each material. In all cases, attempting to implement a realistic and severely degrading behavior of the steel or concrete fibers beyond their maximum strength was found to generate convergence problems. Thus, generous assumptions are made regarding the post-capping behavior to ease convergence. The resulting static pushover capacity curve for a first-mode-proportional lateral load pattern appears in Figure 4.8. The effect of the relaxed material deterioration appears in the residual plateau of nearly 40% the maximum strength that appears beyond a roof displacement of 0.6m, or approximately a maximum interstory drift of 3%. To make sure the structural performance is not artificially boosted by this assumption, global collapse has been set at the 3% drift, essentially assuming a vertical drop to zero strength, rather than an extended plateau beyond this deformation.

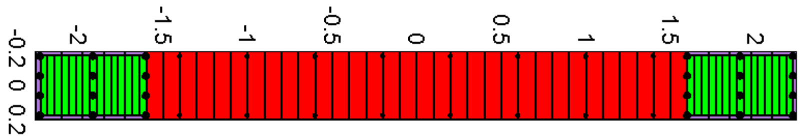

Figure 4.7: Coupled wall: Typical section fiber discretization used to model the wall showing rebars (black), semi confined (red) and confined (green) concrete fibers, (dimensions in m)

The initial (uncracked) period of the model is 0.88sec. This period corresponds to ultra-low deformations. In that case, to achieve better fidelity in the performance assessment, an appropriate increased period the structure is calculated using the secant stiffness at 60% of the maximum base shear V_{max}

$$T_{\mathrm{eff}} = T_1 \sqrt{\frac{k_{in}}{k_{eff}}} = 1.51\mathrm{sec} \tag{4.1}$$

matching fairly well with the 1.54sec estimated in design. Thus, in the following the first-mode period will be taken as $T_1 = T_{\mathrm{eff}} = 1.51$sec.

In Tables 4.1 and 4.2 the acceptance criteria for wall and coupling beam plastic rotations, respectively, are presented.

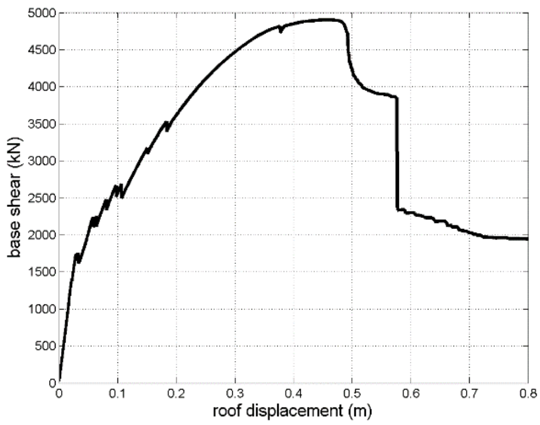

Figure 4.8: Static pushover curve resulting from a first mode proportional lateral load pattern – twelve story coupled wall building designed using method A.

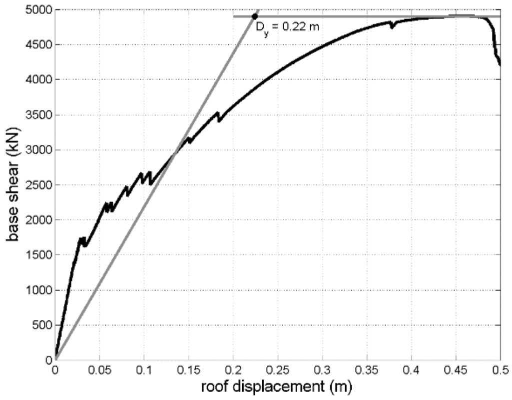

Computed performance:

V_{max} = 4903 kN

$\Delta_y^{60\%Vmax}$ = 0.22.m

$C_y = V_{max}/W$ = 4903/27546 = 0.178

T_{eff} = 1.51sec

Figure 4.9: Calculation of nominal Δ_y by fitting the elastic segment at the 60%V_{max} point of the pushover – twelve story coupled wall building designed using method A.

Table 4.1: Acceptance criteria for wall plastic rotations – twelve story coupled wall building designed using method A.

PO	IO	LS	CP
$\theta_{p,max}$ (rad)	0.005	0.017	0.020

Table 4.2: Coupled wall: Acceptance criteria for coupling beam plastic rotations – twelve story coupled wall building designed using method A.

PO	IO	LS	CP
$\theta_{p,max}$ (rad)	0.006	0.030	0.050

4.5 Performance evaluation of the initial design by nonlinear dynamic analysis

The acceptability of interstory drift ratio of 2%, ductility limit of 3.3 and plastic hinge rotations is assessed versus a 10% in 50yrs MAF at the 50%, 50%, and 60% confidence levels, respectively, using IDA, single and double stripe analysis. For each performance objective, the results are summarized in Table 4.3 and Table 4.4. For IDA, the first two values of each PO correspond to estimated and allowable MAF, and for the stripe analysis they correspond to factored demand and factored capacity, respectively.

Table 4.3: Verification of the maximum interstory drift and beam plastic rotations for the twelve story coupled wall building designed using method A.

	IDR			beam plastic rotation		
	IDA	Single	Double	IDA	Single	Double
	(yrs^{-1})	–	–	(yrs^{-1})	(rad)	(rad)
Demand	0.0005	0.0115	0.0116	0.0002	0.2472	0.2040
Capacity	0.0021	0.0190	0.0182	0.0021	0.9571	0.9816
Check	✓	✓	✓	✓	✓	✓
Confidence		50 %			60%	

Table 4.4: Verification of wall plastic rotations and global ductility limits for the twelve story coupled wall building designed using method A.

	wall plastic rotation			global ductility		
	IDA (yrs^{-1})	Single (rad)	Double (rad)	IDA (yrs^{-1})	Single –	Double –
Demand	0.0002	0.1215	0.0983	0.0005	0.0091	0.0093
Capacity	0.0021	0.9593	0.9736	0.0021	0.0165	0.0163
Check	✓	✓	✓	✓	✓	✓
Confidence	60 %			50 %		

The seismic hazard curve properly scaled to $S_a(T_{\mathrm{eff}})$ at 10% in 50 years, is shown in Figure 4.10

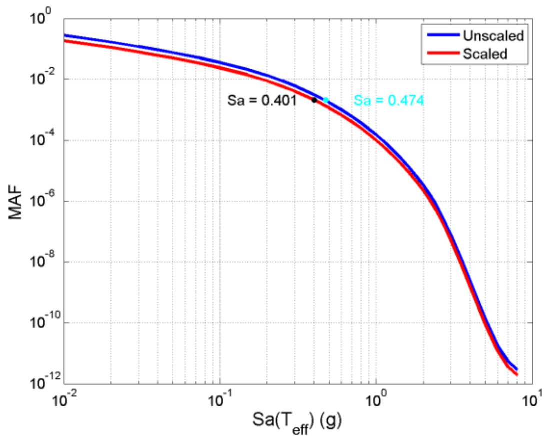

Figure 4.10: Seismic site hazard curve properly scaled to 10% in 50 years for $S_a(T_{\mathrm{eff}})$ used in for the performance assessment of the twelve story coupled wall building designed using Method A.

IDA is first employed to estimate the MAF of exceeding the maximum interstory drift ratio of 2%. The median value of the fragility curve is equal to 0.78g and the standard deviation is 36% (Figure 4.11 (b)). The hazard curve used to estimate the MAF is the one presented in Figure 4.10. The estimated mean annual frequency of exceeding the ductility limit, at 50% confidence, equals 0.00050, which is lower than the corresponding code value of 0.0021 (10% probability of exceeding PO in 50 years). This means that the performance objective is met.

Interstory drift values are calculated for 17 records for S_a^{design}=0.40g (red points) (Figure 4.12 (a)). The points of the hazard curve that define the slope k are presented in Figure 4.12 (b). FD and FC at 50% confidence are estimated as:

$$FD_{RPo}=\theta_{max,50}\ \exp(0.5\cdot k\cdot \beta_{\theta max|Sa}{}^2/b) = 0.0113\ \exp(0.5\cdot 2.53\cdot 0.11^2/1.0) = 0.0115$$
$$FC_R=\theta_{max,C}\ \exp(-0.5\cdot k\cdot \beta_{CR}{}^2/b) = 0.02\ \exp(-0.5\cdot 2.53\cdot 0.20^2/1.0) = 0.0190$$

Since the factored capacity of 0.0190 is greater than the factored demand of 0.0115 the result is satisfactory at the 50% confidence level.

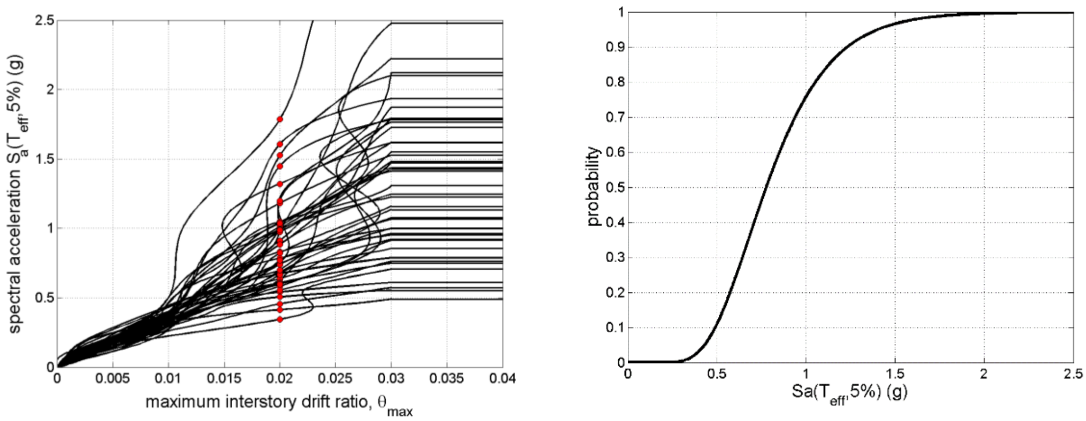

(a) (b)

Figure 4.11: IDA approach for estimating mean annual frequency of exceeding the maximum interstory drift ratio of 2%: a) the $S_a(T_{eff},5\%)$ values calculated for $\theta_{max} = 0.02$, and (b) corresponding fragility curve – twelve story coupled wall building designed using Method A.

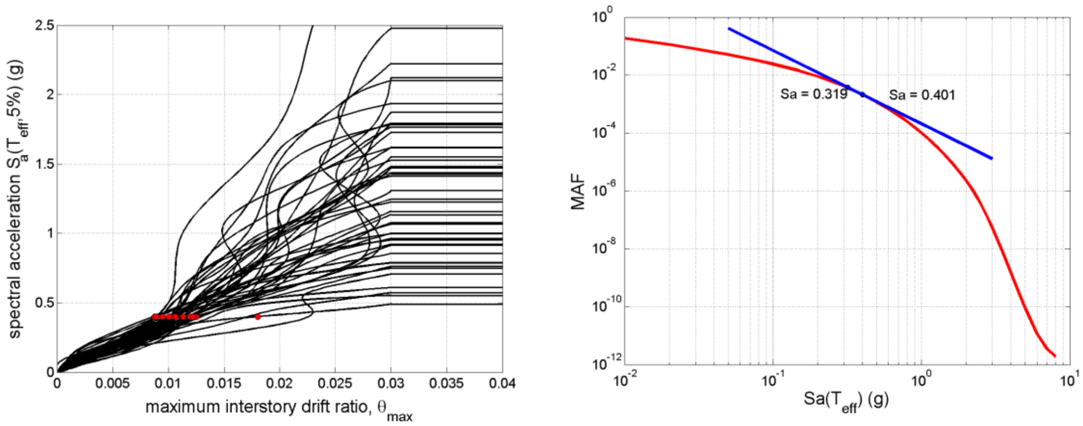

(a) (b)

Figure 4.12: Single stripe analysis method for estimating FD_{RPo} and FC_R for 2% maximum interstory drift ratio: (a) maximum interstory drifts calculated for S_a^{design} (red points). The cut-off value of 3% drift becomes evident by the flatlines. (b) The local fit of the seismic hazard curve – twelve story coupled wall building designed using Method A.

Interstory drift values are calculated for 17 records for S_a^{design}=0.40g (red points) and for 1.1S_a^{design}=0.44g (green points) (Figure 4.13 (a)). The points of the hazard curve needed to estimate the slope k are presented in Figure 4.13 (b). FD and FC at 50% confidence are estimated as:

$$FD_{RPo}=\theta_{max,50}\ \exp(0.5\cdot k\cdot \beta_{\theta max|Sa}{}^2/b) = 0.0113\ \exp(0.5\cdot 2.22\cdot 0.11^2/0.48) = 0.0116$$
$$FC_R=\theta_{max,C}\ \exp(-0.5\cdot k\cdot \beta_{CR}{}^2/b) = 0.02\ \exp(-0.5\cdot 2.22\cdot 0.20^2/0.48) = 0.0182$$

Since the factored capacity of 0.0182 is greater than the factored demand of 0.0116 the result is satisfactory at the 50% confidence level.

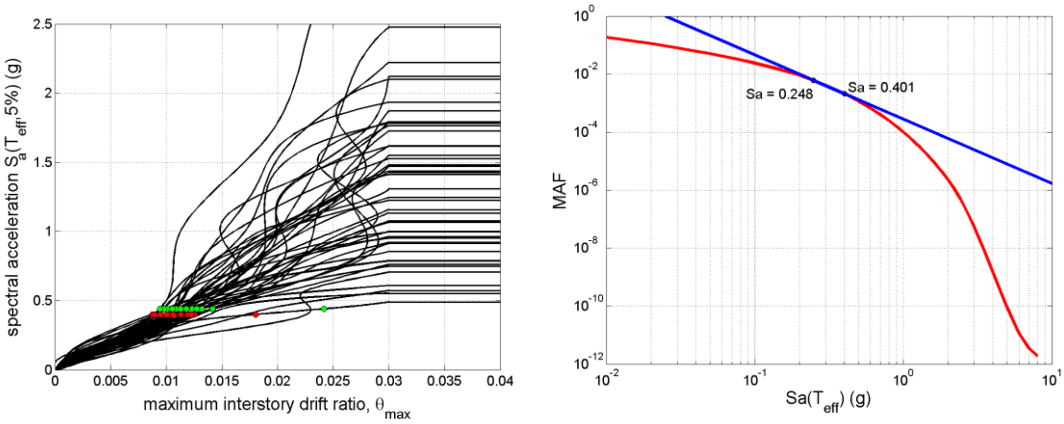

(a) (b)

Figure 4.13: Double stripe analysis method for estimating FD_{RPo} and FC_R for 2% maximum interstory drift ratio: (a) maximum interstory drifts calculated for S_a^{design} (red points) and for $1.1S_a^{design}$ (green points). The cut-off value of 3% drift becomes evident by the flatlines. (b) The local fit of the seismic hazard curve – twelve story coupled wall building designed using Method A.

The mean annual frequency of beams exceeding DCR=1 is calculated by convolving the hazard curve presented in Figure 4.10 with the fragility curve shown in Figure 4.14 (b) (median = 1.22g and dispersion = 44%). The resulting mean annual frequency of exceeding DCR=1, at 50% confidence, is equal to 0.00019 which is lower than the corresponding code value of 0.0021 (10%/50yrs), which means that the performance objective is met.

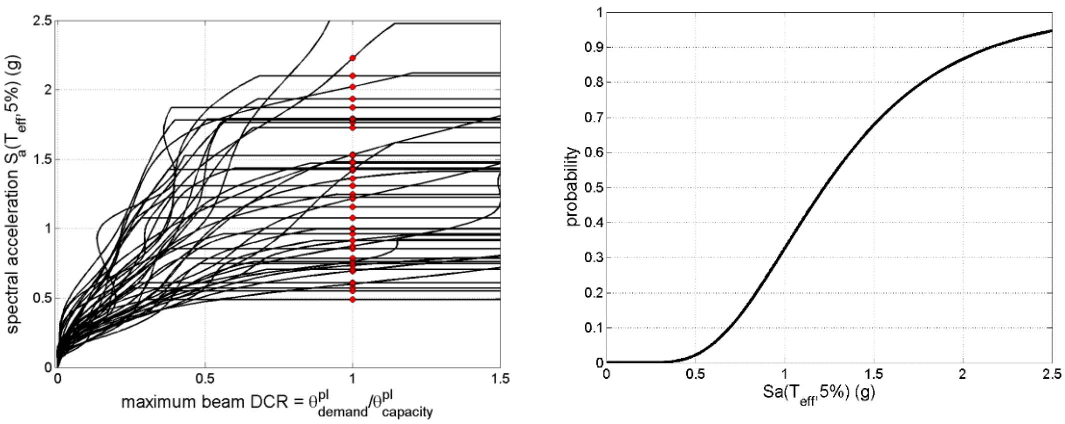

(a) (b)

Figure 4.14: IDA approach for estimating mean annual frequency of exceeding DCR=1 for beams: a) the $S_a(T_{eff},5\%)$ values calculated for DCR=1. 0, and (b) corresponding fragility curve – twelve story coupled wall building designed using Method A.

The coupling beam plastic rotation DCR values are also calculated at S_a^{design}=0.40g (red points), as shown in Figure 4.15 (a).

It is noted here that there are cases (i.e., records) where the coupling beams yield and others where they do not; thus we often encounter zero (or near-zero) plastic rotations mixed together with non-zero ones. This does not abide with the lognormal assumption for demand that is required for utilizing the FC and FD approach for assessment. Actually, this may easily cause a gross overestimation of demand dispersion, often making it appear as larger than 100% when typical values are less than 60%. This can cause the check to fail, even though it should actually pass quite easily. This can be resolved by simply discarding such low values (in our case all records with DCR<0.03) to perform a slightly more conservative assessment that is actually a lot more accurate under a lognormal assumption.

The points of the hazard curve needed to estimate the slope k are presented in Figure 4.15 (b). FD and FC are estimated as:

FD_{RPo}=$DCR_{max,50}$ $\exp(0.5\cdot k\cdot\beta_{DCRmax|Sa}^2/b) = 0.168 \exp(0.5\cdot 2.19\cdot 0.55^2/1.0) = 0.2350$
FC_R=$DCR_{max,C}$ $\exp(-0.5\cdot k\cdot\beta_{CR}^2/b) = 1.0 \exp(-0.5\cdot 2.19\cdot 0.20^2/1.0) = 0.9571$

For a confidence level of 60%, the lognormal standard variate is K_x=0.253 and the evaluation inequality becomes:

$FC_R > FD_{RPo} \exp(K_x\cdot\beta_{TU}) = 0.2350 \exp(0.253\cdot 0.20) = 0.2472$

Since the factored capacity of 0.9571 is greater than the factored demand of 0.2472 the result is satisfactory at the 60% confidence level.

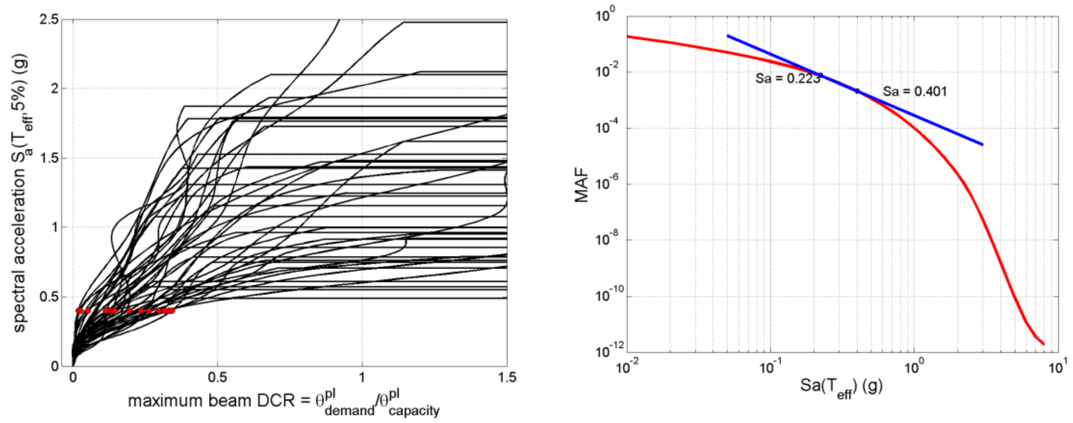

(a) (b)

Figure 4.15: Single stripe analysis method for estimating FD_{RPo} and FC_R for beam DCR=1: (a) maximum beam DCR calculated for S_a^{design} (red points), and (b) the local fit of the seismic hazard curve – twelve story coupled wall building designed using Method A.

The coupling beam plastic rotation DCR values are also calculated at S_a^{design}=0.40g (red points) and for 1.1S_a^{design}=0.44g (green points) (Figure 4.16 (a)). The points of the hazard curve needed to estimate the slope k are presented in Figure 4.16 (b). FD and FC are estimated as:

FD_{RPo}=$DCR_{max,50}$ $\exp(0.5\cdot k\cdot\beta_{DCRmax|Sa}^2/b) = 0.168 \exp(0.5\cdot 2.60\cdot 0.55^2/2.80) = 0.1939$
FC_R=$DCR_{max,C}$ $\exp(-0.5\cdot k\cdot\beta_{CR}^2/b) = 1.0 \exp(-0.5\cdot 2.60\cdot 0.20^2/2.80) = 0.9816$

For a confidence level of 60%, the lognormal standard variate is K_x=0.253 and the evaluation inequality becomes:

$FC_R > FD_{RPo} \exp(K_x\cdot\beta_{TU}) = 0.1939 \exp(0.253\cdot 0.20) = 0.2040$

Since the factored capacity of 0.9816 is greater than the factored demand of 0.2040 the result is satisfactory at the 60% confidence level.

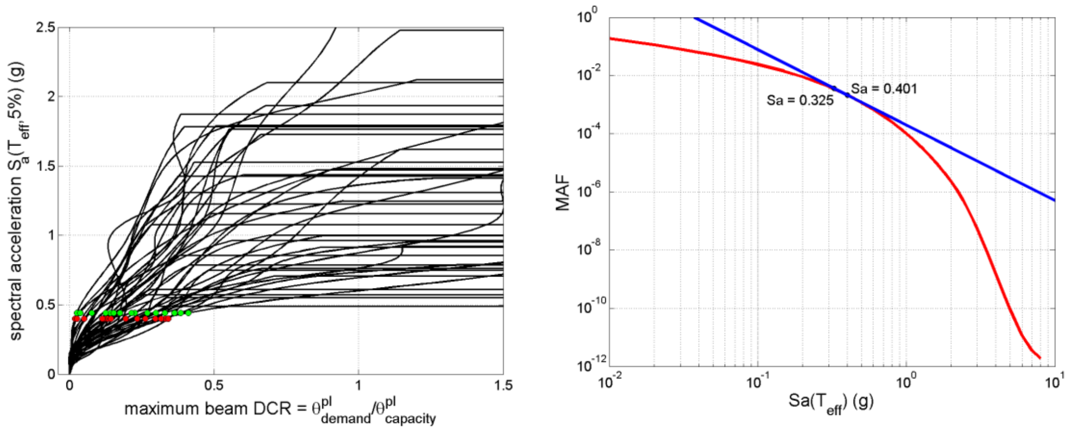

(a) (b)

Figure 4.16: Double stripe analysis method for estimating FD_{RPo} and FC_R for beam DCR=1: (a) maximum beam DCR calculated for S_a^{design} (red points) and for $1.1S_a^{design}$ (green points), and (b) the local fit of the seismic hazard curve – twelve story coupled wall building designed using Method A.

The mean annual frequency of exceeding DCR=1 for wall plastic rotations is calculated by convolving the hazard curve presented in Figure 4.10 with the fragility curve calculated for DCR=1 according to IDA curves (Figure 4.17 (a)), and is shown in Figure 4.17 (b) (median = 1.28g and dispersion = 44%). The resulting mean annual frequency of exceeding DCR=1, at 50% confidence, is equal to 0.00016 which is lower than the corresponding code value of 0.0021 (10%/50yrs), which means that the performance objective is met.

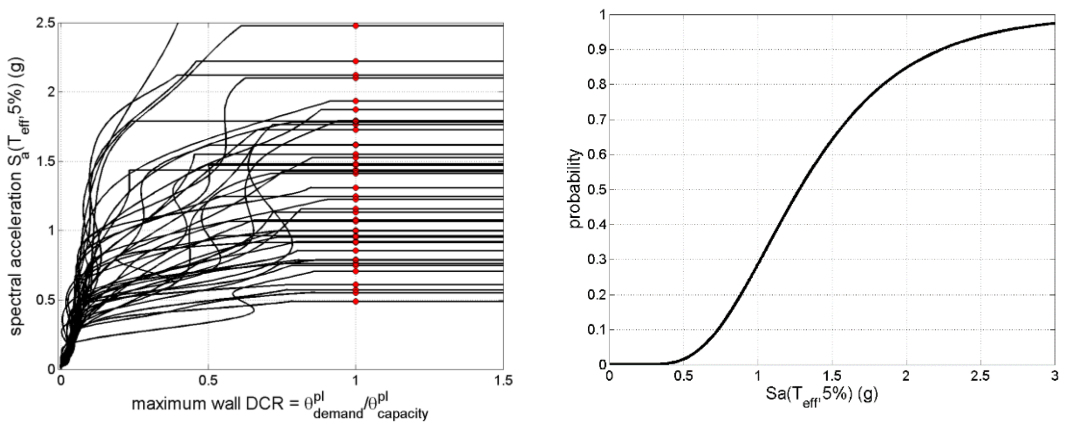

(a) (b)

Figure 4.17: IDA approach for estimating mean annual frequency of exceeding DCR=1 for wall plastic rotation: a) the $S_a(T_{eff},5\%)$ values calculated for DCR =1.0, and (b) corresponding fragility curve – twelve story coupled wall building designed using Method A.

For the single stripe analysis, DCR values are calculated for columns for 17 records for S_a^{design}=0.40g (red points), as shown in Figure 4.18 (a). The points of the hazard curve needed to estimate the slope k are presented in Figure 4.18 (b). FD and FC are estimated as:

$FD_{RPo}=DCR_{max,50}\exp(0.5\cdot k\cdot\beta_{DCRmax|Sa}{}^2/b) = 0.064\exp(0.5\cdot 2.68\cdot 0.75^2/1.0) = 0.1155$
$FC_R=DCR_{max,C}\exp(-0.5\cdot k\cdot\beta_{CR}{}^2/b) = 1.0\exp(-0.5\cdot 2.68\cdot 0.20^2/1.0) = 0.9593$

For a confidence level of 60%, the lognormal standard variate is K_x=0.253 and the evaluation inequality becomes:

$FC_R > FD_{RPo} \exp(K_x \cdot \beta_{TU}) = 0.1155 \exp(0.253 \cdot 0.20) = 0.1215$

Since the factored capacity of 0.9593 is greater than the factored demand of 0.1215 the result is satisfactory at 60% confidence level.

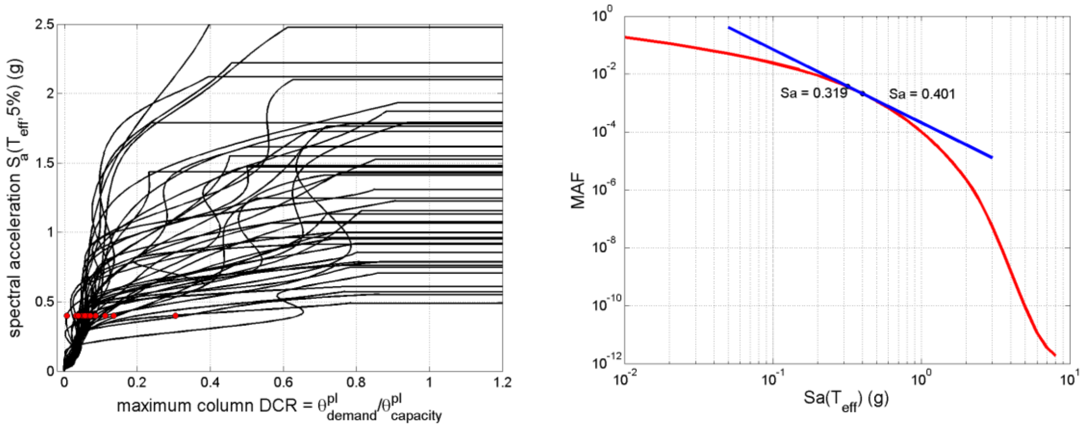

(a) (b)

Figure 4.18: Cantilever wall: Single stripe analysis method for estimating FD_{RPo} and FC_R for column DCR=1: (a) maximum column DCR calculated for S_a^{design} (red points), and (b) the local fit of the seismic hazard curve – twelve story coupled wall building designed using Method A.

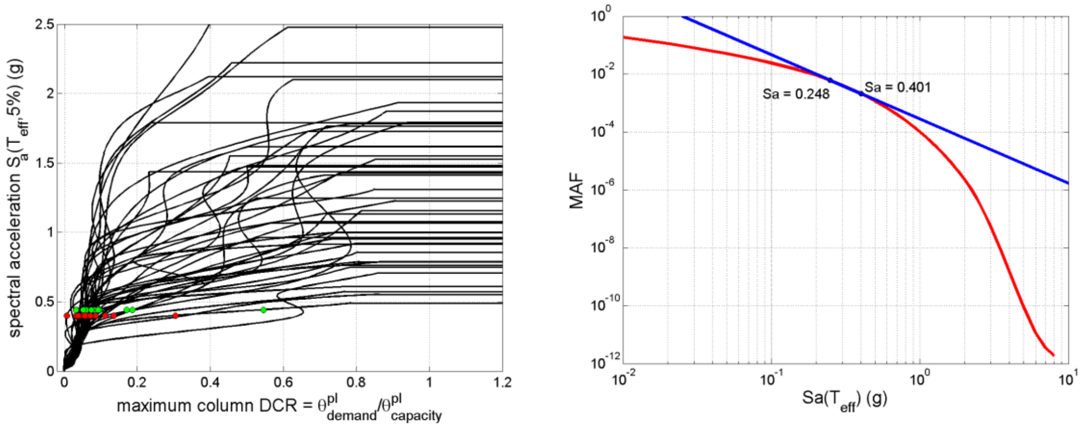

(a) (b)

Figure 4.19: Cantilever wall: Double stripe analysis method for estimating FD_{RPo} and FC_R for column DCR=1: (a) maximum column DCR calculated for S_a^{design} (red points) and for $1.1S_a^{design}$ (green points), and (b) the local fit of the seismic hazard curve – twelve story coupled wall building designed using Method A.

DCR values are also calculated for 17 records for S_a^{design}=0.40g (red points) and for $1.1S_a^{design}$=0.44g (green points) (Figure 4.19(a)). The points of the hazard curve that define the slope k are presented in Figure 4.19 (b). FD and FC are estimated as:

$FD_{RPo}=DCR_{max,50} \exp(0.5 \cdot k \cdot \beta_{DCRmax|Sa}{}^2/b) = 0.064 \exp(0.5 \cdot 2.22 \cdot 0.75^2/1.66) = 0.0935$
$FC_R=DCR_{max,C} \exp(-0.5 \cdot k \cdot \beta_{CR}{}^2/b) = 1.0 \exp(-0.5 \cdot 2.22 \cdot 0.20^2/1.66) = 0.9736$

For a confidence level of 60%, the lognormal standard variate is K_x=0.253 and the evaluation inequality becomes:

$FC_R > FD_{RPo} \exp(K_x \cdot \beta_{TU}) = 0.0935 \exp(0.253 \cdot 0.20) = 0.0984$

Since the factored capacity of 0.9736 is greater than the factored demand of 0.0984 the result is satisfactory at 60% confidence level.

IDA is first employed to estimate the MAF of exceeding the ductility limit of 3.3. The fragility curve is calculated based on the $S_a(T_{\mathrm{eff}}, 5\%)$ values that correspond to θ_{roof} = 3.3·0.22/41.9 = 0.017 (Figure 4.11 (b)). The median value of the lognormal distribution is equal to 0.85g and the standard deviation is 43%. The hazard curve used to estimate the MAF is the one presented in Figure 4.10. The estimated mean annual frequency of exceeding the ductility limit, at 50% confidence, equals 0.00046, which is lower than the corresponding code value of 0.0021 (10% probability of exceeding PO in 50 years), thus the performance objective is met.

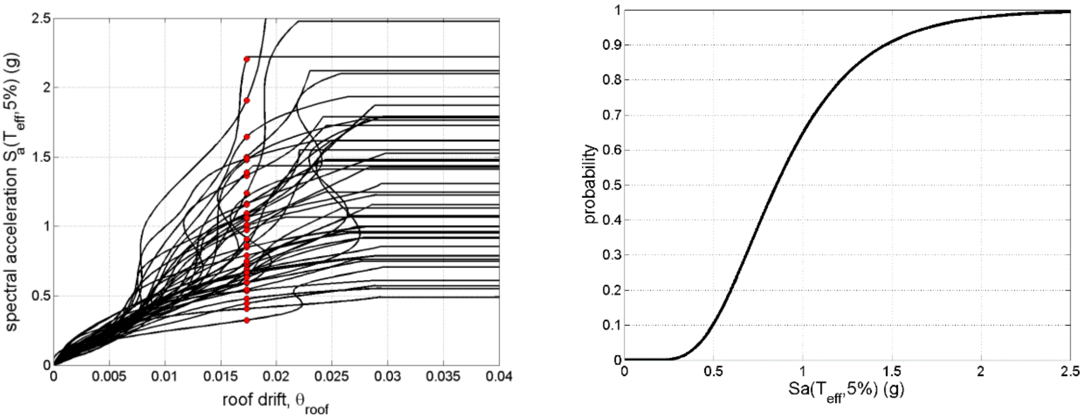

(a) (b)

Figure 4.20: IDA approach for estimating mean annual frequency of exceeding the ductility limit of 3.3: a) the $S_a(T_{\mathrm{eff}},5\%)$ values calculated for θ_{roof} = 0.017, and (b) corresponding fragility curve – twelve story coupled wall building designed using Method A.

To verify the limit on global ductility, θ_{roof} values are calculated for 17 records for S_a^{design}=0.40g (red points) (Figure 4.224.21 (a)). The points of the hazard curve that define the slope k are presented in Figure 4.21 (b). FD and FC at 50% confidence (K_x=0) are estimated as:

$FD_{RPo}=\theta_{roof,50} \exp(0.5 \cdot k \cdot \beta_{\theta roof|Sa}{}^2/b) = 0.0087 \exp(0.5 \cdot 2.34 \cdot 0.22^2/1.0) = 0.0091$
$FC_R=\theta_{roof,\mathrm{C}} \exp(-0.5 \cdot k \cdot \beta_{CR}{}^2/b) = 0.0225 \exp(-0.5 \cdot 2.34 \cdot 0.20^2/1.0) = 0.0165$

Since the factored capacity of 0.017 is greater than the factored demand of 0.0091 the result is satisfactory at the 50% confidence level.

θ_{roof} values are also calculated for 17 records for S_a^{design}=0.40g (red points) and for $1.1S_a^{desigm}$=0.44g (green points) (Figure 4.22(a)). The points of the hazard curve that define the slope k are presented in Figure 4.22(b). FD and FC at 50% confidence (K_x=0) are estimated as:

$FD_{RPo}=\theta_{roof,50} \exp(0.5 \cdot k \cdot \beta_{\theta roof|Sa}{}^2/b) = 0.0087 \exp(0.5 \cdot 2.31 \cdot 0.22^2/0.74) = 0.0093$
$FC_R=\theta_{roof,\mathrm{C}} \exp(-0.5 \cdot k \cdot \beta_{CR}{}^2/b) = 0.017 \exp(-0.5 \cdot 2.31 \cdot 0.20^2/0.74) = 0.0163$

Since the factored capacity of 0.0163 is greater than the factored demand of 0.0093 the result is satisfactory at the 50% confidence level.

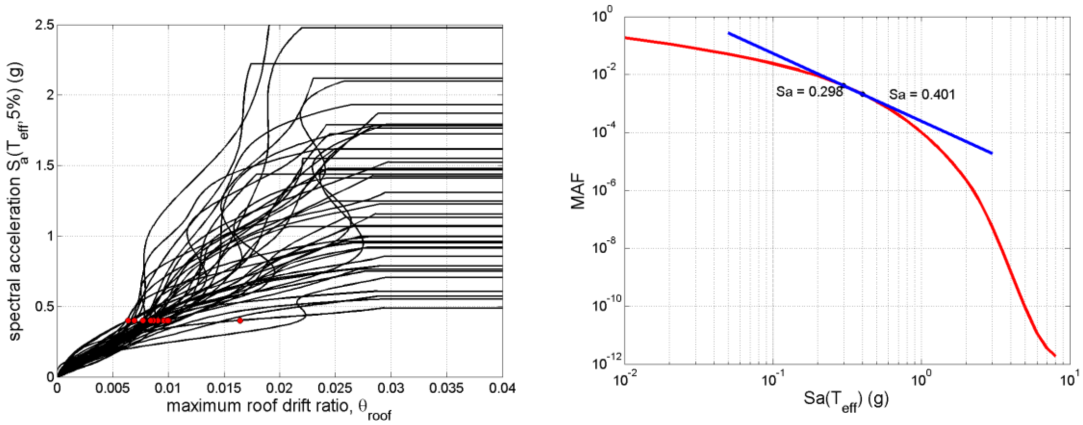

(a) (b)

Figure 4.21: Single stripe analysis method for estimating FD_{RPo} and FC_R for ductility limit of 3.3: (a) roof drift ratio calculated for S_a^{design} (red points), and (b) the local fit of the seismic hazard curve – twelve story coupled wall building designed using Method A.

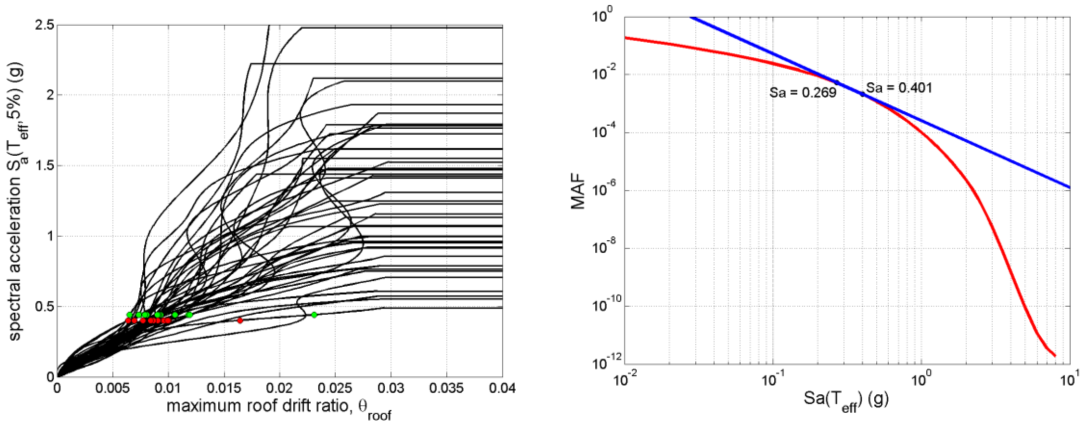

(a) (b)

Figure 4.22: Double stripe analysis method for estimating FD_{RPo} and FC_R for ductility limit of 3.3: (a) roof drift ratio calculated for S_a^{design} (red points) and for $1.1Sa^{design}$ (green points), and (b) the local fit of the seismic hazard curve – twelve story coupled wall building designed using Method A.

5 Cantilever wall

5.1 Building geometry

A 7-story reinforced concrete shear wall building is examined. The plan of the building is shown in Figure 5.1 (b), having dimensions equal to 35x15 m. The perimeter shear walls resist all the seismic loading in the two directions, while the inner columns carry only the gravity loads. Only one out of the four coupled walls is studied in the direction of interest. The cantilever walls have plan length of 5.3m and thickness of 0.3m. The height of the first story is 5.0m while the rest of the stories are 4.0m height, resulting in a total height of 29.0m. The cantilever wall is presented in Figure 5.1 (a).

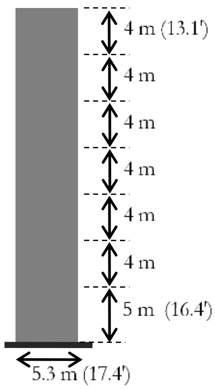

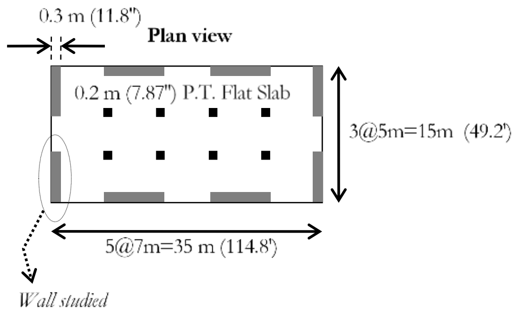

Figure 5.1: Seven story cantilever wall building: (a) shear wall consisting of a rectangular cross section wall, and (b) typical plan of the building.

5.2 Material properties

C30 concrete and B500 steel reinforcement is used. The cantilever wall is designed using nominal material properties, thus the compressive strength of the concrete is f_{ck} = 30MPa and the yield strength of the steel rebars is f_{yk} = 500MPa. The material safety factors used in the design are γ_s = 1.0 and γ_c = 1.0. For the performance assessment, the expected material properties are used, thus f_{ce}= 38MPa, f_{ye}= 575MPa and f_{ue}= 680MPa. The elastic modulus is estimated as Ec = $4700(f_{ce})^{0.5}$, where f_{ce} and E_c are expressed in MPa units.

5.3 Initial design

The initial design of the shear wall using the YFS and an estimation of the slope of the hazard curve within the range of interest (design method B) can be found in detail in Aschheim et al., [7] along with an analytical description of this design method. Only some of the key points of the design are listed in this documentation. The performance objectives that are taken into account are:

- ❖ Limit the mean annual frequency of exceeding an interstory drift ratio of 0.02 to 10%/50 years, at the 50% confidence level
- ❖ Limit the mean annual frequency of plastic hinge rotation demand exceeding plastic hinge rotation capacity at the base of the wall to 10%/50 years, at the 75% confidence level

The first mode parameters of the shear wall building are estimated as Γ_1=1.50 and α_1 =0.65.The yield displacement is estimated as Δ_y = 0.23m. Based on the interstory drift ratio limit of 0.02, the peak roof displacement is estimated as $D_{u,drift}$ = 0.374m, so the resulting ductility is μ = 0.374/0.23 = 1.63. The second performance objective concerns the plastic hinge rotation at the base of the wall. Following the aforementioned procedure for the design, the plastic rotation should be used in order to estimate the corresponding roof drift limit. In order to account for the uncertainty, the plastic hinge rotation capacity of 0.017 for the Life Safety (Table 5.1) is reduced to 0.01rads. Allowing for a plastic hinge equal to l_w/2=5.3/2=2.65m, the roof displacement is estimated as $D_{u,pl.rot.}$=0.517m, thus μ = 0.517/0.23=2.25.

Because we have different confidence levels for the two PO, the Yield Frequency Spectra is derived for the 50% and 75% confidence level using an estimation of the slope of the hazard curve, as shown in Figures 5.2 and 5.3, respectively. The greatest value of the normalized design base shear coefficient is used in the design, thus C_y^*=max{0.278;0.177}=0.278. The design base shear coefficient is $C_y=C_y^*\cdot\alpha_1$=0.278·0.65=0.181 and the design base shear at yield is $V_y=C_y\cdot W$=0.181·8744=1582.7kN. The corresponding period is estimated as 1.51sec using the Equation (3.5).

An inverted triangular distribution of the base shear over the height of the building is assumed, according to the provisions of EC-8. The resultant is at a height of 20.76m, which differs from the value of 22.33(=0.77h) that is the estimated resultant of the first mode distribution of forces. So, a modified base shear is used with the inverted triangular distribution, thus 1582.7·20.76/22.33=1471.4kN. The resulting longitudinal and shear reinforcement at the base of the wall are shown in Figure 5.4.

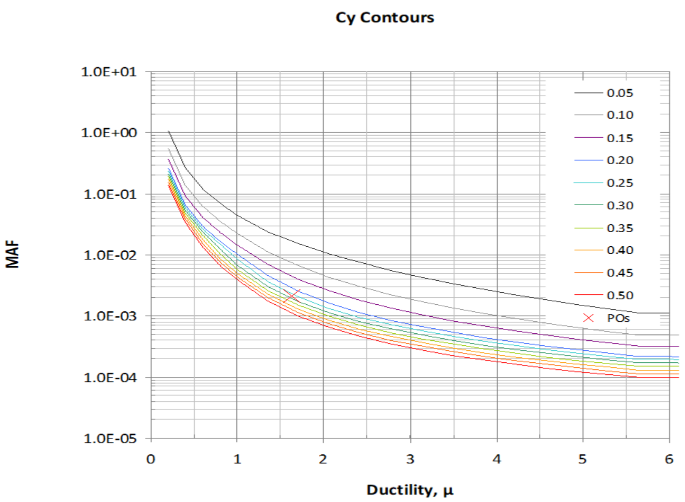

Figure 5.2: Yield Frequency Spectrum (YPS) contours at C_y = 0.05, …, 0.50 determined for a system with Δ_y^*=0.15m at the 50% confidence level. The x symbol represent the performance objective (μ=1.63 and 10% probability of exceedance in 50 years), thus C_y^*=0.278, (seven story cantilever wall building designed using method B), (from Aschheim et al., forthcoming [7]).

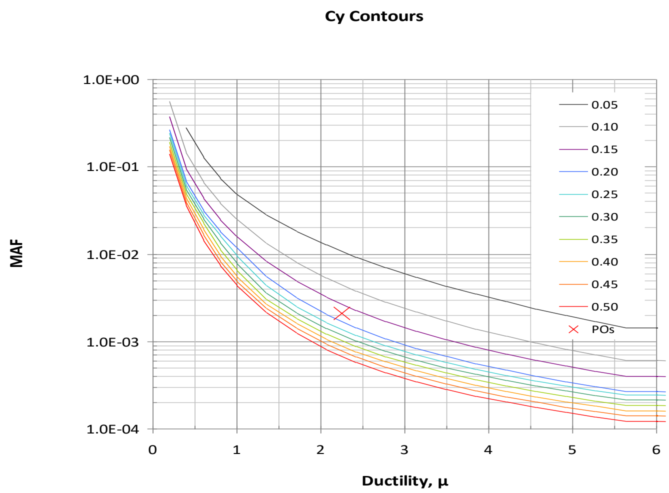

Figure 5.3: Yield Frequency Spectrum (YPS) contours at C_y = 0.05, …, 0.50 determined for a system with Δ_y^*=0.15m at the 75% confidence level. The x symbol represent the performance objective (μ=2.25 and 10% probability of exceedance in 50 years), thus C_y^*=0.177, (seven story cantilever wall building designed using method B), (Aschheim et al., forthcoming [7]).

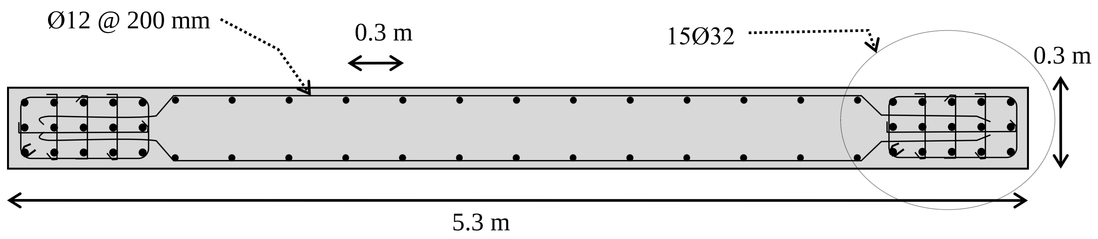

Figure 5.4: Reinforcement at the base of the cantilever wall – seven story cantilever wall building designed using method B (from Aschheim et al., forthcoming [7]).

The initial design is preliminarily evaluated through an eigenvalue analysis. The modal parameters calculated through SeismoStruct are T_1 = 0.58s, Γ_1 = 1.43 and α_1 = 0.61. A non-linear static analysis using a lateral force vector proportional to the fist mode distribution is carried out using SeismoStruct and the resulting pushover curve is presented in Figure 3.10. The period associated with secant stiffness representative of cracked section behavior is estimated as

$$T_{\text{eff}} = T_1 \sqrt{\frac{k_{in}}{k_{eff}}} = 0.89\text{sec} \tag{5.1}$$

which is quite lower than the T^* = 1.51sec.The base shear at yield is 1910kN also is higher than the design base shear which equal to 1471kN. The yield displacement of the building is estimated as 0.19m which in lower than the estimated value of 0.23m. The lower period will result in a smaller spectral displacement, so it is likely that the drift control design will be adequate. Otherwise, the new values can be used for a re-design circle.

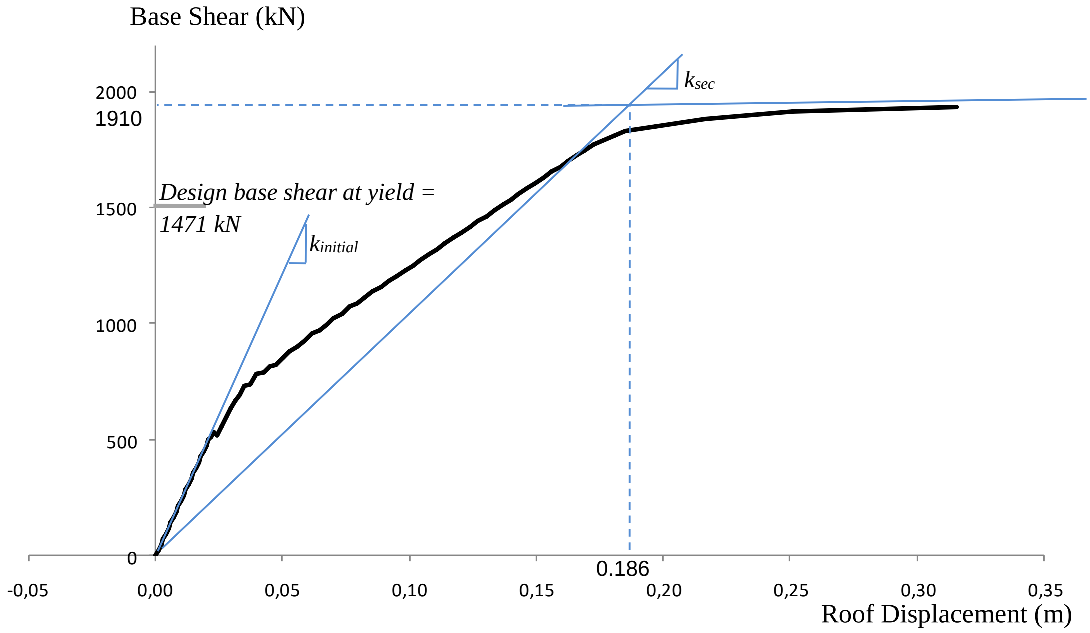

Figure 5.5: Capacity curve observed in a first-mode pushover analysis – seven story cantilever wall building designed using method B (from Aschheim et al., forthcoming [7]).

5.4 Non-linear modeling and acceptance criteria

A two dimensional model of the structure is prepared, as shown in Figure 5.6. Only one out of the four cantilever walls is modeled in the direction of interest. A leaning column is added to simulate the effect of the columns that carry the gravity loads. The leaning column is pinned at the foundation and modeled using linear elastic elements having area and moment of inertia that match the corresponding cross sectional properties of one quarter of the gravity columns of the building plus one cantilever shear wall oriented along the other direction bending around its weak axis. A beam-column element is placed at the centerline of the wall (blue color). The leaning column (red color) is constrained to the nodes of the coupled wall at each floor.

The wall is modelled by using a single displacement-based distributed plasticity element per each story, with fiber section representation monitored at five integration points along the member's length. Following a similar strategy as in the coupled-wall example (Section 4.4) displacement-based elements are preferred to improve convergence. Again, since all plastic rotations are expected to appear at the base, the first-story wall is discretized into five displacement based elements per member having progressively diminishing length with the height from the ground, as shown in Figure 5.6. A comparison of the model to its force-based analogue shows excellent agreement at all levels of inelasticity, as presented in Figure 5.8.

The wall section is discretized into longitudinal steel and concrete fibers (Figure 5.7), the latter having different confinement factors for the cover, the well-confined core at the edges (green) and the semi-confined core of the web (red). The effect of confinement is calculated on the basis of the Mander et al. (1988) model with a resulting confinement ratio of 1.5 for the edge core concrete (green) at the base of the wall. The confinement ratio of the web core concrete (red) is estimated at 1.1. Furthermore, steel reinforcing bars (black color in Figure 5.7) are modelled using a bilinear constitutive law accounting for pinching and stiffness degradation. The expected material properties are used for the analysis, i.e., f_{ce} = 39MPa and f_{ye} = 575MPa.

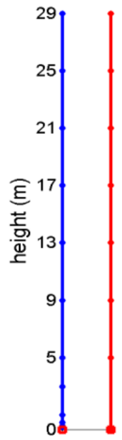

Figure 5.6: Two dimensional structural model used for the analysis showing the shear wall (blue color) and the leaning column (red color) used to model the seven story cantilever wall.

Similarly to the coupled wall example, a number of different assumptions were tested for the post-capping behavior of each material. For easing convergence, generous assumptions were made, resulting in the static pushover capacity curve of Figure 5.8 (for a first-mode-proportional lateral load pattern). To counter the effect of the relaxed material deterioration beyond a roof displacement of 0.3m, global collapse has been enforced at the 3.5% drift, essentially assuming a vertical drop to zero strength, rather than an extended plateau beyond this deformation.

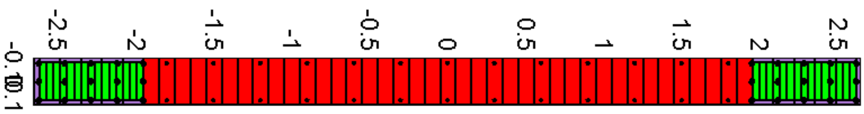

Figure 5.7: Cantilever wall: Typical section fiber discretization used to model the wall showing rebars (black), semi-confined (red) and confined (green) concrete fibers.

The initial (uncracked) period of the model is 0.83sec. A more useful effective period of the structure is calculated using the secant stiffness at 60% of the maximum base shear V_{max}

$$T_{\text{eff}} = T_1\sqrt{\frac{k_{in}}{k_{eff}}} = 1.12\text{sec} \tag{5.2}$$

This is stiffer than the value of 1.51sec assumed in design. The latter better matches the secant period at the point of maximum strength (100% V_{max}), equal to 1.46sec by re-applying Equation 19.2 above. Still, the stiffer period is a better representation of the MDOF system, thus in the following the first-mode period will be taken as $T_1 = T_{\text{eff}} = 1.12$sec.

In Table 5.1 the acceptance criteria for wall plastic rotation, are presented.

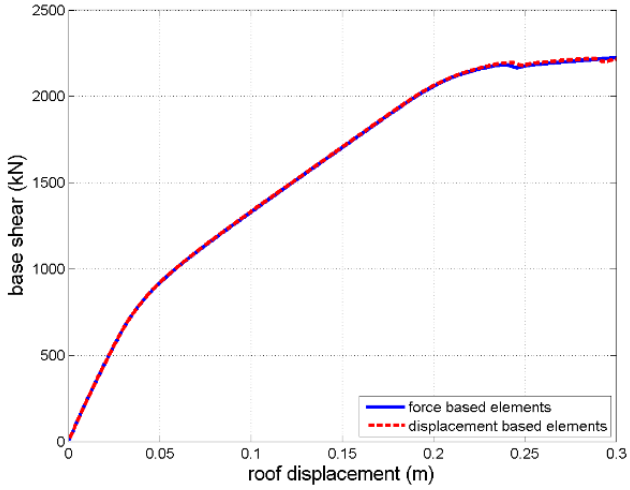

Figure 5.8: Cantilever wall: static pushover curve.

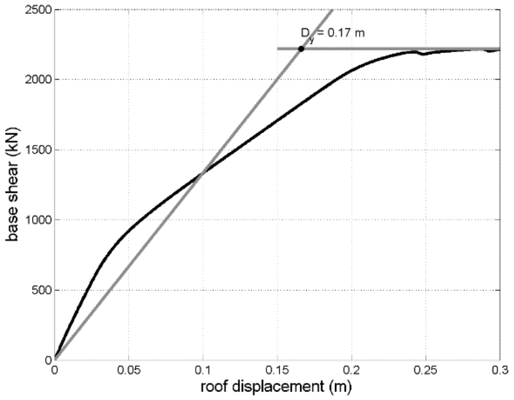

<u>Computed performance:</u>

V_{max} = 2218 kN

Δ_y = 0.17 m

C_y = Vmax/W = 2218/8744 = 0.253

T_{eff} = 1.12sec

Figure 5.9: Calculation of nominal Δ_y of the seven story cantilever wall building by fitting the elastic segment at the 60%V_{max} point of the pushover.

Table 5.1: Acceptance criteria for wall plastic rotations – seven story cantilever wall building designed using method B.

Story	Positive rotation		
	IO	LS	CP
$\theta_{p,max}$ (rad)	0.005	0.017	0.020

5.5 Performance evaluation of the initial design by nonlinear dynamic analysis

The acceptability of interstory drift ratio of 2%, and plastic hinge rotation at the base of the wall is assessed versus a 10% in 50yrs MAF at the 50%, and 75% confidence levels, respectively, using IDA, single and double stripe analysis. For each performance objective, the results are summarized in Table 5.2. For IDA, the first two values of each PO correspond to estimated and allowable MAF, and for the stripe analysis they correspond to factored demand and factored capacity, respectively. The seismic hazard curve scaled to $S_a(T_{eff})$ at 10% in 50 years, is shown in Figure 5.10.

Table 5.2: Verification of the maximum interstory drift and wall plastic rotations for the seven story cantilever wall building designed using method B.

	IDR			wall plastic rotation		
	IDA (yrs^{-1})	Single –	Double –	IDA (yrs^{-1})	Single (rad)	Double (rad)
Demand	0.0005	0.0133	0.0133	0.0002	0.0490	0.0367
Capacity	0.0021	0.0190	0.0190	0.0021	0.9570	0.9832
Check	✓	✓	✓	✓	✓	✓
Confidence	50 %			75%		

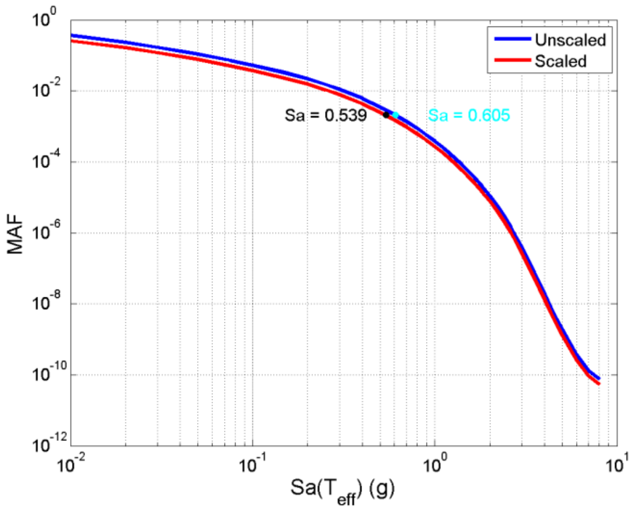

Figure 5.10: Seismic site hazard curve properly scaled to 10% in 50 years for $S_a(T_{eff})$ used for the performance assessment of the seven story cantilever wall building designed using method B.

The mean annual frequency of exceeding maximum interstory drift ratio of 2% is estimated by convolving the seismic hazard curve presented in Figure 5.10 with the fragility curve presented in Figure 5.11 (b) (median value = 0.92g and standard deviation = 25%). The resulting mean annual frequency of exceeding θ_{max} = 2%, at 50% confidence, is 0.00051 which is lower than the code value of 0.0021 (10% in 50 years), thus this performance objective is met.

Interstory drift values are calculated for 17 records for S_a^{design}=0.54g, as shown in Figure 5.12 (a). The points of the hazard curve needed to estimate the slope k are presented in Figure 5.12 (b). FD and FC at 50% confidence are estimated as:

$$FD_{RPo}=\theta_{max,50}\ \exp(0.5\cdot k\cdot \beta_{\theta max|Sa}{}^2/b) = 0.0128\ \exp(0.5\cdot 2.44\cdot 0.18^2/1) = 0.0133$$
$$FC_R=\theta_{max,C}\ \exp(-0.5\cdot k\cdot \beta_{CR}{}^2/b) = 0.02\ \exp(-0.5\cdot 2.44\cdot 0.20^2/1) = 0.0190$$

Since the factored capacity of 0.0190 is greater than the factored demand of 0.0133 the result is satisfactory at the 50% confidence level.

Interstory drift values are also calculated for 17 records for $1.1S_a^{design}$=0.59g, as shown in Figure 5.13 (a). The points of the hazard curve defining the slope k are presented in Figure 5.13 (b). FD and FC at 50% confidence are estimated as:

$FD_{RPo}=\theta_{max,50}\ \exp(0.5\cdot k\cdot \beta_{\theta max|Sa}{}^2/b) = 0.0128\ \exp(0.5\cdot 2.45\cdot 0.18^2/1.003) = 0.0133$
$FC_R=\theta_{max,C}\ \exp(-0.5\cdot k\cdot \beta_{CR}{}^2/b) = 0.02\ \exp(-0.5\cdot 2.45\cdot 0.20^2/1.003) = 0.0190$

Since the factored capacity of 0.0190 is greater than the factored demand of 0.0133 the result is satisfactory at the 50% confidence level.

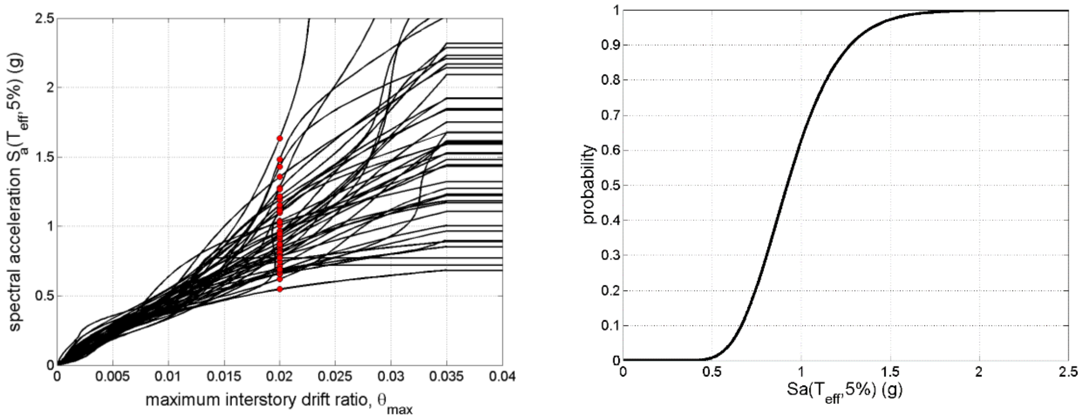

(a) (b)

Figure 5.11: IDA approach for estimating the mean annual frequency of exceeding the interstory drift ratio of 2%: a) the $S_a(T_{eff},5\%)$ values calculated for $\theta_{max} = 0.02$. The cut-off value of 3.5% drift becomes evident by the flatlines. (b) The corresponding fragility curve – seven story cantilever wall building designed using method B.

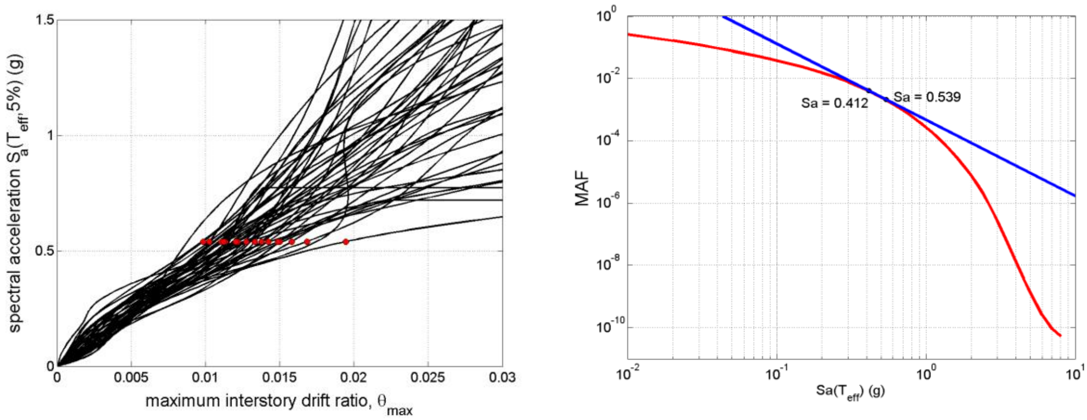

(a) (b)

Figure 5.12: Single stripe analysis method for estimating FD_{RPo} and FC_R for 2% maximum interstory drift ratio: a) maximum interstory drifts calculated for S_a^{design}, and b) the local fit of the seismic hazard curve – seven story cantilever wall building designed using method B.
building designed using method B.

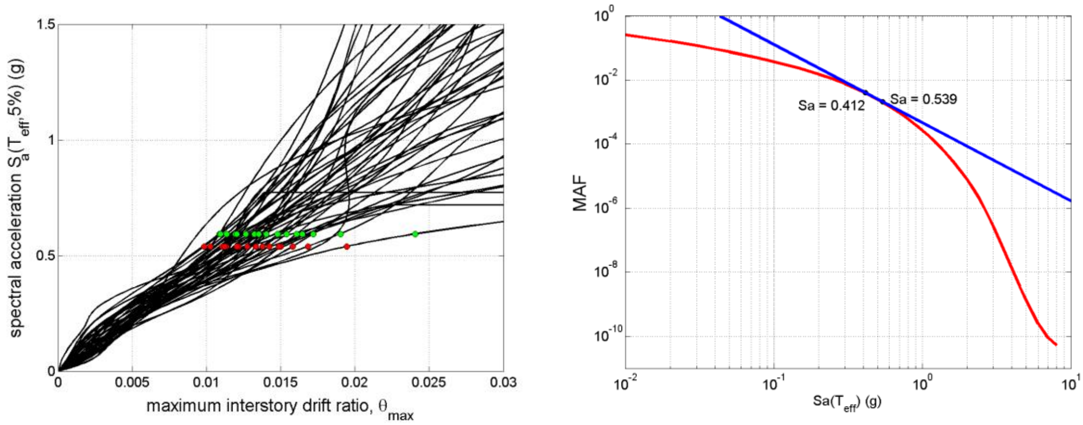

(a) (b)

Figure 5.13: Double stripe analysis method for estimating FDRPo and FCR for 2% maximum interstory drift ratio: a) maximum interstory drifts calculated for Sadesign (red points) and for 1.1 Sadesign (green points), and b) the local fit of the seismic hazard curve – seven story cantilever wall.

The mean annual frequency of exceeding demand capacity ratio of 1 at the base of the wall is estimated by convolving the seismic hazard curve presented in Figure 5.10 with the fragility curve presented in Figure 5.14 (b) (median value=1.60g, dispersion = 40%). The resulting mean annual frequency of exceeding *DCR* = 1.0, at 75% confidence, is 0.00023 which is lower than the code value of 0.0021 (10% in 50 years), thus this performance objective is met.

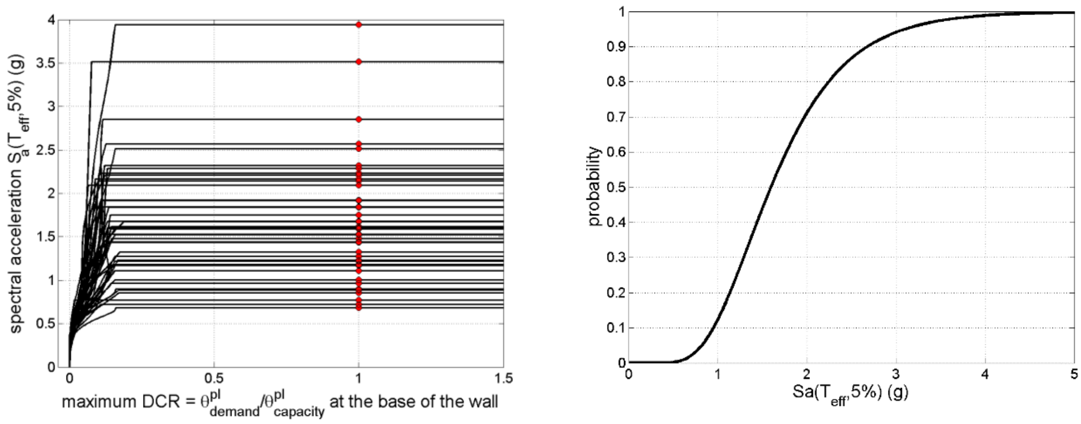

(a) (b)

Figure 5.14: IDA approach for estimating mean annual frequency of exceeding DCR=1 at the base of the wall: a) the $S_a(T_{eff},5\%)$ values calculated for DCR = 1.0, and (b) the corresponding fragility curve – seven story cantilever wall building designed using method B.

DCR values for the base of the wall are calculated for 17 records for S_a^{design}=0.54g, as shown in Figure 5.15 (a). The points of the hazard curve that define the slope *k* are presented in Figure 5.15 (b). FD and FC are estimated as:

$FD_{RPo}=DCR_{max,50}\ \exp(0.5\cdot k\cdot \beta_{\theta max|Sa}{}^2/b) = 0.0268\ \exp(0.5\cdot 2.20\cdot 0.65^2/1.0) = 0.0429$
$FC_R=DCR_{max,C}\ \exp(-0.5\cdot k\cdot \beta_{CR}{}^2/b) = 1.0\ \exp(-0.5\cdot 2.20\cdot 0.20^2/1.0) = 0.9570$

For a confidence level of 75%, the lognormal standard variate is K_x=0.6745 and the evaluation inequality becomes:

$FC_R > FD_{RPo} \exp(K_x \cdot \beta_{TU}) = 0.0429 \exp(0.6745 \cdot 0.20) = 0.0490$

Since the factored capacity of 0.9570 is higher than the factored demand of 0.0490 the result is satisfactory at the 75% confidence level.

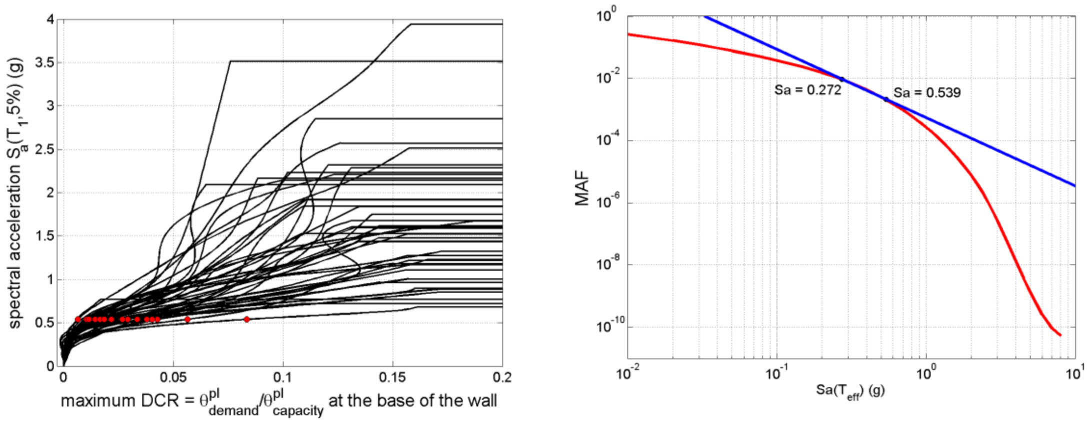

(a) (b)

Figure 5.15: Single stripe analysis method for estimating FD_{RPo} and FC_R for DCR=1 of the base of the wall: (a) maximum DCR at the base of the wall calculated for S_a^{design}, and (b) the local fit of the seismic hazard curve – seven story cantilever wall building designed using method B.

DCR values for the base of the wall are also calculated for 17 records for $1.1S_a^{design}$=0.59g, as shown in Figure 5.16 with green points (a). The points of the hazard curve that define the slope *k* are presented in Figure 5.16 (b). FD and FC are estimated as:

$FD_{RPo}=DCR_{max,50} \exp(0.5 \cdot k \cdot \beta_{\theta max|Sa}{}^2/b) = 0.0268 \exp(0.5 \cdot 2.54 \cdot 0.65^2/3.0) = 0.0368$
$FC_R=DCR_{max,C} \exp(-0.5 \cdot k \cdot \beta_{CR}{}^2/b) = 1.0 \exp(-0.5 \cdot 2.54 \cdot 0.20^2/3.0) = 0.9833$

For a confidence level of 75%, the lognormal standard variate is K_x=0.6745 and the evaluation inequality becomes:

$FC_R > FD_{RPo} \exp(K_x \cdot \beta_{TU}) = 0.0368 \exp(0.6745 \cdot 0.20) = 0.0321$

Since the factored capacity of 0.9833 is higher than the factored demand of 0.0321 the result is satisfactory at the 75% confidence level.

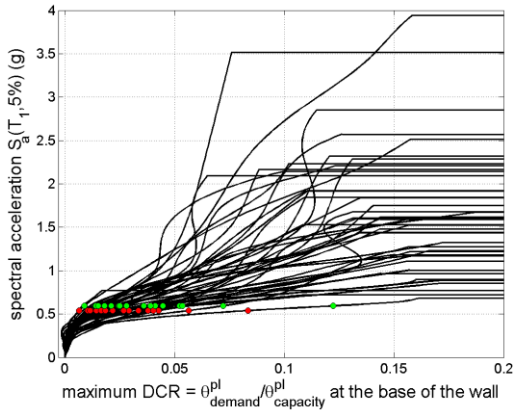

(a)

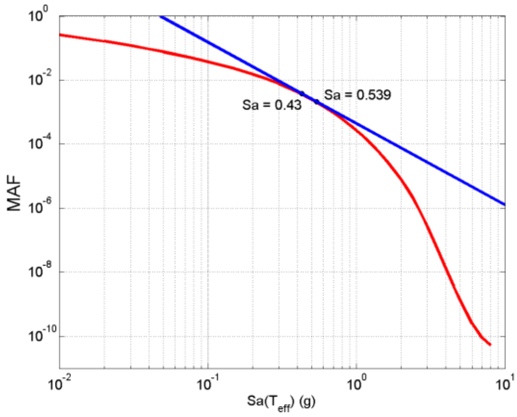

(b)

Figure 5.16: Double stripe analysis method for estimating FD_{RPo} and FC_R for DCR=1 of the base of the wall: (a) maximum DCR at the base of the wall calculated for S_a^{design} (red points) and for 1.1 Sa^{design} (green points) and (b) the local fit of the seismic hazard curve – seven story cantilever wall building designed using method B.

6 Conclusions

Structural design using the Yield Point Spectrum offers a design compatible to the current codes. It does not account for the uncertainties directly, but code specific reduction factors are applied. The results of the performance assessment of the buildings indicate that the YPS offers a design able to meet the performance objectives that are related to a probability of exceedance equal to 10% in 50 years (compatible with the code Sa values). However, the results concerning performance objectives with probability of exceedance different than the 10%/50years are not satisfactory.

The Yield Frequency Spectrum calculated using an approximation of the hazard curve offers an improved design compared to the YPS, as it accounts for the uncertainties, at least at the SDOF level. Thus, the results of the performance assessment of the buildings designed using method B are satisfactory, given that all performance objectives set in the design are finally met. If actual seismic hazard data are used to compute the YFS (method C), then the accurate shape of the hazard is also incorporated, leading to an improved design approach that better accounts for site characteristics. The results of the performance assessment of the building designed using method C are also satisfactory. It is important to note that a desired MAF can be targeted in the design process when the YFS is used, and the focus is on the MAF of exceeding the parameter value of interest (output) rather than on the MAF of exceeding the ground motion intensity (input), as in the design using the YPS.

The three different methods used for the performance assessment of the structures are the single stripe, the double stripe and the IDA approach. In some cases, the results of the single stripe were not satisfactory whereas, following the double stripe analysis or the full IDA, we gain better accuracy and are thus more confident that the specific performance objective was (or was not) met. This is the price we pay for using a simpler approach and it is acceptable assuming one is fully aware of the consequences. So, if the difference of Factored Demand and Factored Capacity calculated through the single stripe analysis is small, one may opt to further test the PO by employing a second stripe or the full IDA. The improved accuracy of the double stripe or the even better accuracy that IDA offers, may allow us to avoid the need of a re-design cycle.

In some cases, the b_{EDP} calculated in the double stripe analysis differed remarkably form the value of 1.0 that is characteristic of moderate-to-long period structures, conforming to the well-known equal displacement rule (and thus used in the single stripe analysis as a default). High values of this slope indicate that the verification is performed relatively close to the onset of global collapse. In such cases, some care should be exercised that no more than 16% of the runs are non-convergent. Otherwise the approximation underlying the FD and FC verification will probably fail. In such cases, IDA is the recommended approach.

Finally, IDA can be conservative close to global collapse as the simple amplitude scaling that it employs may not allow capturing the appropriate spectral shape of the high intensity ground motions. So if collapse is to be assessed, the analyst may attempt more accurate assessment methods.

7 References

1. ACI Committee, American Concrete Institute, & International Organization for Standardization. (2008). Building code requirements for structural concrete (ACI 318-08) and commentary. American Concrete Institute.
2. American Concrete Institute. (2005). Building Code Requirements for Structural Concrete (ACI 318-05) and Commentary (ACI 318R-05), Farmington Hills, MI.
3. American Society of Civil Engineers. (2005). ASCE7-05: Minimum Design Loads for Buildings and Other Structures, Reston, VA.
4. ASCE, 2007a, Seismic Rehabilitation of Existing Buildings, ASCE Standard ASCE/SEI 41-06, American Society of Civil Engineers, Reston, Virginia.
5. ASCE. (2010). Minimum Design Loads for Buildings and Other Structures. ASCE/SEI Standard 7-10.
6. Aschheim, M. (2002). Seismic design based on the yield displacement. Earthquake spectra, 18(4), 581-600.
7. Aschheim, M., Hernández-Montes, E., Vamvatsikos, D.. Design of Reinforced Concrete Buildings for Seismic Performance: Practical Deterministic and Probabilistic Approaches 1st Edition, Forthcoming.
8. Baker JW, Cornell CA. 2006. Spectral shape, epsilon and record selection. Earthquake engineering and structural dynamics, 35(9):1077–1095.
9. Black, E., and Aschheim, M., 2000. Seismic Design and Evaluation of Multistory Buildings Using Yield Point Spectra, CD Release 00-04, Mid-America Earthquake Center, University of Illinois, Urbana, July
10. Code, P. (2005). Eurocode 8: Design of structures for earthquake resistance-Part 1: General rules, seismic actions and rules for buildings. Brussels: European Committee for Standardization.
11. Cornell CA, Krawinkler H. (2000). Progress and challenges in seismic performance assessment, PEER Center News
12. Cornell, C. A., Jalayer, F., Hamburger, R. O., & Foutch, D. A. (2002). Probabilistic basis for 2000 SAC federal emergency management agency steel moment frame guidelines. Journal of structural engineering, 128(4), 526-533.
13. FEMA (2009). Quantification of Building Seismic Performance Factors. FEMA P-695, prepared by the Applied Technology Council for the Federal Emergency Management Agency, Washington, D.C.
14. Haselton, C. B., Liel, A. B., Dean, B. S., Chou, J. H., & Deierlein, G. G. (2007). Seismic collapse safety and behavior of modern reinforced concrete moment frame buildings. In Structural Engineering Research Frontiers (pp. 1-14).
15. Kohrangi M., Bazzurro P., Vamvatsikos D., Spillatura A. (2017). Conditional spectrum based ground motion record selection using average spectral acceleration. Earthquake Engineering and Structural Dynamics, 46(10):1667-1685.
16. Lin T, Haselton CB, Baker JW. (2013). Conditional spectrum-based ground motion selection. Part I: Hazard consistency for risk-based assessments. Earthquake Engineering and Structural Dynamics, 42(12):1847–1865
17. Luco N, Bazzurro P. (2007). Does amplitude scaling of ground motion records result in biased nonlinear structural drift responses? Earthquake Engineering and Structural Dynamics, 36(13):1813–1836.
18. Mander, J. B., Priestley, M. J., & Park, R. (1988). Theoretical stress-strain model for confined concrete. Journal of structural engineering, 114(8), 1804-1826.

19. McKenna, F., Fenves, G. L., & Scott, M. H. (2000). Open system for earthquake engineering simulation. University of California, Berkeley, CA.
20. Miranda, E., & Bertero, V. V. (1994). Evaluation of strength reduction factors for earthquake-resistant design. Earthquake spectra, 10(2), 357-379.
21. PEER (2005). PEER NGA Database. Pacific Earthquake Engineering Research Center, Berkeley, CA, http://peer.berkeley.edu/nga/.
22. Priestley, M. J. N. (2000). Performance based seismic design. Bulletin of the New Zealand society for earthquake engineering, 33(3), 325-346.
23. SeismoSoft, S. (2006). A computer program for static and dynamic nonlinear analysis of framed structures. Disponível online em: http://www. seismosoft. com.
24. Vamvatsikos, D. (2012). Accurate application and second-order improvement of SAC/FEMA probabilistic formats for seismic performance assessment. Journal of Structural Engineering, 140(2), 04013058.
25. Vamvatsikos, D., & Cornell, C. A. (2002). Incremental dynamic analysis. Earthquake Engineering & Structural Dynamics, 31(3), 491-514.